ISTANBUL TECHNICAL UNIVERSITY ★ GRADUATE SCHOOL OF SCIENCE ENGINEERING AND TECHNOLOGY

# EFFECT OF HYDRODYNAMIC PARAMETERS ON PARTICLE-BUBBLE INTERACTIONS IN FLOTATION

PH.D. THESIS

Ahmad HASSANZADEHMAHALEH

Department of Mineral Processing Engineering
Mineral Processing Engineering Programme

DECEMBER 2018

**ISTANBUL TECHNICAL UNIVERSITY ★ GRADUATE SCHOOL OF SCIENCE ENGINEERING AND TECHNOLOGY**

# EFFECT OF HYDRODYNAMIC PARAMETERS ON PARTICLE-BUBBLE INTERACTIONS IN FLOTATION

**Ph.D. THESIS**

**Ahmad HASSANZADEHMAHALEH**
**(505142102)**

**Department of Mineral Processing Engineering**
**Mineral Processing Engineering Programme**

**Thesis Advisor: Prof. Dr. Mehmet S. ÇELIK**

**DECEMBER 2018**

İSTANBUL TEKNİK ÜNİVERSİTESİ ★ FEN BİLİMLERİ ENSTİTÜSÜ

# FLOTASYONDA HİDRODİNAMİK PARAMETRELERİN TANE-KABARCIK ÜZERİNE ETKİSİ

**DOKTORA TEZİ**

**Ahmad HASSANZADEHMAHALEH**
**(505142102)**

**Cevher Hazırlama Mühendisliği Anabilim Dalı**
**Cevher Hazırlama Mühendisliği Programı**

**Tez Danışmanı: Prof. Dr. Mehmet S. ÇELIK**

**ARALIK 2018**

Ahmad HASSANZADEHMAHALEH, a Ph.D. student of ITU Graduate School of Science Engineering and Technology student ID 505142102, successfully defended the thesis/dissertation entitled "Effect Of Hydrodynamic Parameters On Particle-Bubble Interactions In Flotation", which he prepared after fulfilling the requirements specified in the associated legislations, before the jury whose signatures are below.

**Thesis Advisor :** **Prof. Dr. Mehmet Sabri ÇELIK**
Istanbul Technical University

**Jury Members :** **Prof. Dr. Mehmet Sabri ÇELIK**
Istanbul Technical University

**Prof. Dr. Ayhan Ali SIRKECI**
Istanbul Technical University

**Prof. Dr. Gulay BULUT**
Istanbul Technical University

**Assoc. Prof. Dr. Orhan ÖZDEMIR**
Istanbul University

**Assoc. Prof. Dr. Oktay SAHBAZ**
Dumlupinar University

**Date of Submission : 19 October 2018**
**Date of Defense : 20 December 2018**

***to my mother, soul of my father, beloved wife, my brother and sisters,***

## FOREWORD

This thesis is comprised of seven chapters. Chapter one represents the fundamental knowledge and basic concepts concerning the macroscopic and microscopic aspects of flotation. It includes the basics and fundamentally novel perceptions of particle-bubble interactions. Chapter two covers the literature studies critically highlighting applications, constrains and privileges of the most common three methods *i.e.* experimental (direct and indirect), analytical and numerical (CFD) for simultaneously estimation of particle-bubble encounter probabilities ($E_c$) in flotation cells. Chapter three briefly describes the individual methodology used for each objective to tackle some research questions on flotation. Chapter four highlights the impact of particle properties such as particle size ($d_p$) and particle density ($\rho_p$) on the probability of particle-bubble encounter using analytical techniques. In addition, the impact of particle inertial effect ($E_c^{in}$), angle of tangency ($\theta_t$) and critical Stokes number ($St_{cr}$) are discussed in detail on the $E_c$ and flotation kinetic rate constant ($k$). Chapter five discusses the role of bubble surface characteristics (degree of retardation), bubble diameter ($d_B$) and bubble velocity ($v_B$) on the particle-bubble interaction phenomena in flotation. The estimation and optimization of encounter efficiencies and flotation kinetic constants are elaborated in chapter six using response surface method (RSM). Chapter seven underlines the general results and conclusions together with the recommendations for future studies.

I'd like to sincerely express my profound appreciation to everybody who helped me to complete the thesis. My warmest gratitude devotes to my supervisor, Prof. Dr. Mehmet Sabri Çelik for his scientific advices throughout these years. I was honored to be a member of his research team.

I'd like to extend my appreciation to my friends and colleagues including Dr. Sabri Kouachi, Behzad Vaziri Hassas, Dr. Zuzana Brabcova, Dr. Mahshid Firouzi, Dr. Boris Albajanic, Dr. Asghar Azizi, Dr. Mohsen Karimi, Dr. Önur Güven who advised and encouraged me throughout my Ph.D. I am grateful to Dr. Fırat Karakaş, Dr. Feridun Boylu and Dr. Ibrahim Ethem Karaağaçlıoğlu who always helped me in every case. I would like to appreciate Scientific and Technological Research Council of Turkey (TÜBİTAK), Erasmus organization and Istanbul Technical University (ITU) due to the financial fund of scientific research program with the project number of 114M483.

I intend to acknowledge the moral and financial support of my parents, my sisters and the sister in law and my beloved brother and the brothers in low for their endless pure love and helping me during the time of this study. More importantly, I would like to thank my kind father, whom I lost him during my studies and played the most important role in completing my Ph.D.

My sincere gratefulness goes to my friends who inspired me throughout my Ph.D. program specially Hamed Feizullahzadeh, Nima Dadashzadeh, Dr. Mohsen

Abbasnia, Eren Gayretly, Nihat Tarhan, Melik Çiftçi and all my friends in Iran, Turkey and Germany.

Eventually, I intend to thank my love, my beautiful and intelligent wife, Zehra Öztürk, for her helps, supports and kindness during last three years in my life. She has always been beside me to cross over my Ph.D. journey at Istanbul.

December 2018 Ahmad Hassanzadehmahaleh

**TABLE OF CONTENTS**

**Page**

## ABBREVIATIONS

| | |
|---|---|
| $\mathbf{E_c}$ | : Particle-bubble encounter efficiency |
| $\mathbf{E_a}$ | : Particle-bubble attachment efficiency |
| $\mathbf{E_s}$ | : Particle-bubble stability efficiency |
| $\mathbf{E_{coll}}$ | : Particle-bubble collection efficiency |
| $\mathbf{E_c^{GSE}}$ | : Generalized Sutherland equation |
| $\mathbf{E_c^{YL}}$ | : Yoon–Luttrell collision model |
| $\mathbf{E_c^{SU}}$ | : Sutherland equation |
| $\mathbf{E_c^{GA}}$ | : Gaudin collision model |
| $\mathbf{E_c^{SC}}$ | : Schulze collision model |
| $\mathbf{E_c^{FH}}$ | : Flint and Howarth collision model |
| $\mathbf{E_c^{LB}}$ | : Langmuir and Blodgett encounter model |
| $\mathbf{E_c^{RR}}$ | : Reay and Ratcliff encounter model |
| $\mathbf{E_c^{AK}}$ | : Afruns-Kitchner collision model |
| $\mathbf{E_c^{WP}}$ | : Weber and Paddock collision model |
| $\mathbf{E_c^{HB}}$ | : Heindel and Bloom collision model |
| $\mathbf{E_c^{NS}}$ | : Nguyen and Schulze collision model |
| $\mathbf{E_a^{DF}}$ | : Modified Dobby–Finch model |
| $\mathbf{E_a^{YL}}$ | : Yoon–Luttrell attachment model |
| $\mathbf{E_s^{SC}}$ | : Modified Schulze stability model |
| $\mathbf{E_c^{ic}}$ | : Interception effect |
| $\mathbf{E_c^{g}}$ | : Gravitational effect |
| $\mathbf{E_c^{in}}$ | : Inertial effect |
| **NB** | : Nanobubble |
| **CCD** | : Central composite design |
| **ANOVA** | : Analysis of variance |
| **MLR** | : Multi linear regression |
| **ANN** | : Artificial neural network |
| **RSM** | : Response surface modeling |
| **TKE** | : Total kinematic energy of turbulence |
| **DF** | : Degree of freedom |

| | |
|---|---|
| **DOE** | : Design of experimental |
| **MB** | : Microbubble |
| **AFM** | : Atomic force microscopy |
| **CFD** | : Computational fluid dynamic |
| **DEM** | : Discrete element method |
| **RCS** | : Reaction cell system |
| **GFK** | : General flotation kinetic |
| **LRHI** | : Long-range hydrodynamic interaction |
| **SRHI** | : Short-range hydrodynamic interaction |
| **$St_{cr}$** | : Critical Stokes number |
| **CMF** | : Conventional mechanical flotation |
| **TPC** | : Three-phase contact line |

## SYMBOLS

| | |
|---|---|
| **A, B** | : Constants in attachment efficiency model |
| $\mathbf{A_s}$ | : Empirical stabilization constant = 0.50 |
| $\mathbf{MRT_b}$ | : Mean bubble residence time |
| $\mathbf{C_p}$ | : Particle circularity |
| $\mathbf{B_O^*}$ | : Bond number |
| **g** | : Gravitational constant |
| $\boldsymbol{\theta_t}$ | : Angle of tangency |
| **σ** | : Surface tension |
| $\mathbf{K_{st}}$ | : Stokes number |
| $\mathbf{Re_b}$ | : Bubble Reynolds number |
| $\mathbf{S_b}$ | : Bubble surface area flux |
| **λ** | : Turbulence dissipation rate |
| **k** | : Flotation rate constant |
| $\mathbf{N_p}$ | : Number of particles per unit volume |
| $\mathbf{N_b}$ | : Number of bubbles per unit volume |
| $\mathbf{Z_{pb}}$ | : Collision frequency |
| $\mathbf{d_p}$ | : Particle size |
| $\mathbf{d_b}$ | : Bubble size |
| $\mathbf{V_p}$ | : Particle relative velocity |
| $\mathbf{V_b}$ | : Bubble relative velocity |
| **ε** | : Turbulence dissipation rate |
| $\boldsymbol{\rho_f}$ | : Fluid density |
| $\mathbf{t_{ind}}$ | : Induction time |
| $\mathbf{G_{fr}}$ | : Gas flow rate |
| $\mathbf{V_{cell}}$ | : Volume of vessel |
| **η** | : Liquid viscosity |
| **ν** | : Kinematic viscosity |
| **f** | : Constant value=2.03 |
| $\mathbf{F_{att}}$ | : Attachment force |
| $\mathbf{F_{dett}}$ | : Detachment force |

| | |
|---|---|
| **$t$** | : Time |
| **$\rho_p$** | : Particle density |
| **$d_{32}$** | : Sauter mean diameter |
| **$\theta_a$** | : Adhesion angle |
| **$I_b$** | : Interfacial area of bubbles |
| **$K_3$** | : Dimensionless numbers |
| **$R_c$** | : Collision radius |
| **$V_s$** | : Particle settling rate |
| **$U$** | : Bubble slip velocity |
| **$\varphi_c$** | : Streamline stream function |
| **$t_{sl}$** | : Sliding time |
| **μHM** | : Microhydrodynamic |

## LIST OF TABLES

**Page**

## LIST OF FIGURES

**Page**

## EFFECT OF HYDRODYNAMIC PARAMETERS ON PARTICLE-BUBBLE INTERACTIONS IN FLOTATION


## SUMMARY

The current thesis studies the impact of particle and bubble characteristics as well as cell hydrodynamic properties on particle-bubble interactions. Additionally, it investigates the estimation and optimization of the encounter probability of particle-bubble ($E_c$) and flotation rate constant ($k$) in the presence and absence of turbulence by means of response surface method (RSM). The present work comprehensively compiles the previous studies implemented on determination and assessment of $E_c$ in laminar and turbulent fluid flows by means of analytical (streamline-based concepts), numerical (CFD and DEM) and practical methods (direct and indirect approaches). The effects of some significant factors such as particle size (1-100µm*)*, particle density (1.3-7.1g/cm$^3$), bubble size (0.05-0.15cm) and velocity (10-30cm/s), bubble surface mobility (contaminated and non-contaminated) and turbulence dissipation rate (18, 21, 24, 27, 30$m^2/s^3$) on the $E_c$ and $k$ are investigated in detail. The comparison between three common methods for estimation of $E_c$ revealed that the analytical modeling mainly disregard the microhydrodynamic (µHM) resistance forces and particle trajectory together with its angle of tangency in greater Stokes values. However, the best correlation among numerical and analytical modeling is obtained in the rangee of fine and ultra-fine particles due to low impact of inertial forces. Initially, it is found in this work that omitting water inertial forces results in two to four times greater estimation of flotation rate constant as a function of particle diameter ($d_p$), particle density ($\rho_p$) and their synergetic effects. For the first-time, the intersection of three collision models (*i.e.* Sutherhland, Schulze and Dukhin) is suggested as an alternative method for estimating the critical Stokes number ($St_{cr}$) as a function of bubble surface properties (bubble size, its diameter and mobility). The results of the presented approach highly comply the data given by Stokes. Also, the exact thresholds for identifying the positive and negative effects of particle inertia are reported. It is found from optimization processes that particle density plays an opposite role on $E_c$ which implies further studies for more clarification. Also, under a limited hydrodynamic circumstances in a flotation cell, particle inertial effect can be solely ignored to a certain extent. The predicted $E_c$ values are sub-classified in three main zones, *i.e.* low (0-4%), intermediate (4-8%) and high (8-14%) regions with respect to the role of bubble size ($d_B$) and its velocity ($v_B$). Using a combination of Yoon-Luttrell's collision ($E_c^{\mathrm{YL}}$) and attachment ($E_a^{\mathrm{YL}}$) models leads to overestimation of collection efficiencies in comparison with generalized Sutherland equation ($E_c^{\mathrm{GSE}}$) and modified Dobby–Finch ($E_a^{DF}$) models. Moreover, the relative significance of key factors (particle size, bubble diameter, bubble velocity, particle density and turbulence) on $E_c$ and $k$ is shown for the first time to be incoherent in the literature.

**FLOTASYONDA HİDRODİNAMİK PARAMETRELERİN TANE-KABARCIK ÜZERİNE ETKİSİ**

## ÖZET

Bu tez çalışmasında tane ve kabarcık özelliklerinin etkileşimleri tane ve hidrodinamik faktörler özelliklerin üzerine etkileri incelenmektedir. Buna ek olarak, yanıt yüzey yöntemi (RSM) ile türbülans hız varlığında ve yokluğunda tane-kabarcık karşılaşma randımanı ($E_c$) ve flotasyon hız sabiti değerlerinin (k) tahmin ve optimizasyonunu araştırılmaktadır.

Bu tez yedi bölümden oluşmaktadır. Birinci bölüm, flotasyonun makroskopik ve mikroskobik yönleriyle ilgili temel bilgileri ve temel kavramları temsil eder. Parçacık-kabarcık etkileşimlerinin temellerini ve temelde yeni algılarını içerir.

İkinci bölüm, flotasyon hücrelerinde partikül-kabarcık karşılaşma olasılıklarının eşzamanlı olarak tahmin edilmesi için deneysel (doğrudan ve dolaylı), analitik ve nümerik (CFD) deneysel (doğrudan ve dolaylı), analitik ve CFD uygulamaların, kısıtların ve ayrıcalıkların eleştirel olarak vurgulanmasıyla ilgili literatür çalışmalarını kapsar.

Üçüncü bölümde, yüzdürmeyle ilgili bazı araştırma sorularının üstesinden gelmek için her bir amaç için kullanılan bireysel metodoloji kısaca açıklanmaktadır.

Dördüncü bölüm, partikül ebadı ($d_p$) ve partikül yoğunluğu ($\rho_p$) gibi partikül özelliklerinin, analitik teknikler kullanılarak partikül kabarcığı karşılaşması olasılığı üzerindeki etkisini vurgulamaktadır. Ek olarak, partikül atalet etkisinin, teğetlik açısının ($\theta_t$) ve kritik Stokes sayısının ($St_{cr}$) etkisi, $E_c$ ve flotasyon kinetik oranı sabiti (k) üzerinde detaylı olarak ele alınmıştır.

Beşinci bölüm, kabarcık yüzey özelliklerinin (geciktirme derecesi), kabarcık çapının ($d_B$) ve kabarcık hızının ($v_B$) flotasyondaki parçacık-kabarcık etkileşimi olayları üzerindeki rolünü tartışmaktadır.

Karşılaşma verimlerinin ve flotasyon kinetik sabitlerinin tahmini ve optimizasyonu, yanıt yüzeyi yöntemi (RSM) kullanılarak altıncı bölümde ayrıntılı olarak açıklanmaktadır.

Yedinci bölüm, gelecekteki çalışmalar için önerilerle birlikte genel sonuçların ve sonuçların altını çizer.

Hesaplamalı akışkanlar dinamiği (CFD) ile, flotasyon hücrelerinde tane-kabarcık etkileşimlerini belirlemek için deneysel yöntemler (doğrudan ve dolaylı yaklaşımlar) dahil olmak üzere analitik ve sayısal modelleme ile ilgili çalışmaları kapsamlı ve eleştirel bir gözle incelenmistir. Elde edilen sonuçlar, çarpışma açısı, Stokes sayısı, tane yoğunluğunun etkisi ve mikrohidrodinamik kuvvetlerin göz ardı edilmesi ve türbülans etkilerle ilgili tahminlerin zayıfligi uygulanabilen modellerin sınırlı olduğunu göstermektedir. Analitik modellemeden farklı olarak, sayısal modelleme tane-kabarcık karşılaşma etkileşimlerini değerlendirmek için çok güçlü bir teknik

olarak tanımlanmaktadır. Bu çalışmada ilk olarak suyun atalet kuvvetlerinin dikkatle alınmamışı durumunde, sayısal yoğunluklarda ve tane boyutlarındaki değişikliklere bağlı olarak, flotasyon kinetiğinin 2-4 kat daha yüksek tahmin edileceği bulunmuştur. Tane boyutu (1-100μm), tane yoğunluğu (1.3-7.1g/cm$^3$), kabarcık boyutu (0.05-0.15cm) ve hızı (10-30cm/s), kabarcık yüzey hareketliliği (temiz ve kontamine olmuş) ve türbülans yayılım oranının (18, 21, 24, 27, 30m$^2$/s$^3$) $E_c$ ve k üzerindeki etkileri ayrıntılı olarak incelenmiştir.

Tane yoğunluğunun, $E_c$ üzerinde önemli bir rol oynadığı bulunmuş olup, daha net bir açıklama yapmak için detaylı çalışmalara ihtiyaç duyulmaktadır. Aynı zamanda, bir flotasyon hücresinde sınırlı hidrodinamik şartlarde, tane eylemsizliği etkisi sadece belli bir ölçüde göz ardı edilebilmektedir. Tahmin edilen $E_c$ değerleri, kabarcık boyutu ve hızının rolüne göre üç ana bölgede, yani düşük (0-4%), ara (4-8%) ve yüksek (8-14%) bölgelerde sınıflandırılır.

Yoon-Luttrell'in çarpışma ve birleşme modellerinin kombinasyonunu kullanıldığınde toplama verimliliğinin diğer genelleştirilmiş Sutherland denklemi ve modifiye Dobby–Finch modellerinde elde edilen değerlere göre kıyasla, daha yüksek tahmin edilmesine yol açmaktadir. Ayrıca bu çalışmada literatürde göreceli olarak önemli role sahip oldukları gösterilen $E_c$ ve k üzerindeki temel faktörlerin (tane boyutu, kabarcık çapı, kabarcık hızı, tane yoğunluğu ve türbülans) ilk kez tutarlı olmadığı gösterilmiştir.

Diğer önemli bulgulardan bazıları aşağıda yeralıyor:

Tane-kabarcık karşılaşma etkinliği ve türbülans dağılma oranının yokluğunda ve varlığında flotasyon kinetik oranının (k) optimizasyonu, DX7 yazılımı tarafından merkezi bir bileşik tasarım (CCD) kullanılarak ilk kez mineral işleme alanında rapor edilmiştir.

Ec ve k'deki faktörlerin (parçacık büyüklüğü, kabarcık çapı, kabarcık hızı, parçacık yoğunluğu ve türbülans) göreceli önemi literatürde ilk kez tutarsız olduğu gösterilmiştir. İncelenen koşullar altında elde edilen sonuçlara göre, partikül büyüklüğü ve kabarcık hızı, partikül-kabarcık karşılaşması ve flotasyon hızı sabiti üzerinde sırasıyla en etkili faktörlerdir.

İlk kez üç çarpışma modelinin (örn. Sutherhland, Schulze ve Dukhin) kesişimi, kabarcık yüzey özelliklerinin (kabarcık büyüklüğü, çapı ve hareketliliğinin bir fonksiyonu olarak kritik Stokes sayısını (Stcr-st) tahmin etmek için alternatif bir yöntem olarak önerilmektedir). Sunulan yaklaşımın sonuçları, Stokes tarafından verilen elde edilen verilerle oldukça ilişkilidir.

İlk defa, partikül ataletinin pozitif ve negatif etkilerini tanımlamak için tam eşikler rapor edilmiştir.

Flotasyon kinetik modellemesinde ana zorluklar ve fırsatlar aşağıda yeralıyor:

Araştırmacıların, köpüklü flotasyon işlemlerinin teorik, deneysel ve sayısal tekniklerle modellenmesi konusundaki çabalarına rağmen, aşağıdaki zorluklar daha ileri araştırmalar gerektirmektedir.

Flotasyon modellemesinin mikroskobik yönlerinin doğrulanması için lokal parçacık-kabarcık etkileşimlerini gözlemlemek için doğru görselleştirme teknikleri geliştirmek

Malzemelerin heterojenliği göz önüne alınarak, kabarcık arayüzlerinde minerallerin dinamik temas açısı ölçümlerinin yapılması

Köpük özelliklerinin modellenmesini parçacık yoğunluğuna odaklanan mevcut toplama bölgesi modelleri ile birleştirmek

Sayısal yöntemler içeren, örneğin; CFD-DEM ve deneysel ve analitik verilerle korelasyonları

Yoğun türbülanslı ortamda lokal parçacık ve kabarcık türbülanslı hızların uygulanması

# 1. INTRODUCTION- CONCEPTS, FUNDAMENTALS AND THEORIES

Flotation is a powerful separation technique with its extensive applications in different industries such as solid-solid separation, paper (Venditti, 2004) and plastic industries (Wang et al., 2015), petrochemical industry (Zheng and Zhao, 1933) electrolyte cleaning, remediation (Vanthuyne et al., 2003) and waste water treatment (Rubio et al., 2002). Flotation takes place in the presence of three different phases (*i.e.*, solid (particles), liquid (water) and gas (bubbles)). The properties of each phase play a vital role in the efficiency of the flotation process.

Flotation processes can be discussed from both microscopic and macroscopic aspects. It is a complicated separation technology which can be studied colloidal to micro scales using batch, pilot and industrial scales. The thermodynamic and kinetic concepts of each scale are different from the other. For example, the macroscopic properties include chemical and physicochemical features (surface tension, water composition and its quality, pH, reagent regime and its dosages), equipment factors (power input, cell hydrodynamics, reactor geometries, gas flowrate and turbulence) and operational properties (throughout, particle size, solids content, particle wettability, circuit design and ore's mineralogy).

On the other side, microscopic aspect of particle–bubble interactions is typically categorized into collision, attachment and detachment (stability) sub–processes. These terms are typically studied under static and a steady state conditions. A large number of studies have been devoted to observe and measure the macroscopic parameters because they are relatively simpler than microscopic characterizations. Nevertheless, over the last two decades, deep comprehension of the particle–bubble interaction mechanisms have been enhanced in the sense of identifying their significant roles in flotation processes. Additionally, elaboration of high technologies and modern devices such as Raman spectroscopy, automated mineralogical analyses, Atomic Force Microscopy (AFM), high–speed cameras oriented many researcher in this field to fundamentally understand the relevant phenomena (Zhang et al., 2001;

Assemi et al., 2008). Figure 1.1 demonstrates a commonly used RSC (reaction system cell) flotation machine representing both macro and microscopic views.

## 1.1 Microscopic Aspect Of Particle-Bubble Interaction

From microscopic point of view, particle-bubble interactions are broadly shown to be the key sub-process in the froth flotation processes. Due to difficulty in observation and measurement of fundamental phenomena taking place in microscopic level, capture efficiency ($E_{cap}$) also known as collection efficiency ($E_{coll}$) has been introduced. It is composed of the probability of three sub-steps (equation 1.1) (Hewitt et al., 1995).

$$E_{cap} = E_c . E_a . E_s \tag{1.1}$$

where $E_c$, $E_a$, and $E_s$ are particle-bubble encounter (collision), attachment and stability (detachment or aggregation) efficiencies, respectively.

A clear understanding of these microprocesses is basically essential in estimation of flotation kinetic rates (Dobby and Finch, 1987; Crawford and Ralston, 1988; Kouachi et al., 2015). Figure 1.1 demonstrates an intensively turbulent system in a typical flotation cell in the vicinity of an impeller.

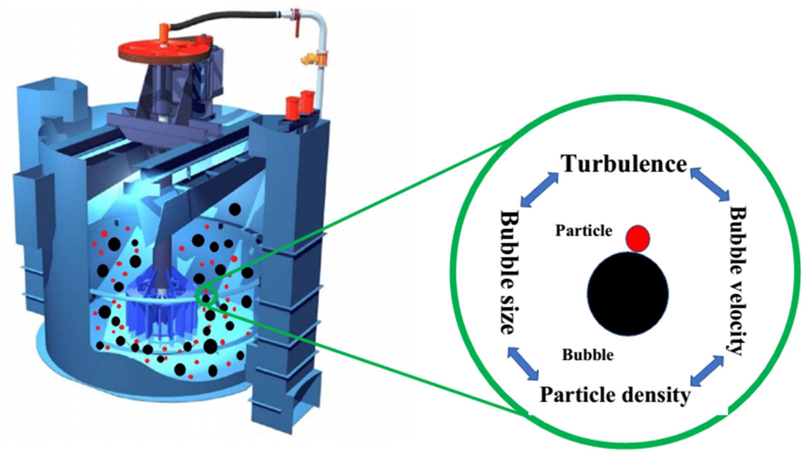


**Figure 1.1 :** Schematic representation of a reaction cell system (RCS) together with a microscopic view.

Particle-bubble encounter sub-process is the most vital and the initial step of interaction of a particle and a rising bubble. This phenomenon can be classified into elastic and non-elastic collisions based on the energy and momentum exchanges between particles and bubbles in an intensive turbulent vessel. Fluid hydrodynamic is mainly controled by these mechanisms. The encounter interaction of particle-bubble is predominantly controlled by the pulp flow, fluid dynamics, cell geometries and the relative motion of particles and bubbles in a turbulent cell. However, particle-bubble attachment and its stability are linked to the physicochemical characteristics of the medium and surface properties of particles and bubbles. Figure 1.2 exhibits the main regions of these sub-processes in a conventional mechanical flotation cell. As shown, particle-bubble encounter and attachment sub-processes are the principle interactions taking place in the pulp zone (collection zone). However, particle-bubble stability is the main interaction that occurs in the froth zone.

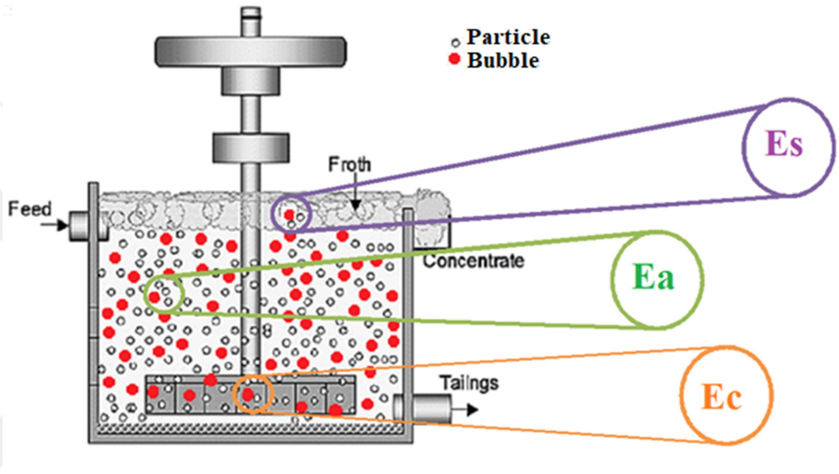


**Figure 1.2 :** Sub-processes of particle-bubble interactions along with their predominant regions.

## 1.2 Theory Of Particle–Bubble Encounter

Particle-bubble encounter so-called collision efficiency is defined as the ratio of the number of particles encountering a bubble per unit time to the number of particles approaching the bubble at a great distance in a flow tube with a cross–sectional area equal to the projection area of the bubble (Schulze 1989). With respect to Navier Stokes equation, a few effects (*i.e.* interceptional ($E_c^{ic}$), gravitational ($E_c^{g}$) and inertial ($E_c^{in}$) effects) may cause deviation of particle trajectories from the straight streamlines in the boarder of a bubble.

In addition to these effects, Brownian, shear–induced and diffusion forces might affect the system which will not be discussed in this chapter due to their insignificant roles on the studied range of particles and bubbles in the froth flotation media. It's worth mentioning that the particle–bubble encounter caused as a consequence of

Brownian diffusion is only important for sub–micron particle sizes surrounding randomly in the fluid. Similarly, the collision arising by shear–induced mechanisms is ordinarily disregarded in the froth flotation because it is solely significant for the collision of spheres of similar sizes (Miettinen et al., 2010).

### 1.2.1 Interceptional effect

According to the interceptional effect ($E_c^{ic}$), particles track streamlines without being deviated from their direction. As a consequence of this effect, coarser particles gain superior chance of being collided with bubbles in the medium. It only takes place if the particle trajectory falls in a streaming cylinder of radius so–called collision radius ($R_C$). Abrahamson (1975) described the $R_C$ as a summation of particle and bubble radii ($R_p$+$R_B$), however, Sutherland (1948) defined it as the radius where all particles have the tendency of colliding with the bubble (Dai et al., 2000).

### 1.2.2 Gravitational effect

The gravitational force ($E_c^g$) of particle may cause a trivial increase in the Ec. The contribution of $E_c^g$ can be simply represented by a dimensionless term ($v_s$) as the ratio of the particle weight less buoyancy to the fluid resistance which gives the scaled particle settling velocity (equation (1.2)) (Nguyen and Schulze, 2004).

$$v_s = V_s / U \tag{1.2}$$

where $V_s$ is the particle settling rate and $U$ is the bubble slip velocity.

### 1.2.3 Inertial effect

The inertial effect ($E_c^{in}$) initiating from the particle inertial power which can be recognized by the dimensionless Stokes number (*St*). Indeed, particle inertial forces are related to the particle masses; the $E_c^{in}$ effect is essentially the accountable factor for inducing the encounter probability of particle–bubble particularly for coarse and dense particles.

Figure 1.3 schematically exhibits the proportion of each effect on the $E_c$ in the bubble diameter of 0–2mm, particle density of 0–10g/cm$^3$ and particle size of 0–100µm. In addition to the particle inertial effect, water inertial effect as an opponent force for encountering particle-bubble is rarely argued in the literature. However, chapter four of the present work covers this discussion in detail.

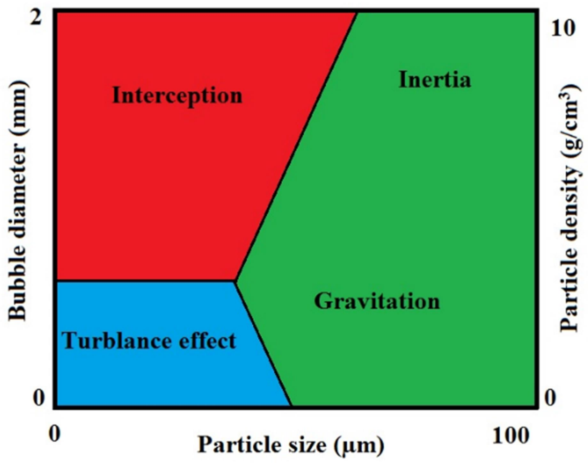


**Figure 1.3 :** Particle-bubble sub-processes versus bubble size, particle density and particle size.

### 1.2.4 Interaction of a single particle with a single bubble

The $E_c$ in a flotation system is schematically demonstrated in Figure 1.4. equation (1.3) represents the motion of a single particle on a rising single bubble in a quiescent condition.

$$(1+0.5\frac{\rho_p}{\rho_f})St\frac{d\vec{v}}{d\tau}-(1.5\frac{\rho_p}{\rho_f})St\frac{d\vec{w}}{d\tau}=\vec{w}-\vec{v}+\vec{v}_g \qquad (1.3)$$

where $\rho_f$ and $\rho_p$ are the liquid and particle densities, respectively. $\vec{w}$ and $\vec{v}$ indicate the dimensionless water and particle velocities around the bubble surface and $\tau$ is dimensionless time. These dimensionless velocities can be acquired by dividing the appropriate dimensional velocities to the velocity of bubble. Also, the dimensionless time is introduced as $\tau = tv_B/R_B$, where $t$ denotes time, $R_B$ indicates the bubble radius and $v_B$ is the bubble velocity. The gravitational force in terms of the particle motion can be calculated by equation 1.4.

$$v_g=\frac{(\rho_p-\rho_f)g2R_P^2}{9\mu v_B} \qquad (1.4)$$

where $v_B$ and $\mu$ are the bubble and liquid velocities, respectively and $v_g$ defines the Stokes velocity of the particle at terminal settling.

Particle Stokes number (*St*) is defined as the ratio of the characteristic time of a particle to a characteristic time of the flow. A particle with a low Stokes number (*St*<<1) follows fluid streamlines and inertial forces have practically no effect on the motion of the particle. However, a particle with a large Stokes number (*St*>>1) is dominated by its inertia and continues along its initial trajectory (equation 1.5).

$$St = \frac{2R_p^2 v_B \rho_p}{9\mu R_B} \tag{1.5}$$

where $v_B$ is the bubble velocity, $\rho_p$ is the particle specific gravity and $\mu$ is the dynamic fluid viscosity. Also, $R_B$ and $R_p$ are the bubble and particle radii, respectively.

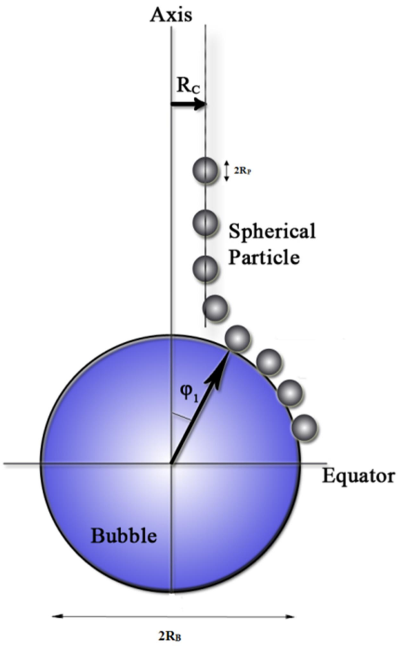


**Figure 1.4 :** Schematic view of interacting single particle with single bubble (Hassanzadeh et al., 2016).

### 1.2.5 Particle settling velocity

In flotation, particle-bubble interaction is affected by particle and bubble terminal velocities. The type of movement of single solid sphere in Newtonian and non-Newtonian liquids is well known; after a short acceleration time, it falls at its terminal settling velocity. For an unbounded liquid, terminal settling velocity can be calculated from the knowledge of the liquid and solid physical properties and from the drag coefficient (Rooki et al., 2012). Nguyen et al., (1994) showed that terminal velocity of a rigid spherical particle can be directly predicted on the basis of the physical properties of solid particle and fluid medium via Archimedes number. Some other models are driven from the correlation between particle Reynolds number and Archimedes number. An improved formula has been developed which provides a unified and useful approximation for terminal velocity of solid particles in the modelling of the flotation process (Nguyen et al., 1997). Various expressions have been described for determination of particle settling velocity. In this study, several models were taken into account in order to evaluate its effectiveness on particle-bubble collision efficiency for two different minerals (*i.e.* quartz and chalcopyrite). Nguyen et al., (1997) described the terminal velocity which is directly driven from the correlation between the Lyashchenko number (Ly) and the Archimedes number (Ar) (Equation 1.6).

$$V = \frac{V_S}{\sqrt[3]{1+\alpha(Ar)^{\beta}}} \tag{1.6}$$

where $V$ is the terminal velocity predicted by the Stokes law, and the parameters $\alpha$ and $\beta$ are given in Table 1.1. The Archimedes number contains parameters that characterize the properties of heterogeneous system and criterion establishing the type of settling. This number represents the ratio of buoyancy and inertial forces. The Lyashchenko number is the same as the dimensionless settling number.

Also, $V_S$ is the commonly known Stokes formula for terminal velocity (denoted by subscript St):

$$V_S = \frac{d_P g \Delta(\rho_P - \rho_f)}{18\mu} \tag{1.7}$$

where $d_P$ is particle size, g is gravity acceleration, $\rho_P$ and $\rho_f$ are particle and fluid densities and $\mu$ is the fluid viscosity. Particles that obey the terminal velocity described by equation 1.7 are sometimes called Stokesian particles (Nguyen et al., 1997).

**Table 1.1 :** The numerical values of constant $\alpha$ and $\beta$ in the related equation (Nguyen et al., 1997).

| **Archimed number** | $\boldsymbol{\alpha}$ | $\boldsymbol{\beta}$ |
|---|---|---|
| $\boldsymbol{Ar \leq 17845}$ | 0.0294 | 0.887 |
| $\boldsymbol{17845 \leq Ar \leq 512000}$ | 0.0014 | 1.198 |

The terminal velocity predicted by the Oseen law is expressed as following formula:

$$V = \frac{2V_S}{1+\sqrt{1+Ar/2}} \tag{1.8}$$

The terminal velocity obtained by Oseen law is mainly accurate for $Ar \leq 24$.

Also Equation 1.9 can be used for calculating particle settling velocity which is presented by Bruce, et al., (2003):

$$V = \frac{20.52}{d_P\rho_f}\left(\left[1 + 0.0921\left(\frac{d_P^3\,(\rho_P-\rho_f)\rho_f g}{0.75\mu_f^2}\right)^{0.5}\right]^{0.5} - 1\right)^2 \tag{1.9}$$

### 1.3 Particle-Bubble Encounter Determination

#### 1.3.1 Experimental techniques

The research studies in this context can be classified into three main approaches; i) analytical modeling approach, ii) numerical techniques and iii) experimental measurements. It is extremely hard to directly observe the interactions due to facing with an intensive turbulence medium. Also, there is a severe lack of technology to dynamically track particles encountering bubbles in a vessel while both moving with different velocities. Therefore, the primary solution for this difficulty is to isolate one sub-process from the rest. However, it is almost impossible to segregate particle–bubble encounter from other sub–processes in a real flotation system. Furthermore, the processes are exceedingly influenced by means of interrelated factors in the system. In this regard, practical works were mostly dedicated to determination of a single particle and single bubble rising in a laminar flow.

Also, experimental studies have conducted by measuring collection efficiency ($E_{coll}$) instead of particle–bubble encounter probability. Huang et al. (2011) recently reported that the error of obtaining $E_c$ value by back calculation of $E_{cap}$ was more than 50%. Lately, several researchers (Dai et al., 1998; Basarova et al., 2010; Ireland and Jameson 2014; Brabcova et al., 2015) measured Ec using practical approaches by taking advantage of virtual techniques (high–speed cameras). These works whether merely used glass beads and/or quartz particles or the trials carried out in the absence of energy dissipation rate (quiescent system). Since these practical studies were performed on quartz/silica particles, impacts of particle density and in turn the particle inertial effect were entirely overlooked. Furthermore, as the bubbles were fixed constantly at the bottom of cells, the liquid motion near the surface of the bubble was modified.

Besides that, as the experiments did not include the cell turbulence and the liquid flow, the probability of particle-bubble interactions were obtained merely on the basis of the settling velocity of particles. Another concern in conjunction with the experimental studies is cleaning methodology of glass beads (silica/quartz) surfaces. Most of the studies used acid and alkali treatments methods (Dai, 1998; Pyke et al., 2003; Hubicka et al., 2013; Guven et al., 2015; Vaziri Hassas et al., 2016). However, it is now evidently shown that the acid or alkaline treatment enhances the negative charge on the particle's surface. Positive disjoining pressure, which is formed because of the negative charge on the glass and bubble surface, leads to the formation of a stable film and this subsequently prohibits the particle–bubble attachment (Mukherjee, 2004).

### 1.3.2 Numerical methods

In addition to applying direct and indirect experimental methods for measuring the particle–bubble encounter interaction, some researchers utilized numerical techniques like discreet element method (DEM) and computational fluid dynamics (CFD) (Koh et al., 2000; Liu and Schwarz 2009; Firouzi et al., 2011; Wang et al., 2018). This method needs profound knowledge of fluid dynamics. It beneficiates both Euler-Euler (E-E) and Lagrangian-Euler (L-E) approaches. However, both cannot truly cover the physical conception that occurs in the complex flotation cell. For this reason, DEM is mainly taken as a useful means of simulating particulate systems for some complex industrial applications. A comprehensive insight regarding the restriction of each method is argued in detail by Wang et al., (2018). Nevertheless, the Newtonian particle methods used in the conventional DEM restricts their usefulness to particle–only systems. For this reason, researchers make use of combination of the fluid modeling strengths of CFD with the particle prowess of DEM, so-called (CCDM) or CFD+DEM.

#### 1.3.2.1 Concepts of microhydrodynamics

Microhydrodynamic (μHM) term was primarily introduced by Batchelor (1976). It deals with predicting macroscopic properties of suspensions from the microscopic behavior of individual and interacting particles in the suspending fluid. Suspension microstructure and particle motions are the main points of the µHM with regard to studying bounded/unbounded flows in the Stokes flows (Davis, 1993). The µHM effect also known as short–range hydrodynamic interaction (SRHI) (Happel and Brenner, 1963) originates from the water flow in the thin liquid film separating the particle with bubble. The µHM interaction at distances comparable to the particle radius grounds the particle trajectory to deviate from the liquid flow line.

While the particle approaches the bubble surface, the drag force deviates from the Stokes equation due to the µHM effect arising from the hydrodynamic resistance of the thin liquid film confined between a bubble and particle. The µHM impact on particle–bubble encounter interaction was surveyed by Dukhin (1983), who introduced the drag coefficient in conjunction with the Stokes drag on a solid sphere moving perpendicularly towards a mobile bubble surface; this was later modified by Dai et al., (1998). Nguyen et al. (2006) developed this hypothesis by putting perpendicular and parallel directions of particle motion into the particle–bubble encounter modeling. Moreover, Grammatika and Zimmerman (2001) expressed the issue of µHM mobility in the froth flotation as the linear relation between the moments of the surface traction on a rigid particle. Figure 1.5 schematically demonstrates the consequence of µHM forces for three minerals colliding to a mobile bubble. The effect of µHM on particle–bubble encounter is discussed in more detail in the chapter five.

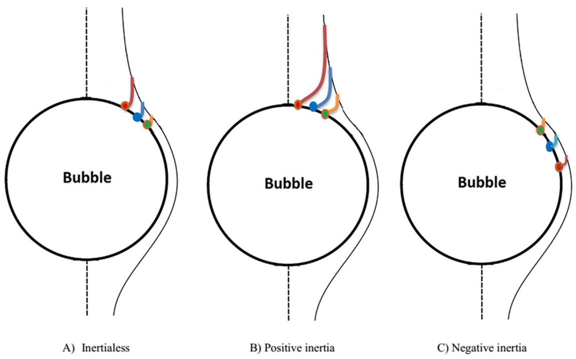


**Figure 1.5 :** schematic view of particle inertial statues duribg interaction with a mobile bubble ( Galena, chalcopyrite and quartz particles).

### 1.3.3 Analytical approaches

In this thesis, more than a dozen of analytical collision models are discussed and compared with each other under certain conditions. These models encompass many factors and assumptions for predicting the $E_c$. The key parameters can be named as particle size, shape and particle and fluid densities, pulp density, the fluid flow regime (potential, intermediate and Stokes flows), static and dynamic contact angle and its wettability, dispersion energy, power input and cell turbulence, bubble surface mobility, bubble diameter, its shape and velocity as well as particle trajectory.

Approximation of $E_c$ by making use of analytical collision models in the presence and absence of cell turbulence has been sufficiently discussed in the literature. Thus, this chapter only covers a brief overview of these models focusing on their downsides; more detailed information can be found elsewhere (Dai et al., 2000; Ralston et al., 2002). The Dukhin model so-called generalized Sutherland equation (GSE) is accepted as one of the accurate models in the sense of considering the particle trajectory and its inertial effect (Dai et al., 1998; Pyke et al., 2003; Miettinen, 2007) which is broadly used in various investigations (Newell and Grano, 2006; Jiang et al., 2010; Karimi et al., 2014; Popli, 2017). However, recent numerical reports demonstrate that the Dukhin's theory does not precisely forecast the particle–bubble encounter interaction for every particle size owing to its poor estimation of collision angle in terms of discounting the microhydrodynamic forces (Nguyen and Nguyen, 2009). This concept has been discussed in detail in chapter 4.

### 1.4 Particle-Bubble Encounter And Designing Concepts

The efficient design and optimization of flotation processes requires robust computational tools able to capture the physics of the process but at the same time versatile enough to allow extensive parametric studies. The first principles of the flotation process is not a viable task since it includes several size scales starting from those of the flotation device and ending to the scale of the thin film separating particle and bubble. At the heart of the modeling of flotation process is the bubble-particle collision function. The vast majority of the relevant literature work refers to non-turbulent flows but a few recent approaches have been also suggested for the derivation of this function for turbulent flows.

At first, all these approaches requires a critical review in order to select the most proper ones valid for the specific conditions of different interests. Then, the selected approaches can be adapted algebraically to be incorporated in a generalized framework for bubble-particle collision in a turbulent flow field. Such an effort might be based on scale decomposition as i) the turbulent flow field creates a relative velocity between particle and bubble ii) the existence of bubble creates a flow field around it iii) the existence of particle creates hydrodynamic interactions with the bubble (microhydrodynamics). The scales (i) and (ii) must be treated in a stochastic manner. In such a framework additional aspects, *e.g.* colloidal forces, can be directly incorporated.

The knowledge of the local collision frequency is not enough to proceed to CFD level simulations. Ignoring mesoscale spatial inhomogeneity, a mean field theory (in the form of population balances) to account for bubble/particle size, attachment time, bubble loading distributions can be developed in the sense of designing point of view. The direct transfer of such a model to 3-D CFD level is computationally intractable since multivariate unknown bubble size/loading distributions have to be dealt with. So, an hierarchy of such models for the zero dimensional case can be elaborated based on physical (*e.g.* variables lumping) and mathematical (*e.g.* method of moments) complexity reduction techniques.

## 1.5 Particle-Bubble Encounter Modeling

### 1.5.1 Sutherland model ($E_c^{SU}$)

Sutherland commenced the first endeavor to propose an encounter model. He simply assumed that particle and bubble size are the main parameters as represented in equation 1.10. Following this, coarser particles have a better chance of intercepting the bubble and the calculated collision rate was directly proportional to the particle size. The particle inertia was overlooked and it was assumed that particles follow the streamlines of the fluid flow (interceptional effect). Additionally, bubble surface was considered completely mobile (not contaminated), and the fluid flow at the bubble surface was potential flow regime.

$$E_c^{SU} = \frac{3d_p}{d_B} \tag{1.10}$$

where $d_p$ and $d_B$ are particle and bubble diameters and $E_c^{SU}$ is indicting Sutherland encounter model.

Afterwards, it was found that $E_c^{SU}$ overestimates the Ec and which was improved by Dukhin through incorporating the particle inertial effects which have a strong influence on $E_c$ of coarse and dense particles. Also it was shown that the $E_c^{SU}$ is invalid at supercritical Stokes numbers because of the influence of particle and water inertial forces. Moreover, because of neglecting the particle inertial effect, the model implies that collision can occur uniformly on the entire upper half of the bubble surface, however, it is recently accepted that the maximum collision angle can be lower than 90º.

### 1.5.2 General Sutherland equation (Dukhin model, $E_c^{GSE}$)

The Sutherland collision model was improved by Dukhin incorporating the positive and negative inertial effects on the basis of the inertial hydrodynamic interaction between solid particles and mobile bubbles. Also, it initially included the particle trajectory on the surface of the bubble. In this regard, the analytical equation (equation 1.11) termed the generalized Sutherland equation (GSE) was introduced by Dai et al., (1998).

According to the assumptions, the particle-bubble encounter efficiency of Dukhin/GSE model ($E_c^{GSE}$) is proposed as in equation 1.11.

$$E_c^{GSE} = E_c^{SU}\, sin^2\theta_t \times exp\left(3K_3\, cos\,\theta_t\left(ln\frac{3}{E_c^{SU}} - 1.8\right) - \frac{9K_3(\frac{2}{3}+\frac{cos^3\theta_t}{3}-cos\,\theta_t)}{2E_c^{SU}\, sin^2\theta_t}\right) \quad (1.11)$$

where $E_c^{SU}$ is Sutherland collision model (equation 1.10), $\theta_t$ (◦) indicates the maximum collision angle (equation 1.12) (angle of tangency) which is defined as the angle above which no encounter was possible and $K_3$ is a dimensionless number given by equation 1.13.

$$\theta_t = arcsin\left(2\beta\left(\sqrt{1+\beta^2}-\beta\right)\right)^{1/2} \quad (1.12)$$

$$K_3 = St\,\frac{(\rho_p-\rho_f)}{\rho_p} = \frac{4v_b(\rho_p-\rho_f)}{9\eta d_b} \quad (1.13)$$

where the St shows the particle Stokes number as $St = \frac{\rho_p v_b d_p^2}{9\,\eta\, d_b}$ and $\eta$ represents the viscosity of liquid. Dimensionless number $\beta$ is calculated by equation 1.14.

$$\beta = \frac{2\,f\,E_c^{SU}}{9\,St} \quad (1.14)$$

where *f* is a constant value equal to 2.034 (Duhkin and Rulyov, 1997).

### 1.5.3 Schulze collision model ($E_c^{SC}$)

Schulze introduced the $E_c$ as the ratio of the number of particles colliding a bubble per unit time to the number of particles approaching the bubble at a great distance in a flow tube with a cross-sectional area equal to the projection area of the bubble (Dai et al., 2000). Schulze model ($E_c^{SC}$) is shown as: $E_c^{SC} = (\frac{R_C}{R_B})^2$.

where $R_C$ representing the collision radius which is dependent on the relationship among $R_B$ and $R_p$.

$E_c^{SC}$ includes three main effects of gravitational, interceptional, and inertial on particle-bubble encounter phenomenon which is obtained from the summation of these three individual effects (equation 1.15):

$$E_c^{SC} = E^{ic} + E^{g} + [(1 - \frac{E^{ic}}{\left(1+\frac{d_p}{d_B}\right)^2}) \times E^{in}] \quad (1.15)$$

where $E^{in}$ is the inertial, $E^{ic}$ is the interceptional and $E^{g}$, the gravitational effects, respectively. $d_p$ and $d_B$ are the same as described in the previous equations.

Particle interception effect ($E^{ic}$) was defined as the reason that particles follow the stream lines in the vicinity of a bubble without any deviation (equation 1.16):

$$E_{c-SC}^{ic} = \frac{2\varphi_c}{(1+\frac{v_p}{v_B}) \times v_B \times Re_B^2} \quad (1.16)$$

where $\varphi_c$ term is the streamline stream function that coincides with the grazing trajectory and $R_{eb}$ is the bubble Reynolds number $Re_b = \frac{v_b \rho_f d_b}{\eta}$ which is defined as described as the inertial forces to the viscous forces of the fluid. In fact, $E^{ic}$ is determined only by the fluid flow regime around the bubble.

In case of the gravitational effect ($E^{g}$), the following equation (equation 1.17) was proposed as:

$$E_{C-SC}^{g} = Sin^2\varphi_c(1 + \frac{d_p}{d_B})^2 \times \frac{v_p}{v_B} \quad (1.17)$$

With regard to the inertial effect, $E_c^{SC}$ was proposed as an approximate equation by consideration of bubble and particle sizes and velocities together with Stokes number and two coefficients (equation 1.18).

$$E_{C-SC}^{in} = \left(\frac{St}{St+a}\right)^b \times \left(\frac{1}{1+\frac{v_p}{v_B}}\right)\left(1 + \left(\frac{d_p}{d_B}\right)\right)^2 \quad (1.18)$$

where *St* denotes the Stokes number and a and b indicate constant numbers which can be simply opted based on $R_{eb}$ given elsewhere (Hassanzadeh et al., 2016).

### 1.5.4 Weber and Paddock collision model ($E_c^{WP}$)

Weber and Paddock collision model ($E_C^{WP}$) presumes that the particles are very fine and the hydrodynamic interaction among the particles and the fluid is negligible. Additionally, $E_C^{WP}$ assumes Stokes flow for the streamlines of the fluid which is approximated via a Taylor series. Weber and Paddock proposed the model as the ratio of the number of particles encountering with the bubble per unit time to the number of particles swept across the projected area of the bubble per unit time. $E_c^{WP}$ is encompassed from two key constituents *i.e.* interceptional ($E_{c-WP}^{ic}$) and gravitational ($E_{c-W}^{g}$ ) forces. The gravitation effect is calculated using the equation 1.19.

$$E_{c-WP}^{g} = sin^2\varphi_c(1 + \frac{d_p}{d_B})^2 \times \frac{v_p}{v_B} \quad (1.19)$$

where the all terms are described before.

Since the fluid velocity is obtained through the stream functions, the equation for calculation of the interceptional component ($E_{c-WP}^{ic}$) highly depends on the applied stream functions. The $E_{c-WP}^{ic}$ for an immobile bubble (completely retarded bubble surface) is represented by:

$$E_{c-WP}^{ic} = \left[1 + \frac{2}{1+\left({}^{37}/_{R_{eb}}\right)^{0.85}}\right]\frac{d_P}{d_B} \quad (1.20)$$

For a mobile bubble (completely unretarded bubble surface), $E_{c-WP}^{ic}$ can be shown by the given formula (equation 1.21).

$$E_{C-WP}^{ic} = 1.5\left[1 + \frac{(3/16)R_{eb}}{1+0.249R_{eb}^{0.56}}\right]\left(\frac{d_P}{d_B}\right)^2 \quad (1.21)$$

Finally, the $E_c^{WP}$ is determined by the summation of the $E_{c-WP}^{ic}$ and $E_{c-WP}^{g}$.

To achieve an accurate interpretation of the $E_c$ values for each model, their assumptions have to be taken into account. Table 1.2 presents the basic suppositions for each collision model.

**Table 1.2 :** Principal features of predictes particle-bubble encounter probability for each model.

| Model | Webber–Padack | Schulz | Sutherland | Dukhin |
|---|---|---|---|---|
| **Bubble's mobility** | Mobile and immobile | Mobile | Mobile | Mobile |
| **Fluid flow type** | Intermediate | Potential | Potential | Potential |
| **Inertial condition** | Inertialless | Positive Inertial | Inertialless | Negative inertial |

### 1.6 Attachment Efficiency ($E_a$)

The attachment sub-process plays a key role on aggregation of particle-bubble and its floating transition to the froth zone. It is controlled by particle and bubble surface properties specially the particle wettability characteristics. After a successful collision, particle slides over the thin liquid film, which forms between the bubble and particle when they come infinitesimally close to each other. Later, this film gets thinner and finally reaches the critical thickness, which leads to the rupture of the film and then the three-phase contact (TPC) line occurs and starts to expand over the surface of particle to reach an equilibrium of contact angle on the particle surface (Nguyen et al., 1997; Nguyen et al., 1998).

The motion of a particle as it slides over the surface of the liquid film has been investigated intensively and constitutes the most complex phenomenon in the modeling. Most of the attachment efficiency models are based on this principle that if the sliding time is equal to or longer than the induction time, the particle will attach to the bubble surface (Nguyen et al., 1998; Dobby and Finch, 1986; Luttrell and Yoon, 1992).

Since in this study only two attachment models have been discussed (*i.e.* Dobby–Finch ($E_a^{DF}$) and Yoon-Luttrell attachment models ($E_a^{YL}$)), other particle-bubble attchment models can be found elsewhere (Dai, 1998; Pyke, 2003).

### 1.6.1 Attachment modeling

#### 1.6.1.1 Dobby–Finch attachment model ($E_a^{DF}$)

The Dobby–Finch attachment model is defined as the ratio of the area on the bubble surface, which corresponds to the angle of adhesion to the area, which corresponding to angle of tangency. In other words, this efficiency is the ratio of the area on top of the bubble, where the bubble actually presents and slides after collision, to the area, through which the particle has a chance of successful attachment before falling away from the bubble surface. The basic mathematical equation of this model is expressed as $E_a = \frac{sin^2\,\theta_a}{sin^2\,\theta_t}$ (Dobby and Finch, 1986).

where $\theta_a$ (◦) the adhesion angle, was the specific collision angle its sliding time being equal to the induction time. The $\theta_a$ was the collision angle where sliding time equaled its induction time ($t_{ind}$):

$$\theta_a = 2arctan\,exp\left[-t_{ind}\frac{2(v_P+v_B)+(v_B)\left(\frac{d_B}{d_p+d_B}\right)^3}{d_p+d_B}\right] \tag{1.22}$$

The induction time was calculated using equation 1.23.

$$t_{ind} = Ad_p^B \tag{1.23}$$

where B is constant and independent of the particle size (~0.6±0.1) (Duan et al., 2003) and A is inversely proportional to the particle contact angle (Dai et al., 1999).

#### 1.6.1.2 Yoon-Luttrell attachment model ($E_a^{YL}$)

Yoon-Luttrell presumed that the value of the adhesion angle is determined by the magnitude of the tangential velocity of the particle as it slides over the bubble surface. In fact, expression of the sliding time ($t_{sl}$) was substituted directly by the induction time $t_i$. Therefore, they derived an equation for the $t_{sl}$ under intermediate flow condition as follow (Yoon, et al., 1989; Nguyen, 1993):

$$t_{sl} = \frac{d_B+d_P}{v_B\frac{d_P(45+8Re^{0.72})}{30\ \ B}}ln\left\{cot\frac{\theta}{2}\right\} \tag{1.24}$$

It is assumed that sliding time is just equal to the induction, the calculated angle in the equation 1.22 is then equal to the adhesion angle. Hence, $\theta_a$ for intermediate flow regime is determined by the equation:

$$\theta_a^{(i)} = 2 \arctan exp\left[\frac{-d_P v_B t_{ind}\, R_P\left(45+8Re^{0.72}\right)}{15 d_B (d_P+d_B)}\right] \qquad (1.25)$$

For the Stokes flow conditions, the angle can be expressed by flowing formula.

$$\theta_a^{(s)} = 2 \arctan exp\left[\frac{-3 d_P v_B t_{ind}}{d_B (d_P+d_B)}\right] \qquad (1.26)$$

For the potential flow conditions the given angle is coming below.

$$\theta_a^{(p)} = 2 \arctan exp\left[\frac{-3 d_P v_B t_{ind}}{(d_P+d_B)}\right] \qquad (1.27)$$

where $v_B$ is the bubble rising velocity, $d_P$ and $d_B$ are the particle and bubble diameters, respectively.

### 1.7 Modified Schulze Stability Model ($E_s^{SC}$)

Modified Schulze (1992) stability model is typically chosen for determining detachment efficiency of particle–bubble as below:

$$E_s = 1 - \exp\left(A_s\left(1 - \frac{F_{att}}{F_{det}}\right)\right) = 1 - \exp\left(A_s\left(1 - \frac{1}{B_O^*}\right)\right) \qquad (1.28)$$

where As is a constant value, 0.5 (Bloom and Heindel, 2002; Govender et al., 2013). The ratio of the detachment force ($F_{det}$) to the attachment force ($F_{att}$) is a dimensionless term indicated as Bond number ($B_O^*$) by equation 1.29 (Pyke et al., 2003; Koh and Schwarz, 2007).

$$B_O^* = \frac{d_p^2\left[(\rho_p-\rho_f)g+1.9\rho_p\varepsilon^{\frac{2}{3}}\left(\frac{d_p}{2}+\frac{d_B}{2}\right)^{-\frac{1}{3}}\right]+1.5d_p\left(\frac{4\sigma}{d_B}-d_B p_f g\right)sin^2\left(\pi-\frac{\theta}{2}\right)}{6\sigma \sin\left(\pi-\frac{\theta}{2}\right)\sin\left(\pi+\frac{\theta}{2}\right)} \qquad (1.29)$$

where $\theta$ (◦) is the contact angle, $\sigma$ (N/m) surface tension, g (m/s$^2$) gravitational constant and $\varepsilon$ (W/kg) is energy input.

The power value of each parameter in equation 1.29 is experimentally examined by Safari and Deglon (2018) with the aim of proposing a new attachment–detachment flotation kinetic model. More detailed information in this regard can be found elsewhere (Newell, 2006).

## 2. COMPREHENSIVE LITERATURE REVIEW

This chapter initially scans the available studies implemented on microscopic principles of particle-bubble encounter interaction in the literature. Three main approaches including analytical, numerical and experimental are presented. In addition to providing a comprehensive and critical review, the effects of some key hydrodynamic parameters *i.e.*, particle density, bubble surface mobility, bubble size and its velocity, turbulent dissipation energy and fluid flow type are discussed. A detailed overview can be found elsewhere (Hassanzadeh et al., 2018).

### 2.1 Analytical Approaches

Over the last two decades, a lot of research studies focused on determination of particle–bubble encounter efficiency using analytical modeling. The main idea was solving the Navier Stokes equation by some specific assumptions concerning the fluid flow, particle and bubble characteristics. Nevertheless, these models are relatively simplified to decrease the natural complexity of the flotation process which involves three phases and their inactions.

Langmuir and Blodgett encounter model ($E_c^{LB}$) is most likely the initial collision model considering the inertial hydrodynamic interaction among a small stationary droplet and a large falling droplet (Langmuir and Blodgett, 1945). However, it is now evidently known that the $E_c^{LB}$ is only valid for particles holding a great St. Since interaction of fine and ultrafine particles with bubbles occurs due to the interceptional effect, the $E_c^{LB}$ does not provide adequate correctness for these particle sizes. A few years later, Sutherland (1948) followed almost the same trend assuming that the particle inertia could be neglected, and therefore particles followed the streamlines of the fluid. It was revealed that coarse particles had a superior chance to interact with the retarded bubbles and the calculated $E_c$ was directly proportional to the $d_p$.

Later in 1957, Gaudin presented a collision model ($E_c^{GA}$) by supposing inertialess particle effect and Stokes fluid flow regime for particles in the vicinity of bubbles. It was later reported that the $E_c^{GA}$ was the model completely underestimated the $E_c$ in compared with the rest of analytical models. The collision model of Flint and Howarth (1971), $E_c^{FH}$ underestimated the actual $E_c$ as if $E_c^{GA}$ (Dai, 1998). Woodburn et al. (1971) introduced the probability of interception of a particle by a bubble as an exponential function of the particle size, bubble size, and particle–bubble relative velocity. Reay and Ratcliff (1973) used the $E_c^{FH}$ by simple modification and proposed a new formula ($E_c^{RR}$) for both collision and diffusion regimes, by counting both gravitational and interceptional forces. The experimental results obtained from a micro-flotation Hallimond tube showed poor correlations for latex in connection with the influence of electrical or surface forces.

Afterwards, Anfruns and Kitchener (1977) ($E_c^{AK}$) used the $E_c^{RR}$ and $E_c^{FH}$ and estimated the $E_c$ values under Stokes fluid flow via combining electrostatic, interceptional and gravitational effects disregarding fluid drag forces and the particle inertial forces. Later, the $E_c^{AK}$ was found only applicable for inertialess and Stokes flow conditions with regards to using stream functions given by Jenson (1959) and Hamielec et al., (1963). Weber and Paddock (1983) encounter model ($E_c^{WP}$) presumes that particles are fairly fine by discounting the hydrodynamic interaction between particles and the fluid Later, Dukhin (1982) extended Sutherland encounter model ($E_c^{SU}$) and named generalized Sutherland equation (GSE), as described by Dai et al. (1998). The generalized Sutherland model ($E_c^{GSE}$) is established on the basis of the $S_c^{SU}$ incorporating particle trajectory on the bubble's surface and inertial forces. It is amplified at the un-retarded bubble surface with a non–zero tangential velocity component of the liquid phase. Also, it includes the influence of both positive and negative inertial forces in terms of the inertial hydrodynamic interaction between solid particles and fresh bubbles (Pyke, 2003). The Schulze collision efficiency, $E_c^{SC}$, takes into account three different effects (*i.e.* interceptional, gravitational and inertial) on the $E_c$. However, it exclude the micro-hydrodynamic forces together with water inertial effects. At the end of 1980s, Yoon and Luttrell (1989) encounter model ($E_c^{YL}$) utilized the basis of Sutherland's assumptions considering three fluid flow regimes including Stokes, potential and intermediate regimes. The model assumed that the particle–bubble encounter probability could take place uniformly on the entire upper half of the bubble surface. However, it was recently accepted that the maximum collision angle could be lower than 90º (Firouzi et al., 2011).

Lately, this model was widely used in the numerical investigtions. Dobby and Finch ($E_c^{DF}$) established their model based on the $E_c^{SU}$ (Dobby and Finch, 1987). The $E_c^{DF}$ model considered Re in the range of 20–300 and the intermediate fluid flow with respect to the calculated trajectory results versus Stokes's numbers (0.1 to 1). In 1999, Heindel and Bloom proposed a model ($E_c^{HB}$) using intermediate flow of $E_c^{YL}$. This model assumed that particles and bubbles are spherical and particle radius is less than bubble radius ($R_p$<$R_B$) to lift the restriction of $R_p$<<$R_B$. One of the most recent model is the collision model defined by Nguyen and Schulze (2004) ($E_c^{NS}$). It is the most developed version of both $E_c^{SC}$ and $E_c^{NK}$, which contains cell turbulence effect and all particle inertial forces.

Figure 2.1 displays the particle-bubble encounter models discussed above. It shows the $E_c$s versus particle size in a semi–logarithmic scale. More specifically, detailed description of the model is presented in the sense of fluid flow regime and particle and bubble properties in Hassanzadeh et al., (2018). It also introduces the key restrictions involved with each model.

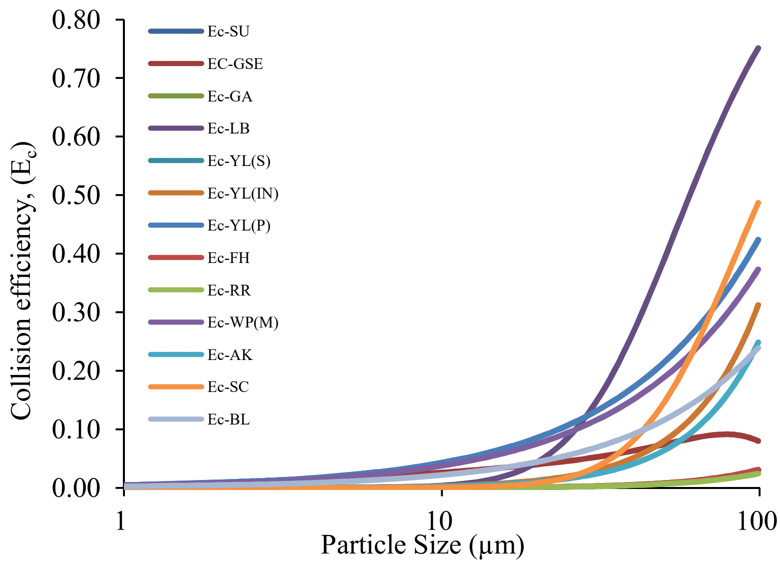


**Figure 2.1 :** Particle-bubble collision probability obtained by common collision models ($\rho_p = 2650\,\frac{kg}{m^3}, d_B = 0.08cm, v_B = 0.316\,\frac{m}{s}$ and $\rho_f = 1000\,\frac{kg}{m^3}$).

Table 2.1 describes in detail the formulas used for calculation of $E_c$ obtained using each model. Description of general assumptions in terms of each model can be found elsewhere (Hassanzadeh et al., 2018).

**Table 2.1 :** List of models in terms of calculating collision efficiency.

| Collision model | Equation |
|---|---|
| **Sutherland** | $E_c^{SU} = \frac{3d_p}{d_B}$ |
| **Gaudin** | $E_c^{GA} = \frac{3}{2}(\frac{d_P}{d_B})^2$ |
| **Flint & Howarth** | $E_c^{FH} = \frac{v_p / v_B}{1 + \frac{v_p}{v_B}}$ |
| **Reay & Ratcliff** | $E_c^{RR} = (\frac{d_p}{d_B})^n$ <br> $1.9 < n < 2.05$ |
| **Langmuir & Blodgett** | $E_c^{LB} = (\frac{St}{St + 0.2})^2$ <br> $St = \frac{\rho_p v_B d_p^2}{9\eta d_B}$ |
| **Anfruns & Kitchener** | $E_c^{AK} = \frac{(1 + d_p / d_B)^2}{1 + v_p / v_B} \times \left[\frac{v_p}{v_B} + \frac{2\varphi_c^0}{(1 + d_p / d_B)^2}\right]$ |
| **Yoon & Luttrell** | Stokes flow; $E_c^{YL} = \frac{3}{2}(\frac{d_p}{d_B})^2$ <br> Intermediate flow; $E_c^{YL} = \frac{d_p}{d_B}(\frac{3}{2} + \frac{4\,\mathrm{Re}_B^{0.72}}{15})$ <br> Potentiel flow; $E_c^{YL} = 3(\frac{d_p}{d_B})$ |
| **Dukhin or GSE** | $E_c^{GSE} = \exp\left[(3K_3(\ln\frac{3}{E_c^{SU}} - 1.8) - \frac{4(\frac{2}{3} + \frac{\cos^3\varphi t}{3} - \cos\varphi t)}{\sin^4\varphi t}) \times \cos\varphi t\right] \times \sin^2\varphi t \times E_c^{SU}$ <br> $\varphi_t = \arcsin(2\beta(\sqrt{1+\beta^2} - \beta))^{1/2}$ <br> $\beta = \frac{2fE_c^{SU}}{9K_3}$ <br> $K_3 = K\frac{\rho_\rho - \rho_f}{\rho_p}$ <br> $St = \frac{\rho_\rho v_B d_\rho^2}{9\eta d_B}$ |

**Table 2.1 (continued):** List of models in terms of calculating collision efficiency.

| | |
|---|---|
| **Weber & Paddock** | **For retarded bubble;**<br>$E_c^{WP} = \left[1+\frac{2}{1+(\frac{37}{\mathrm{Re}_B})^{0.85}}\right]\frac{d_p}{d_B} + \sin^2\varphi_t(1+\frac{d_p}{d_B})^2 \times \frac{v_p}{v_B}$<br>$\mathrm{Re}_B = \frac{d_B V_B \rho_w}{\mu_w}$<br>**For unretarded bubble;**<br>$E_c^{WP} = 1.5\left[1+\frac{\frac{3}{16}\mathrm{Re}_B}{1+0.249\,\mathrm{Re}_B^{0.56}}\right](\frac{d_p}{d_B})^2 + \sin^2\varphi_t(1+\frac{d_p}{d_B})^2 \times \frac{v_p}{v_B}$ |
| **Schulze** | $E_c^{SC} = \frac{2\varphi_c}{(1+\frac{v_p}{v_B})v_B\,\mathrm{Re}_B^2} + \sin^2\varphi_c(1+\frac{d_p}{d_B})^2(\frac{v_p}{v_B}) + [(1-\frac{\frac{2\varphi_c}{(1+\frac{v_p}{v_B})v_B\,\mathrm{Re}_B^2}}{(1+\frac{d_p}{d_B})^2}) \times ((\frac{St}{St+a})^b(\frac{1}{1+\frac{v_p}{v_B}})(1+(\frac{d_p}{d_B}))^2)]$ |
| **Nguyen & Kmet** | $E_c^{NV} = \frac{2D}{9Y(1+v_p/v_B)}(\frac{d_p}{d_B})^2\{(X+C)^2+3Y^2)^{1/2}+2(X+C)\}^2$<br>$X = \frac{3}{2}+\frac{9\,\mathrm{Re}_B}{32+9.888\,\mathrm{Re}_B^{0.694}}$<br>$Y = \frac{3\,\mathrm{Re}_B}{8+1.736\,\mathrm{Re}_B^{0.518}}$<br>$C = \frac{v_p}{v_B}(\frac{d_B}{d_p})^2$<br>$D = \frac{\sqrt{(X+C)^2+3Y^2}-(X+C)}{3Y}$ |
| **Dobby & Finch** | Low particle inertia (St<0.1);<br>$E_c^{DF} = \frac{(1+d_p/d_B)^2}{1+v_p/v_B}(1+\frac{d_p}{d_B})^2\sin^2\varphi + \left[1+\frac{2}{1+(\frac{37}{\mathrm{Re}_B})^{0.85}}\right]\frac{d_p}{d_B}$<br>If $400 < \mathrm{Re} < 20$; $\varphi_C = 78.1 - 7.37\log\mathrm{Re}$<br>If $1 < \mathrm{Re} < 20$; $\varphi_C = 85.5 - 12.49\log\mathrm{Re}$<br>If $0.1 < \mathrm{Re} < 1.0$; $\varphi_C = 85.0 - 2.5\log\mathrm{Re}$<br>Intermediate particle inertia (St>0.1);<br>$E_c^{DF} = \{\frac{(1+d_p/d_B)^2}{1+v_p/v_B}(1+\frac{d_p}{d_B})^2\sin^2\varphi + \left[1+\frac{2}{1+(\frac{37}{\mathrm{Re}_B})^{0.85}}\right]\frac{d_p}{d_B}\} \times [1.627\,\mathrm{Re}^{0.06}\,St^{0.54}(\frac{v_p/v_B}{U})^{0.16}$ |
| **Nguyen & Schulze** | $E_c^{NS} = 1-(1-\frac{v_s}{v_s+U})(1-f(R)\frac{v_s}{v_s+U}[X+Y\cos\varphi_{c,i}]\sin^2\varphi_{c,i})(1-\frac{(St)^a-b}{(St)^a+C})(1-18\sqrt{\frac{3}{15}\frac{\rho_f}{\rho_p-\rho_f}\frac{\lambda_k}{R_p+R_B}})$<br>$\varphi_{c,i} = a\cos[\frac{\sqrt{X^2+3Y^2}-X}{3Y}]$<br>$R = \frac{R_p}{R_B}$<br>For mobile bubble surface; $f(R) = R - R^2$<br>For immobile bubble surface; $f(R) = R$ |

As noted previously, the analytical models presented for estimation of the $E_c$ in quiescent systems disregard the energy dissipation rate and microhydrodynamic's effect (μMH) (Firouzi *et al*., 2011). The former one diminishes $E_c$, whereas the turbulence effect increases the $E_c$. By incorporation of their effects on the bubble–particle encounter process, its modeling gets more complex and thus requires numerical methods to resolve. Historical perspectives of numerical methods used for estimation of the $E_c$ together with its basic and fundamental concepts are noted below.

## 2.2 Numerical Techniques

This section scans the literately published manuscripts concerning the application of computational fluid dynamics (CFD) modelling on particle-bubble interaction in a flotation system.

Nguyen and Kme (1992) proposed the first numerical method to estimate the $E_c$ in a single interaction of particle-bubble while the fluid flow varies at intermediate *Re*. It considers the effect of particle and bubble densities on the $E_c$. The results of the model were compared analytically with mentioned collision angles obtained by Weber (1981) and their own experimental data. It was reported that there is a considerable disagreement between Weber's models and experimentally obtained data for dense particles holding large Reb. The reason is that particle densities were discounted in the Weber model unlike the numerical model proposed by Nguyen Van and Kme (1992). Indeed, these outcomes emphasized the significant role of particle specific gravity on estimation of $E_c$ and k.

Nguyen (1994) developed the previous model for pridiction of $E_c$ by introducing a novel term for the liquid radial velocity which igoned the particle and water inertial forces. Also they derived by presuming a retarded (immobile) bubble surface regarding the bubble's contamination. However, experimental results did not support the bubble surface retardation (Sam et al., 1996). As a second elaboration, the equations were solved numerically focusing on inertial effect and the bubble surface mobility (Nguyen et al. (2006). As recently reported in detail (Hassanzadeh et al., 2018), the particle movement on the bubble surface in the rotational spherical coordinate system can be described by equation 2.1 and equation 2.2.

$$K'\frac{\mathrm{d}v_r}{\mathrm{d}\tau}=K'\frac{v_\varphi^2}{r}+K''\left(w_r\frac{\partial w_r}{\partial r}+\frac{w_\varphi}{r}\frac{\partial w_r}{\partial\varphi}-\frac{w_\varphi^2}{r}\right)-v_r+w_r \tag{2.1}$$

$$K'\frac{\mathrm{d}v_\varphi}{\mathrm{d}\tau}=-K'\frac{v_\varphi v_r}{r}+K''\left(w_r\frac{\partial w_\varphi}{\partial r}+\frac{w_\varphi}{r}\frac{\partial w_\varphi}{\partial\varphi}-\frac{w_\varphi w_r}{r}\right)-v_\varphi+w_\varphi \tag{2.2}$$

where, vφ and vr represent the tangential and radial proportions of the particle velocity. Also, $w_\varphi$ and $w_r$ indicate respectively the tangential and radials contributions of the liquid velocity. St is the particle Stokes number which was defined in detail in section one.

They elaborated equation 2.1 and equation 2.2 to incorporate the $E_c^g$ (Nguyen and Nguyen, 2009).

Additionally, the microhydrodynamic resistance effects for interaction of particles and (mobile/immobile) bubbles in two and three-phases were introduced and developed in numerical studies by Brenner, 1961, Nguyen and Evans 2002 and Firouzi et al., 2011.For instance, Firouzi et al. (2011) used Eqs 2.3 and equation 2.3 and solved them numerically for both retarded and un-retarded bubbles.

$$K'\frac{\mathrm{d}v_r}{\mathrm{d}\tau}=K'\frac{v_\varphi^2}{r}+K''\left(w_r\frac{\partial w_r}{\partial r}+\frac{w_\varphi}{r}\frac{\partial w_r}{\partial\varphi}-\frac{w_\varphi^2}{r}\right)-f_1v_r+f_2w_r-v_g\cos\varphi \tag{2.3}$$

$$K'\frac{\mathrm{d}v_\varphi}{\mathrm{d}\tau}=-K'\frac{v_\varphi v_r}{r}+K''\left(w_r\frac{\partial w_\varphi}{\partial r}+\frac{w_\varphi}{r}\frac{\partial w_\varphi}{\partial\varphi}-\frac{w_\varphi w_r}{r}\right)-f_3v_\varphi+f_4w_\varphi+v_g\sin\varphi \tag{2.4}$$

The results obtained by numerical methods for estimation of the Ec reasonably supported the existing analytical outcomes solely for ultrafine particle range where the inertial force is negligible. Apart from the fine particles, coarse particles deviate from fluid streamlines in the vicinity of bubbles in the light of their inertial impacts. This phenomenon is the matter of discussion in chapter four where the intersection point of Dukhin and Schulze encounter models manifests the particle and water inertial forces.

The main difficulty of the numerical methods is that they consider two phases into account viz. whether liquid-gas or liquid-solid. However, in flotation processes all three phases are involved and interact differently in mainly three zones (collection (pulp), quiescence and froth). For this reason, nowadays combination of DEM+CFD appears to be very useful for principal understating and modeling of flotation processes. For instance, Table 2.2 summarizes the list of studies worked on CFD modeling of column flotation in last decades. As seen, none of the studies used the numerical and population balance approaches for modeling both zones.

A comprehensive investigation on the application numerical methods to particle-bubble interactions was recently reviewed by Hassanzadeh et al., (2018) through summarizing the studies of Koh et al., 2000 and 2003; Nguyen et al., 2016; Liu and Schwarz 2009 a,b; Koh and Schwarz 2006; Maxwell et al., 2012). Most recently, Wang et al., (2018) presented a solid literature review on CFD modeling in connection with the processes in three mostly used flotation cells *i.e.* conventional mechanical flotation (CMF) cell, flotation column and dissolved air flotation device. The concluded results at the end were in absolute agreement with the presented insights by Hassanzadeh et al., (2018) with respect to applying both CFD and DEM for analyzing the interactions between three phases.

### 2.3 Experimental Methods

Observation of the particle-bubble interactions in an intensive turbulent cell is still one of the main challenges that flotation processes are facing with. For this reason, measurement techniques take advantage of some simplified systems by reducing the effect of these factors or isolating one sub-process from the rest. It leads to a better control of the system by dealing with a few parameters. With respect to particle-bubble encounter measurements, researchers used a single particle counterbalancing with a single bubble in the absence of energy dissipation rate. Firstly, floatability and wettability behavior of a single (pure) particle in the absence of gangue minerals were foubd significantly different from a mineral in a deposit. Secondly, the results could only be applied to quiescent zone which is substantially lower than an intensively turbulent zone around the impeller (Nguyen and Kmet, 1992; Wang et al., 2003; Verrelli et al., 2014).

Generally speaking, the measurement techniques can be classified into two parts *i.e.* direct and indirect methods which are reviewed below.

**Table 2.2 :** CFD modeling of column flotation focusing on particle-bubble sub-procsses.

| Zone | Author | year | Model | Turbulence |
|---|---|---|---|---|
| **Collection** | Deng et al., | 1996 | E-E | Lam |
| **Collection** | Xia et al., | 2006 | E-E | Lam |
| **Froth** | Ciliers et al., | 2006 | - | - |
| **Collection** | Chakraborty et al., | 2009 | E-E | k-e model |
| **Collection** | Nadeem et al., | 2009 | E-E | k-e model |
| **Collection** | Koh and Schwarz | 2009 | E-E | k-e model |
| **Collection** | Rehman et al., | 2011 | E-E | Standard k-e model |
| **Froth** | Brito et al., | 2012 | - | - |
| **Collection** | Sarhan et al., | 2016 | E-E | Standard k-e model |
| **Collection** | Nasirimoghadam et al., | 2017 | E-E | Standard k-e model |
| **Collection** | Khorasani et al., | 2017 | E-E | Realizable k-e model |
| **Collection** | Yang et al., | 2017 | E-E | Realizable k-e model |
| **Collection** | Guoa et al., | 2017 | E-E | Realizable k-e model |

### 2.3.1 Direct and indirect methods

As mentioned previously, operating factors is controlled thoroughly to enable studying the microscopic sub-processes of the particle-bubble interactions. In direct methods, bubble is kept constant in the presence of liquid (water) and zero velocity while particles (normally pure materials) falling on its surface (Schulze and Gottschalk, 1981; Verrelli and Albijanic, 2015; Brabcova et al., 2015). The observation is recorded using high-speed cameras and particle tracking together with the probably of encountering particle with the bubble calculated by considering of reasonable assumptions. Figure 2.2 shows a typical measurement performed by Brabcova et al., (2015). It was found that particle trajectory is in very tight connection with distance of particles from bubbles which is relevant to the bubble surface property, particle size and its density. However, it is now proven that only fine particles with lower densities follow the streamlines. Also, the results cannot be extended to an actual system due to disregarding the bubble velocity and cell turbulence (Nguyen and Schulze, 2004). More specific concepts in this regards are discussed on the effect of particle specific gravity in upcoming sections. The restrictions of direct methods for measuring $E_c$ can be listed as below:

- Whether water velocity is ignored or considered negligible compared to the real flotation system.
- A captive bubble is assumed entirely immobile in the disperse system. While, surface contamination of bubble is changing based on the reagent dosage and its size providing both mobile and immobile bubbles.
- Particle density is always lower due to accessing to only silica, glass beads or quartz particles.
- Streamlines assumed to be stationary while they change in space and time in an actual cell.

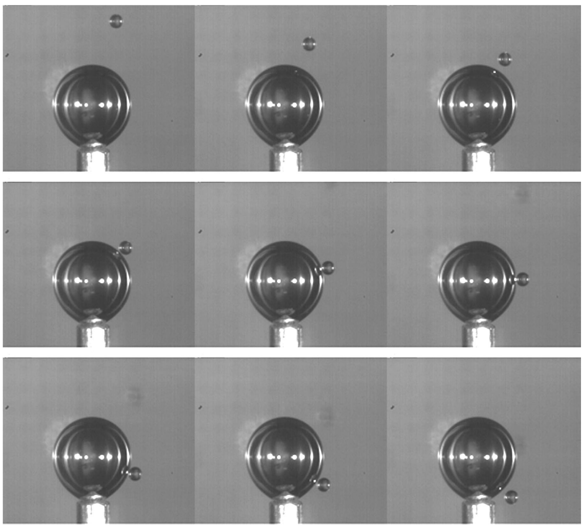

**Figure 2.2 :** Direct observations of bubble-particle collision interactions. Each image was taken after 40ms (Brabcova et al., 2015).

A group of researchers used indirect measurement techniques for studying the microscopic aspect of the flotation. A device as shown in Figure 2.3 was used for generating a single bubble (Hewitt et al., 1994), while a dispersion system mimicked the flotation system. Bubbles were generated by capillary technique from the bottom of the apparatus while the interacting of particles with bubbles were recored using a high-speed camera alongside of the tube. More specific information concerning its operation, assumptions, applicability and limitations are presented elsewhere (Hassanzadeh et al., 2018).

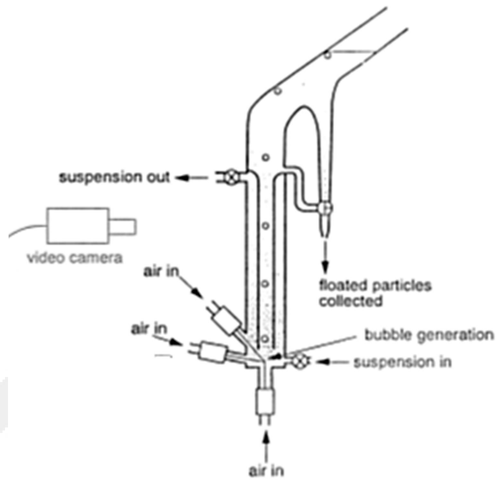


**Figure 2.3 :** A representative diagram of a single-bubble flotation device (Hewitt et al., 1994).

### 2.4 Impact Of Fluid Properties, Bubble And Particle Characteristics On $E_c$

#### 2.4.1 Effect of particle specific gravity

Specific gravity of particle is one of the factors significantly affecting flotation processes. Unlike other particle properties, the role of $\rho_p$ on the $E_c$ has not been adequately studied owing to main practical difficulties involved in the process. It is still very hard to dynamically observe the interaction of particles with different densities colliding with bubbles at certain velocities. For this reason, recent analytical and numerical investigations were focused to evaluate this issue.

Conceptually, during the collision sub–process, the higher the $\rho_p$ is the greater $V_s$ that leads to stronger deviation of particle trajectories from the fluid streamlines. This deviation may potentially cause the particles to collide with bubbles.

A great number of studies worked on determination the role of particle specific gravity on the $E_c$ (Derjaguin and Dukhin, 1960; Levin 1961; Michael and Norey 1969; Nguyen and Kmet, 1992; Nguyen and Kmet, 1994; Dai et al., 1998; Phan et al., 2003; Ralston et al., 2002; Sarrot et al., 2005; Sarrot et al., 2007; Bournival et al., 2016; Kouachi et al., 2017; Hassanzadeh et al., 2016; 2017 and 2018). A detailed review compiled the findings of all these studies comprehensively which is reported elsewhere (Hassanzadeh et al., 2018). To avoid any redundancy, short explanations regarding some of these works are presented below.

Pyke (2003) calculated the $E_c$ using $E_c^{GSE}$ for quartz ($\rho_p = 2.6\ \frac{g}{cm^3}$), chalcopyrite ($\rho_p = 4.1\ \frac{g}{cm^3}$) and galena ($\rho_p = 7.4\ \frac{g}{cm^3}$). It was found that $E_c^{GSE}$ reliably predicts the particle-bubble encounter efficiencies for quartz and chalcopyrite particles. However, it exhibits a substantially overestimation for intermediate and coarse galena particles. In the same context, Hassanzadeh et al. (2017) and Kouachi et al. (2017) beneficiated the differences among $E_c^{SC}$and $E_c^{GSE}$ to identify the effect of particle density on the Ec. They found that there are two distinct areas where the $\rho_p$ plays entirely different role which was in a close agreement of numerical results of Firouzi et al., (2011). In the first zone, enhancing particle density resulted in diminishing the $E_c$, however, in the second zone, increasing $\rho_p$ followed by an increase in the $E_c$. Nevertheless, the effect of turbulent dissipation energy and fluid density on the $E_c$ in these analytical studies was not discussed sufficiently.

By comparing these similar studies together, it was revealed that Pyke (2003) and Kouachi et al., (2017) mainly discussed the influence of $\rho_p$ on flotation kinetic rates while Hassanzadeh et al. (2017) concentrated on the particle and bubble inertial aspects. Nguyen et al., (2006), Nguyen and Nguyen (2009) and Firouzi et al., (2011) used CFD technique to determine the Ec. They compared the numerical results with corresponding outcomes of $E_c^{GSE}$. The comparison only showed reasonable agreement between the $E_c^{GSE}$ and the CFD results particles finer than <10µm. Contrarily, a significant deviation between $E_c^{GSE}$ and CFD was observed for non–ultrafine particles (>10µm). The principal difference apparently originated from the angle of tangency.

In this regards, Nguyen et al. (2006) reported that there is a particle diameter where the angle of tangency has a minimum in the presence of mobile bubbles which cannot be observed by $E_c^{GSE}$. They concluded that for coarse particles, the particle inertial force is comparably greater than the centrifugal force. As a consequence, the angle of tangency increases with increasing particle diameter towards 90°. The simulation results obtained by Liu and Schwarz (2009) using 3-D CFD method along with Lagrangian particle tracking model indicated that the SRHI should be considered for accurate prediction of the $E_c$ because it increases the hydrodynamic resistance on the particle approaching a bubble surface which is so-called microhydrodynamic effect.

Furthermore, it is reported in several woks that (Levin 1961; Michael and Norey 1969; Ralston et al., 2002) the inertial deposition of particles on the bubble surface can take place at while St is greater than 1/12 so-called critical Stokes number ($St_{cr}$). It is defined as a critical value of the St where above that a particle can reach the surface of a sphere or a bubble under the action of inertial forces (Dai, 1998). According to the definition of St, it exemplifies the ratio of the magnitude of the inertial force to the viscous resistance of the medium. When St>>Stcr, the inertial forces have a positive effect on $E_c$ ,however, for St<<Stcr, particles move alongside the streamlines of the fluid flow and then the interception effect is the foremost collision mechanism. In this context, Derjaguin and Dukhin (1960) pointed out that for a given $d_B$, there is a specific particle size below which no collisions can occurr. They also reported that if $St>St_{cr}$, an increase in bubble diameter can result in increasing the $E_c$ considering $St_{cr}=1.212$ and $St_{cr}=1/12$ for Stokes and potential fluid flows, respectively. More detailed discussions were presented elsewhere (Kouachi et al., 2017; Hassanzadeh et al., 2016; 2017 and 2018).

Hassanzadeh et al. (2016) found that the resistant water inertial force on $E_c$ can be overlooked for fine particles while $v_B$ is exceeded. However, under the same bubble velocity, it was highly suggested to take the water inertial effect (negative inertial force) into account for coarse particles. Ralston et al. (2002) discussed the long-range (LRHI) and short-range (SRHI) hydrodynamic interaction forces on the particle-bubble interactions. It was reported that deviation of the trajectory of a fine particle from the straight path towards the bubble surface at a distance of the order of the bubble size is caused by LRHI *i.e.* hydrodynamic drag forces. However, in the case of a coarse particle, the inertial forces considerably exceed the LRHI. The negative effect of inertial forces clearly increased with bubble size and particle density.

### 2.4.2 Bubble velocity and its size effects

This section reviews the role of bubble diameter and its velocity on Ec which is discussed in detail elsewhere (Hassanzadeh et al., 2018). Bubble velocity ($v_B$) and its size ($d_B$) are two very imperative elements influencing the particle–bubble collision efficiency. Many studies focused on understanding their effects on flotation processes (Reay and Ratclitf 1975; Motarjemi and Jameson, 1978; Ahmed and Jameson, 1985; Yoon and Luttrell, 1989; Wang et al., 1996; Sam et al., 1996; Han et al., 2001; Ralston et al. 2002; Lehr et al., 2002; Tao, 2004; Kulkarani et al., 2005; Hassanzadeh et al., 2016). However, their impacts on Ec are still not well-understood and require further studies.

According to the literature, it's now known that $d_B$ and $v_B$ in different flotation cells vary in the ranges of 0.05 to 0.25cm (Banisi and Finch, 1994; Sam et al., 1996; Chen et al., 2001; Cho and Laskowski, 2002) and 10 to 40cm/s. It's worth mentioning that these ranges highly depend on the reagent type and dosages, presence or absence of particles, their types and sizes, agitation rate in mechanical flotation cells, aeration rate and type of equipment and some other relevant operating parameters. Figure 2.4 presents the role of both $v_B$ and $d_B$ on $E_c$. As seen, smaller bubbles show more affinities for encountering with fine particles (Reay and Ratcliff, 1973; Schulze, 1989) which leads to using micro or nano-bubbles in the flotation system.

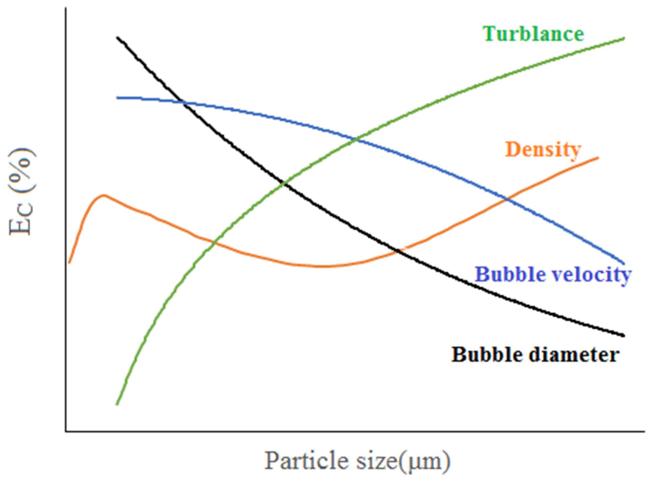


**Figure 2.4 :** Variation of probability of particle-bubble encounter with particle size of different density, cell turbulence and bubble velocity.

In addition to $d_B$ and $v_B$, bubble mobility is another main property of the bubbles in interacting with bubbles. The behavior of bubbles with various degrees of contaminations are diverse in the vicinity of particles and in turbulent cells. Typically, the bubble surface can be with impurities in water composition or being exposed with additive reagents (especially frothers) contaminated. These chemical agents reduce $d_B$ and in turn its velocity (Quinn et al., 2007; Firouzi and Nguyen, 2014a, b, c and 2017; Firouzi et al. 2015). The profile of $d_B$ and $v_B$ can be shown by Figure 2.5. It is reported that there is a critical bubble size where its movement start changing which leads to a significant effect on $E_c$ (Sam et al., 1996; Hassanzadeh et al., 2016). This is discussed in detail in chapter five.

In this thesis $d_B$ and $v_B$ are the main focuses while bubble surface mobility and its impact on $E_c$ can be found elsewhere (Malysa et al., 2005) and (Temesgen et al., 2017).

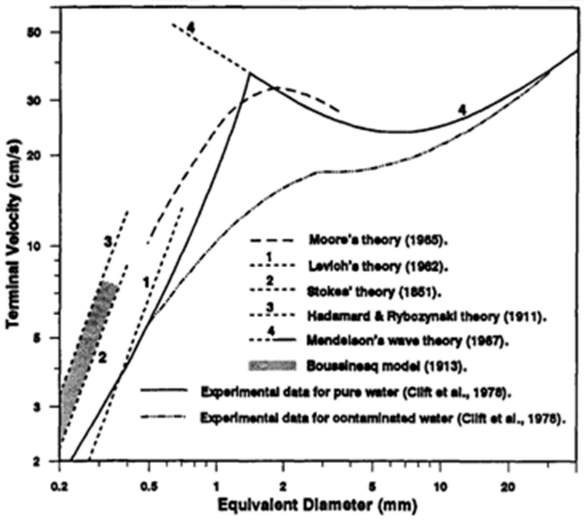


The terminal velocity of air bubbles in water

**Figure 2.5 :** Profile of bubble's terminal velocity as a function of bubble diameter for different theoretical models (Sam et al., 1996).

### 2.4.3 Impact of cell turbulence

Energy dissipation rate so-called cell turbulence plays a very crucial role in flotation cells in achieving a desirable flotation rate constant and acceptable grade-recovery curve. More specifically, the cell turbulence leads to a remarkable increase of particle-bubble collision frequency (Pyke et al., 2003) and contrarily decreases the particle-bubble aggregate stability particularly for dense minerals (Hassanzadeh et al., 2018). Schubert (2008) assumed that the collision frequency could be improved by use of an efficient impeller-stator system, increase of the power input by means of a higher rotational speed, dispersion of flotation slurry and reduction of solids concentration in the feed pulp. Hoang et al. (2018) investigated the impact of turbulent hydrodynamics to help understanding the role of turbulence in flotation of fine particles (grade, recovery and flotation kinetics). It was found that the turbulent hydrodynamics condition should be optimizated in order to improve grade or recovery for each flotation stage (*i.e.* rougher, scavengers and cleaners). Furthermore, (Hoang et al., 2018c; Hoang et al., 2018b); Hoang et al. (2018) reported that in case flotation of high grade ore, not only the pulp properties but also the froth properties which are influenced by the impeller speed, air flowrate and pulp density are significantly change over flotation time. Thus, identification of its optimal value is a mandatory term in flotation processes. In addition to its direct impact, cell turbulence is affected by other factors *e.g.* pulp density. For example, a high %S and/or attractive interaction between fine particles can also enhance the pulp viscosity resulting in a decrease in turbulent energy dissipation rate, which in turn has a negative effect on the particle–bubble collision frequency (Fornasiero and Filippov, 2017).

Because of the natural complexity of three-phases in the flotation systems, quantification of the energy dissipation rate is hard to obtain (Meng et al., 2016). In this regard, the mean turbulent kinetic energy dissipation rates and power number are normally measured in order to estimate the cell turbulence.

The cell mean turbulent kinetic energy dissipation rates can be calculated on the basis of the motor power and the mass of pulp in the flotation cell as follows:

$$\bar{\epsilon} = \frac{P_{loaded} - P_{unloaded}}{m_{pulp}} \quad (2.5)$$

where $P_{unloaded}$ and $P_{loaded}$ are power drawn of the motor with empty cell, and with a flotation cell and pulp together, respectively. Also, mpulp is the pulp mass in the cell.

The power number ($C_p$) as ratio of actual to theoretical power consumption, is shown in equation 2.6:

$$c_P = \frac{P}{\rho_f n^3 D^5} \quad (2.6)$$

where P is the net power input (Nm/s), ρf is the specific gravity of the pulp (density) (kg/m$^3$), n is the impeller rotational speed (s$^{-1}$), D is the impeller diameter (m).

In the literature, there are several models presented for calculating the collision frequency as shown in Table 2.3. Each model, its description together with the assumptions is described in detail by Hassanzadeh et al., (2018).

**Table 2.3 :** Common models used for calculation of particle-bubble collision frequency.

| **Author(s)** | **Formula** |
|---|---|
| **Smoluchowski** | $Z_{PB} = \frac{4}{3} N_p N_B d_{12}^3 G$ |
| **Camp & Stein** | $Z_{PB} = \frac{4}{3} N_p N_B d_{12}^3 \sqrt{\frac{\varepsilon}{v}}$ |
| **Shaffman & Turner** | $Z_{PB} = (\frac{8\pi}{15})^{1/2} N_p N_B d_{12}^3 (\varepsilon / v)^{1/2}$ <br> $Z_{PB} = (8\pi)^{1/2} N_p N_B d_{12}^2 [(1 - \frac{\rho_p}{\rho_f})^2 (\tau_p - \tau_B)^2 (\overline{a^2} + g) + \frac{d_{12}}{9} \frac{\varepsilon}{v}]^{1/2}$ |
| **Abrahamson** | $Z_{PB} = 5 N_p N_B d_{12}^2 \sqrt{v_p^2 + v_B^2}$ <br> $v_1^2 = \frac{v^2}{1 + 1.5\tau_1 \varepsilon \sqrt{v^2}}$ |

### 2.4.4 The challenge of particle diameter

Flotation technology has faced the challenge of fine particles practically from the very first years of its application, in other words, this task is more than 110 years old. The sole kinetic parameter dependent on the particle size is the efficiency of their capture by a rising bubble. In the case of fine inertia free particles, this parameter can be conveniently described by a formula given below:

$$E(d_p, d_b) = \frac{4j(d_p)}{\pi d_b^2 v_B n_p} \tag{2.7}$$

where np is numerical concentration of particles and $j(d_p)$ is a total flow of particles attached to a bubble. The specific calculations of function $j(d_p)$ is based on considering a particle trajectories in the hydrodynamic field of a rising bubble with the account of a hydrodynamic particle-bubble interaction as well as surfaces forces which manifest when the surfaces of a particle and a bubble draw close at a distance roughly less than 100nm.

If a particle has a spherical shape, surface forces presented only a dispersion component and a bubble surface is entirely retarded by absorption layer of surfactants, the function $E\left(d_p, d_b\right)$ follows the law

$$E(d_p, d_B) \sim \frac{d_p^{1.45}}{d_B^{1.83}} \tag{2.8}$$

In the event when a bubble surface is completely tangentially moveable, the following relation is valid:

$$E(d_p, d_B) \sim \frac{d_p^{0.8}}{d_B} \tag{2.9}$$

Considering that, the flotation rate constant is in the direct proportion to the value of $E(d_p, d_B)$, then the relation between equation 2.8 and equation 2.9 show that acceleration of fine particles flotation process can be achieved either through application possibly finest bubbles and/or through the increase in the size of floated objects. The latter can be achieved by using particles flocculation (or coagulation) or by using relatively coarse flotation carriers. Regrettably, in minerals beneficiation the first method implies significant difficulties related to selectivity. The second option looks more promising. Quite often, we use flotation carriers as particles of similar nature as the floated ones, but sufficiently coarser in size. Rarely carriers are applied with nature different from the floated particles, *e.g.* paraffin or 2 polystyrene balls, oils drops etc. The more promising approach involves application of microbubbles as flotation carriers, but the size of microbubbles shall be less than 50 µm.

The major improvement for the current challenge is using micro and nano-bubbles in flotation system. The major impediment in practical implementation of this technique is the difficulty of producing the sufficient quantities of microbubbles. In terms of the potential capacity, the most promising is the method of mechanical dispersion of air in the concentrated solution of a frother. This technique allows producing air-in-water micro-dispersion (AWMd), in which the microbubbles concentration amounts to 60 vol.%. This dispersion can be then fed in the flotation cell, specifically in the area of vigorous mixing, by a special pipeline, and in this zone it quickly falls into separate very flotation active microbubbles. In line with the CMF-theory, the flotation rate constant k at relatively small volume dosages of microbubbles per the unit feed weight (ml/g) can be presented by relation:

$$k = k_0 + \alpha f \quad (2.10)$$

where $\alpha$ is a certain constant. The findings of laboratory tests conducted at actual and artificial mineral mixtures demonstrate that at dosages $f$ of around 0.1(ml/g) we can achieve more than 2 time increase of the flotation rate alongside with the significant increase in recovery.

The major advantage of CMF-technique is that it can be easily implemented for any industrial flotation cell (either of pneumo-mechanical or column types) and does not require significant capital costs or reconstruction of flotation cells. Air-in-water microdispersion can be fed by a pipeline from the AWMd-generator outlet into the pulp flow directed into a column cell or alternatively directly into a zone of vigorous mixing of a mechanical type flotation cell. AWMd-generator can be placed on the cover of a flotation cell or close to the pipeline feeding the pulp.

### 2.4.5 Particle encounter efficiency and flotation rate constant

The flotation rate constant has been studied extensively over the past decades macroscopically through modeling represented in categories such as empirical and phenomenological (population balance, mathematical and probabilistic) models (Gharai and Venugopal, 2016). From the 1930's to early 1990, various mathematical and practical flotation kinetic models were proposed and examined under different flotation conditions (Zuniga, 1935; Kelsall, 1961; Arbiter and Harris, 1962; Imaizumi and Inoue, 1963; Woodburn, 1970; Jowett, 1974; Trahar and Warren, 1976; Harris, 1978; Klimple, 1980; Agar et al., 1989; Mehrotra and Padmanabhan, 1990; Kelly and Carlson, 1991; Ek, 1992; Yuan et al., 1996). Nevertheless, it is now accepted that there is no unique flotation kinetic model applicable to the froth flotation processes (Dowling et al., 1985; Nguyen and Schulze, 2004; Bu et al., 2017; Sahoo et al., 2017). The majority of the empirical models have fitted the first order kinetic models to the experimental data which are valid only at steady–state conditions (Azizi et al., 2015; Albijanic et al., 2015; Ni, et al., 2016; Hassanzadeh and Karakaş, 2017a). The inability of flotation sub–processes to describe the flotation rate constant under flotation conditions has made them unsuitable for assessment, control and monitoring purposes. Therefore, it appears that the fundamental analytical modeling of flotation rate constant can provide a universal way of evaluating the flotation kinetics with a distribution of particle floatabilities (Nguyen and Schulze, 2004).

Several factors such as particle and bubble sizes, percent solids, particle residence time distribution, angle of tangency, particle roughness, morphology, density and particle terminal settling velocity, contact angle, bubble surface contamination, bubble velocity and turbulent dispersion rate play significant roles in maximizing both $E_c$ and k in the froth flotation processes (Trahar, 1981; Fallenius, 1987; Tao, 2004; Guven and Celik, 2016; Hassanzadeh, 2017). A brief explanation describing the effect of each parameter on both particle–bubble encounter efficiency and flotation rate constant is elaborated here.

Turbulence dissipation rate: An optimum flotation rate constant is aimed not only to maximize the particle–bubble encounter efficiency but also to minimize the particle–bubble detachment (Schubert, 2008). More specifically, the cell turbulence leads to a small increase in the flotation rate constant of fine and intermediate sizes of dense particles and in turn to an increase in particle–bubble collision frequency and volume of pulp that sweeps through the bubble ($V_{path}$). On the contrary, a substantial decrease in the flotation rate constant of coarse particles occurs due to a decrease in the particle–bubble aggregate stability particularly for denser minerals.

Contact angle: Particle contact angle leads to an increase in the flotation rate constant due to an increase in the attachment efficiency.

Bubble size: A decrease in the bubble size increases the particle–bubble encounter and attachment efficiencies and in turn causes an increase in the flotation rate and recovery of fine particles (Reay and Ratcliff, 1973; Hassanzadeh et al., 2016). Increasing the bubble size at a constant bubble velocity results in an increase in the flotation rate constant of coarse particles but leads to a decrease in the flotation rate constant of fine particles (Pyke, 2003).

Percent solids: A high percent solids and/or attractive interaction between fine particles can also increase the pulp viscosity resulting in a decrease in turbulent energy dissipation rate, which in turn has a negative effect on the particle–bubble collision frequency (Fornasiero and Filippov, 2017). An increase in the solids concentration leads to a decrease in flotation rate constant (Azizi et al., 2015).

Particle size: There is a large amount of evidence indicating that Ec increases with increasing the particle size. However, the behavior of k versus dp follows different trends. As a general rule, k decreases gradually when the range of particle size becomes finer due to an increase in the number of particles per unit weight, the deteriorating conditions for particle–bubble collision, and such effects as increasing surface oxidation of the particles; it also decreases suddenly above an optimum particle size either due to low degree of mineral liberation or reduced ability of bubbles to lift the coarse particles (Trahar, 1981; Hassanzadeh and Karakas, 2017b).

Particle density: It is believed that increasing particle density enhances the Ec, however, numerical results reveals that there are two distinct zones where the particle density plays completely different roles. In the first zone, increasing particle density reduces the $E_c$, whereas in the second zone, increasing particle density leads to an increase in the $E_c$ (Liu and Schwarz, 2009). Increasing the particle density at a constant particle size, in general, reduces the flotation rate constant (Shi and Fornasiero, 2009).

Angle of tangency: The analytical results predict a continuous decrease on the angle of tangency with increasing the particle size (Kouachi et al., 2017). However, numerical outcomes indicate that there is a critical particle size where the angle of tangency is minimal (Firouzi et al., 2011).

Bubble velocity: Increasing bubble velocity above a threshold decreases the Ec due to a decrease in the maximum possible collision angle and likewise, k is reduced owing to the substantial reduction in the attachment efficiency (Pyke, 2003).

# 3. THEORY AND METHODOLOGY

## 3.1 Methodology Of Chapter Four

This chapter deals with the effect of particle density on particle-bubble interaction and flotation kinetic rate. To fundamentally understand the concepts, quartz and chalcopyrite with specific gravities of 2.65 and 4.3 g/cm$^3$ were studied while particle size varied from 1-100µm. Bubble size and its velocity were selected in the ranges of 0.1-0.15cm and 18-31cm/s, respectively. Bubble surface was assumed not contaminated (mobile). Moreover, energy dissipation rate together with gas flow rate were kept constant as 38m$^2$/s$^3$ and 3.5×10$^{-3}$ m$^3$/min, respectively.

Schulze ($E_c^{SC}$) and Dukhin ($E_c^{GSE}$) particle-bubble encounter models were selected due to their different assumptions with respect to the effect of particle density (particularly the inertial effect). The general flotation kinetic (GFK) model was used for calculation of the flotation rate constant. With this regard, modified Dobby–Finch attachment ($E_a^{DF}$) and modified Schulze stability ($E_s^{SC}$) models were used for determination of the particle-bubble attachment and detachment probabilities, respectively.

More specifically, the $E_c^{SC}$ was applied to the GFK model instead of using $E_c^{GSE}$ to better understand either particle or water inertial effects. Finally, particle-bubble encounter probabilities along with flotation constant rates were determined and critically analyzed in the presence of turbulent and variation of particle size, its density, bubble size and bubble velocity. In this chapter, we elaborate the original and modified flotation rate constants. Former kinetic approach is the broadly-known flotation rate constant based on $E_c^{GSE}$ and the latter is the one in which $E_c^{GSE}$ was substituted with $E_c^{SC}$.

It is worth mentioning that detailed definitions of the particle-bubble interaction modeling were presented in chapter 1. Additionally, the general flotation kinetic model was described in section 3.3.

### 3.2 Methodology Of Chapter Five

In this chapter, the effect of bubble surface properties, bubble size and its velocity were studied on the particle-bubble encounter efficiency. This investigation was divided into two parts. First, the particle density, fluid flow regime and bubble surface mobility were considered constant (*i.e.*, chalcopyrite with specific gravity of 4.3g/cm$^3$, potential flow and mobile bubble) to understand the phenomena clearly. The collision probability has been determined by Schulze and GSE models in the particle size range of 1 to 100µm. Bubble diameters of 0.08, 0.12, and 0.15cm and bubble velocities of 10, 20 and 30cm/s were selected to study the parameters involved in the flotation of chalcopyrite.

In the second part, impact of bubble surface characterization (mobility and immobility), its diameter and velocity were investigated concentrating on inertial forces in the $E_c$. Three encounter models including Sutherland ($E_c^{SU}$), Schulze ($E_c^{SC}$) and Generalized Sutherland Equation ($E_c^{GSE}$) were taken into account with regard to their differentiations from the inertial point of view in the particle size range of 1-100µm. Bubble diameter and its velocity were selected as in the first section. Weber and Paddock collision model ($E_c^{WP}$) was taken for evaluation of the effect of bubble surface mobility on $E_c$.

A detailed description concerning the $E_c^{SU}$, $E_c^{SC}$, $E_c^{WP}$ and $E_c^{GSE}$ were presented in section 1.5.

### 3.3 Methodology Of Chapter Six

In this section, the most common flotation kinetic equation was used (equation 3.1) (Pyke et al., 2003; Duan et al., 2003; Govender et al., 2013; Karimi et al., 2014 a, b; Popli et al., 2015). It was initially proposed by Ahmed and Jameson (1989) based on the assumptions that the reaction is the first order, bubble concentration in pulp is constant, and the volume of particles removed is negligible. According to Derjaguin and Dukhin (1993), the collection efficiency ($E_{coll}$ the so–called capture efficiency, $E_{cap}$) was calculated as the product of three probability functions ($E_c.E_a.E_s$), quantifying the collision, attachment, and detachment (stability) efficiencies.

$$\frac{dN_p}{dt} = kN_p = -Z_{pb}E_cE_aE_s \tag{3.1}$$

where $t$ *(s)* is time, $N_p$ the number of particles and $k$ the flotation rate constant. $E_c$, $E_a$ and $E_s$ were consecutive sub–processes comprising the particle–bubble collision, attachment and stability. $Z_{pb}$ ($m^3/s$) is the collision frequency per unit volume between particles and bubbles of diameters $d_p$ and $d_b$ ($m$), respectively.

To calculate $Z_{pb}$, several formulas were presented by Smoluchowski (1917), Camp and Stein (1943), Saffman and Turner (1956), and Abrahamson (1975) which were discussed in detail elsewhere (Hassanzadeh et al., 2018). Abrahamson (1975)'s model (equation 3.2), well–accepted for the flotation processes, was used in this study (Schubert, 1999; Koh et al., 2000; Liu and Schwarz, 2009):

$$Z_{pb} = 5N_pN_b(\frac{d_p+d_b}{2})^2\sqrt{(\vec{V}_p^2 + \vec{V}_b^2)} \tag{3.2}$$

where $N_p$ and $N_b$ were the number of particles and bubbles per unit volume, $\vec{V}_p$ and $\vec{V}_b$ (m/s) were turbulent root–mean square (RMS) velocities of particle and bubble relative to the turbulent fluid velocity which could be approximated by the following expression (equation 3.3) (Schubert and Bischofberger, 1978; Schubert,1999):

$$(\vec{V}_i^2)^{1/2} \approx 0.33\frac{\varepsilon^{\frac{4}{9}}d_i^{\frac{7}{9}}}{v^{\frac{1}{3}}}(\frac{\rho_p-\rho_f}{\rho_f})^{\frac{2}{3}} \tag{3.3}$$

where the subscript i refers to the particle or bubble, $\varepsilon$ (W/kg) denotes the dispersion rate of the turbulent kinetic energy per unit mass, $v$ ($m^2/s$) is the kinematic viscosity of the fluid, $\rho_p$ and $\rho_f$ ($kg/m^3$) are particle and fluid densities, respectively.

By combining equation 3.1 and equation 3.2, it could be shown that;

$$k = 5N_b\frac{d_b^2}{4}[0.33\frac{\varepsilon^{\frac{4}{9}}d_b^{\frac{7}{9}}}{v^{\frac{1}{3}}}\left(\frac{\rho_p-\rho_f}{\rho_f}\right)^{\frac{2}{3}}]E_cE_aE_s \tag{3.4}$$

where $N_b$ represented by gas flow rate $G_{fr}$ ($cm^3/min$) and bubble residence time, $MRT_b$ (min) per unit volume of vessel ($V_{cell}$). The $MRT_b$ is defined as the time that bubbles of velocity $v_b$ remain in the unit volume.

Eventually, equation 3.5 was shown as:

$$k = 2.39\frac{G_{fr}}{d_bV_{cell}}[0.33\frac{\varepsilon^{\frac{4}{9}}d_b^{\frac{7}{9}}}{v^{\frac{1}{3}}}\left(\frac{\rho_p-\rho_f}{\rho_f}\right)^{\frac{2}{3}}\frac{1}{v_b}]E_cE_aE_s \tag{3.5}$$

The capability of equation 3.5 was experimentally examined for the flotation of quartz, chalcopyrite and galena in several studies (Pyke et al., 2003; Pyke, 2004; Duan et al., 2003; Newell, 2006; Newell and Garno, 2007). Additionally, Karimi et al., (2014a, b) presented a good agreement between the experimental and numerical data on the flotation of quartz, chalcopyrite and galena using computation fluid dynamics (CFD) under various contact angles and agitation and gas flow rates. Therefore, the agreement of experimental and numerical results with the theoretical model of equation 3.5 was led us to confidentially calculate the flotation rate constants.

According to assumptions of Abrahamson's model (*i.e.* highly turbulent condition and infinity Stokes number), particle–bubble encounter probability is approximately 1. However, in an actual flotation condition, as the turbulent is not infinitive, the use of collision efficiency model provides much less value in serving as a correction factor for $Z_{pb}$ (Sherrell, 2004).

Considering the existing analytical models of collision, attachment and detachment, two most common model configurations were selected as (I) Dukhin so–called generalized Sutherland equation ($E_c^{\mathrm{GSE}}$), modified Dobby–Finch attachment ($E_a^{DF}$) and modified Schulze stability ($E_s^{SC}$) models (*i.e.* ($E_c^{\mathrm{GSE}}$, $E_a^{DF}$, $E_s^{SC}$) and (II) Yoon–Luttrell ($E_c^{YL}$), Yoon–Luttrell (intermediate) ($E_a^{YL}$) and modified Schulze stability ($E_s^{SC}$) models (*i.e.* ($E_c^{YL}$, $E_a^{YL}$, $E_s^{SC}$)).

Dukhin (1983) collision model (so–called $E_c^{\mathrm{GSE}}$) was experimentally verified by Dai (1998), Pyke, (2003), Duan et al., (2003) and Newell (2006). However, recent numerical studies demonstrated its inaccuracy due to poor estimation of the collision angle and disregarding the microhydrodynamics and bubble wall effects (Phan et al., 2003; Liu and Schwarz 2009; Firouzi, et al., 2011). On the other hand, the collision model of Yoon–Luttrell (1989) was accepted as an accurate model and used by several researchers in their investigations (Koh and Schwarz, 2006; Shahbazi et al., 2009; Govender et al., 2012; Yoon et al., 2016). However, it was only applicable to particles finer than 100µm and bubbles smaller than 1mm with immobile surfaces which did not completely cover particle and bubble ranges in flotation conditions.

The $E_c^{\mathrm{GSE}}$ (equation 1.7) was selected to estimate the particle–bubble encounter efficiency as described in section 1.6.1.

Measured attachment efficiencies by several studies (Dai, 1998; Duan et al., 2003; Pyke et al., 2003) aimed to test the particle–bubble attachment model showed good agreement with those predicted using the modified Dobby and Finch attachment efficiency model ($E_a^{DF}$) (Dobby and Finch, 1987). Likewise, other researchers used $E_a^{DF}$ in their studies (Dai, 2000; Pyke, 2004; Newell, 2006; Karimi et al., 2014a; Hassanzadeh et al., 2016; Kouachi et al., 2017; Popli, 2017). Thus, modified Dobby–Finch attachment model (equation 1.19) was selected to calculate the attachment efficiency (Ea) (Dobby and Finch, 1987) as explained in section 1.7.1.

### 3.3.1 Optimization technique–response surface method (RSM)

It is broadly–known that the flotation process is affected by many interlinked factors. For instance, changing bubble size impacts significantly on bubble velocity (Sam et al., 1996) and varying surface contamination of bubble is highly effective on bubble diameter and bubble velocity (Laskowski et al., 2003; Kulkarani and Joshi, 2005; Rafiei, 2009). Also, turbulence has a major effect on bubble size (Amini et al., 2013) and its velocity (Nesset et al., 2006) in a flotation cell. Bubble size can also be influenced by solids concentration (Finch et al., 2008; Vazirizadeh, 2015). Moreover, interaction of air flow rate and froth thickness (pulp level) induces a significant effect on flotation rate constant (Cilek, 2004). The inter–related relation of gas hold–up, interfacial area of bubbles and bubble surface area flux significantly affect k (Vazirizadeh et al., 2015). Therefore, it is not preferred to use one–factor at a time (OFAT) method due to neglecting the interaction effects of the factors.

Design of experimental (DOE) methodology was used to incorporate the interaction effects into the modeling technique. The response surface methodology (RSM), a well–known statistical technique (Martinez–L et al., 2003; Kalyanin et al., 2005; Dashti and Eskandari Nasab, 2013), was utilized for modeling and optimization of flotation process. In this regard, second–order models were applied as they provide a high degree of flexibility and applicability in a wide variety of functional forms. These advantages lead to a well approximated the true response surface. Also, it is very easy to estimate the parameters in a second–order model using the method of least squares.

# 4. EFFECT OF PARTICLE DENSITY

## 4.1 Assessment Of The Particle-Bubble Encounter Efficiency Models

As seen in chapter two, there is a threshold where below and above the behavior of particle size and its density on particle-bubble encounter interaction is entirely different. Additionally, it is impossible to track and observe this mechanism practically. Therefore, the only solution is taking advantage of analytical and numerical modeling approaches. To disclose this phenomenon, two collision models *i.e.* $E_c^{GSE}$ and $E_c^{SC}$ were applied under a certain hydrodynamic condition. These models were chosen based on their assumptions concerning the role of particle inertial forces. In this regards, the selective theoretical method is to create a physical definition and functional features of the parameters which are regarded in one and disregarded in the other model.

The role of particle inertia on the $E_c$ was introduced in section 1.3.3. In addition to that, the concept was elaborated in detail in section 2.4.1. In equation 4.1, St number differs under various flotation conditions which is used to investigate the particle inertial impact on $E_c^{SC}$. Since St might fluctuate either by varying the particle size for one mineral, or for changing mineral types containing different densities. Consequently, two minerals *i.e.* quartz and chalcopyrite with respective densities of 2.65g/cm$^3$ and 4.1g/cm$^3$ were studied in this section. Top particle size for both minerals was considered 100µm. As seen Figure 4.1, Ec is depicted for both minerals against particle size using both $E_c^{GSE}$ (equation 1.7) and $E_c^{SC}$ inertial (equation 4.1). According to Figure 4.1, both models predict that Ec is increasing by increasing both particle size and density with different rates under the defined flotation condition.

$$E_C^{in} = \left(\frac{1}{1+{}^{v_P}/_{v_B}}\right)\left(1 + {}^{d_P}/_{d_B}\right)^2 \left(\frac{St}{St+a}\right)^b \tag{4.1}$$

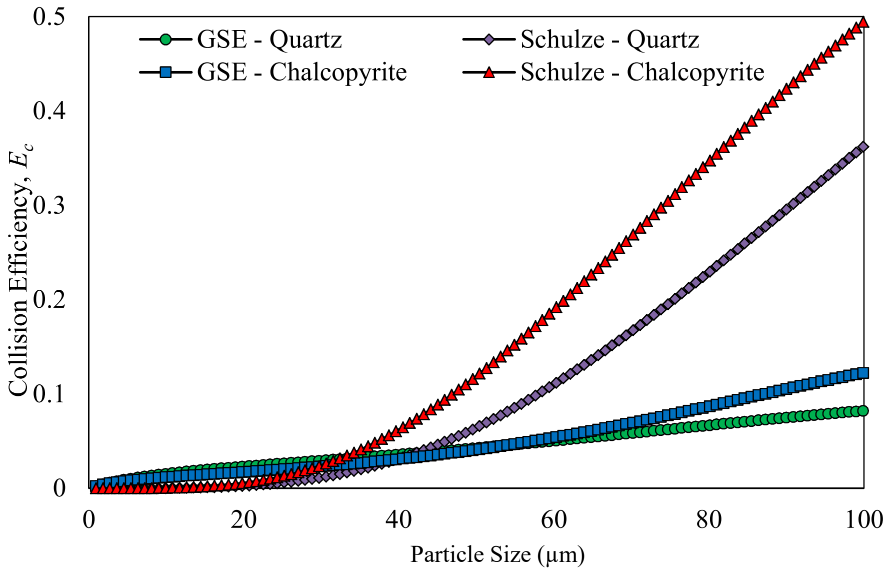


**Figure 4.1 :** Encounter probability of bubble with quartz and chalcopyrite parties calculated by both $E_c^{GSE}$ and $E_c^{SC}$ ($d_B$=1.2×10$^{-3}$m, $v_B$=31.6×10$^{-2}$m.s$^{-1}$).

Figure 4.1 also exhibits that Schulze model overestimates the particle-bubble encounter efficiencies for both minerals with a considerable enhancement in intermediate and coarse sizes. Moreover, it can be found that the predicted increase tendencies by $E_c^{SC}$ is relatively uniform for both minerals in the studied particle range. However, $E_c^{GSE}$ displays two separate areas at particle diameter of ca. 57µm.

Despite $E_c^{SC}$-quartz is high under this particle diameter; it becomes greater for chalcopyrite particles over this critical spot. This deviation clearly indicates the water density impact as an opponent force in counterbalancing the inertial forces in Dukhin's model where the chalcopyrite particle diameter approaches 57µm. Consequently, for the particles finer than 57µm, the particle-bubble encounter probability reduces by increasing particle density. In fact, particle deposition from the flow onto the bubble surface becomes weaker by diminishing particle diameter and a corresponding decrease in inertial forces and the St (Ralston et al., 1999). This reduction is mainly because of the negative effect of the water flow at the slip surface of air bubbles (Phong et al., 2009) which is in conjunction with the microhydrodynaic forces. While particle sizes increase, due to a larger St, the effect of water flow (negative inertial force) at the bubble surface is overcome by the particle inertial force (positive force).

On the other side, in the inertialess domain ($St<<St_{cr}$), the Ec is strongly varying by $d_B$ and $d_p$. In the case of inertial deposition ($St>>St_{cr}$), Ec depends on St itself. For intermediate particle sizes (40-60μm) which correspond to the closer $E_c$ values between quartz and chalcopyrite, the encounter probability needs to be considered as a function of both the St and particle/bubble diameters (Dai et al., 1998; Ralston et al., 1999). More specifically, a slight variation in inertial forces induces a substantial change in collision $E_c$ (Ralston et al., 1999). As shown in Figure 4.2, for particles coarser than 57μm, the influence of particle size and its density becomes more significant and correspondingly notable differences in Sts among the minerals become evident. When the Stokes number of particles is low, they follow the streamlines. However, when the Stokes number increases to a certain extent, particles gain sufficient momentum to deviate from the streamlines (Yoon et al., 1989). In other words, for coarser particles, the $E_c$ is mainly influenced by St, however, finer particles cannot resist the flow streams around the bubble due to their low momentum. For this reason, Stokes number is not a function in calculation of the $E_c$ in this region. In a similar context, Ralston et al., (1999) reported that for two mineral densities, the difference in the value of Stokes number for particles of the same diameters is possible.

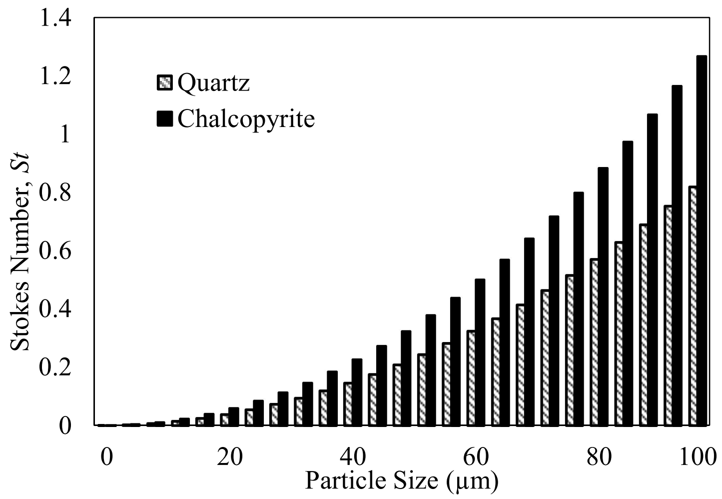


**Figure 4.2 :** *St* number versus particles size.

As noted previously, dimensionless number β is the ratio of $E_c^{SU}$ to the St (equation 1.10). By consideration of equation 1.9 in equation 1.10, it is almost evident that K3 and consequently St includes the inertial effects, whereas, the Sutherland equation characterizes the interceptional mechanism. Indeed, this coupling manifests the resistance influence of the inertial forces on the particle-bubble interaction (Dukhin et al., 1998).

Figure 4.3 displays the contribution of angle of tangency ($\theta_t$) versus dimensionless number β which is calculated based on equation 1.8. It is shown that θt increases with increasing β which in turn demonstrates the effect of St on the maximum collision angle. On the other side, β reduces by increasing St in the light of inverse relationship of β and St accordingly (Figure 4.4). By taking both Figure 4.3 and Figure 4.4 (equations 1.8−1.10) into accounts, one can anticipate a decrease in angle of tangency by increasing St as depicted in Figure 4.4. It is important to note that the St affects $\theta_t$ term through parameter β. This difference can be seen as a variation in slopes of Figure. 4.4 and Figure 4.5. Since this parameter comprises other functional features, this relation becomes essential for different particles with a variety of sizes, densities, and velocities (Equations 1.1 and 1.8−1.10).

Figure 4.3 presents the interval of $\theta_t$ for chalcopyrite and quartz while their particle sizes is in the range of 1−100μm. This discrepancy indicates why $E_c$ obtained for chalcopyrite is relatively lower than that for quartz in the case of finer sizes contrary to what is anticipated without taking the inertial forces into account (Figure 4.1).

It can be observed in Figure 4.3 when the $\theta_t$ approaches π/2 (bubble's equator), β increases (*i.e.* $\beta >> 1$). This contributes to a lower Stokes number (*i.e.* $St << 1$), as shown in Figure 4.4. These circumstances stand for inertialess conditions that is to say inertial forces do not interfere with the interceptional forces, which validates and prevails Sutherland equation (Dukhin et al., 1998). Under the opposite conditions (*i.e.* $\beta << 1$), $\theta_t$ varies away from the equator of the bubble (π/2) as clearly shown in Figure 4.3; it leads to an increase in St illustrated in Figure 4.4, which declines the interception and inertial impacts. Firouzi et al., (2011) using numerical techniques found that for retarded and unretarded bubbles, there is a critical set of particle diameter and its density where the $\theta_t$ is minimal. Comparing $E_c$ obtained from CFD and $E_c^{GSE}$ values showed that particle density has a very strong effect on the collision angle and its efficiency.

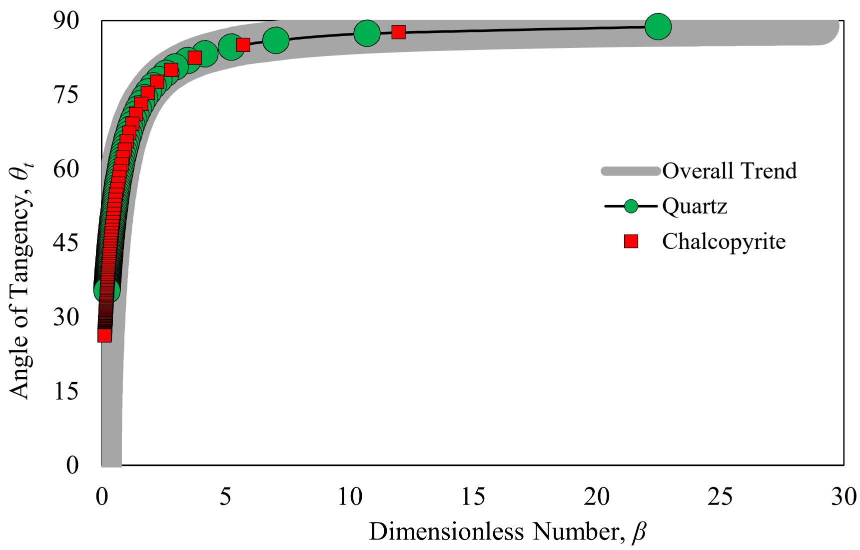


**Figure 4.3 :** Calculated tangency angle ($\theta_t$) versus dimensionless number ($\beta$) based on equation 1.8).

Combining results in Figure 4.3 and Figure 4.4, and Figure 4.5 it is clear that the chalcopyrite particles have lower $\theta_t$ and $\beta$, which is related to greater St in comparison with the quartz particles. The consequence of these figures can be summarized as below:

a) For particles finer than 57µm, $E_c^{GSE}$ of chalcopyrite is lower than that of quartz which is in connection with the smaller Stokes numbers (Figure 4.2). In other words, in this region the water inertial force (negative inertial effect) prevails particles to interact with bubbles which eventually results in reducing the $E_c$. It can be because of lower $\theta_t$ of chalcopyrite which corresponds to smaller effective collision area on the bubble surface.

b) For the particles coarser than 57µm, *St* is greater and the effect of particle density on particle-bubble attachment/detachment process becomes significant which can counterbalance the water inertial forces. Therefore, positive effect of inertia (particle inertial force) overcomes the negative effect (water inertial effect). This term is excluded in $E_c^{Sc}$ which causes an overestimation of particle-bubble encounter efficiency approximately 2-4 times.

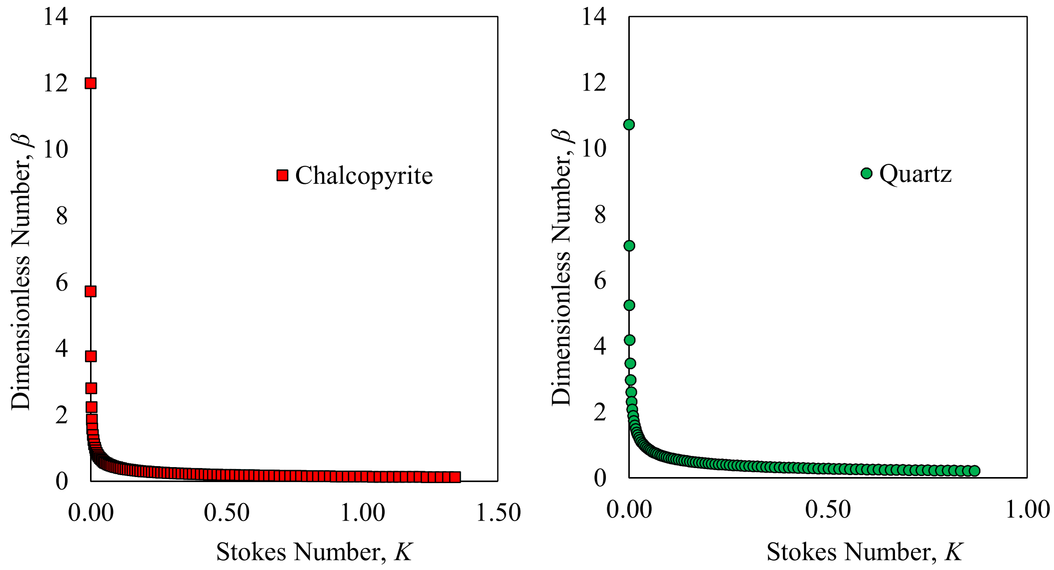


**Figure 4.4 :** Dimensionless number ($\beta$) as a function of *St* number obtained for quartz and chalcopyrite.

### 4.2 Particle Density's Role On Schulze Collision Model

Both $E_c^{GSE}$ and $E_c^{SC}$ assume that the Ec is dependent on St under inertial deposition given in Equations 1.7 and 4.1. Thereby, the present study focuses on the role of Stokes (St) and critical Stokes ($St_{cr}$) numbers. The $St_{cr}$ for quartz and chalcopyrite for specific bubble and particle features is given in Figure 4.4 which is falling in the particle sizes of ca. 43µm and 30µm, respectively. As known (Dai et al., 2000) beyond these values, the mechanism of particle-bubble encounter is different. As presented in Figure 4.1, $E_c$ for quartz particles by $E_c^{SC}$ overcomes that using $E_c^{GSE}$ for the particles coarser than 43µm. This is the threshold point where exactly St becomes higher than Stcr and inertial impact sets off to become effective (Hassanzadeh et al., 2016). However, for chalcopyrite the interrelation of $St>St_{cr}$ falls in for the particle size exceeding 30µm. Also, it is reported by Dai et al., (1998) that below and above the Stcr, the negative and positive effects of the inertial forces respectively become dominated effects on the particle-bubble interaction.

Nowadays, it is broadly known that at $St<<St_{cr}$, $E_c^{ic}$ is the main mechanism for the particle-bubble encounter interaction as the particles moving along the streamlines of the fluid (Dai et al., 1998; Ralston et al., 1999, Dai et al., 2000). In this case, the $E_c^{SU}$ (equation 1.11), can be the simple and relatively appropriate approach for calculating the $E_c$. The reason is attributed to the impact of inertial forces which can be neglected

and the $E_c$ simply depends on $d_p$ and $d_B$ (Dukhin et al., 1977). The same conclusion can be achieved in Figure 4.1 where both models provide approximately the same results for quartz and chalcopyrite particles finer than 45µm and 35µm, respectively.

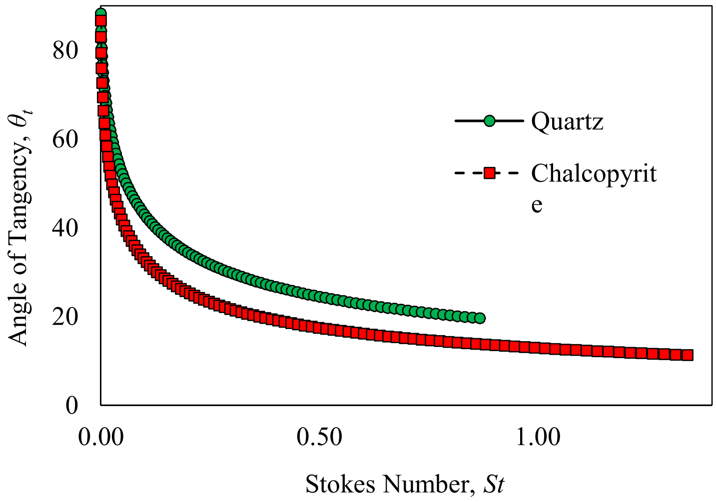


**Figure 4.5 :** Calculated angle of tangency ($\theta_t$) for quartz and chalcopyrite particles on the basis of Equations 1.8-1.10.

### 4.3 Incorporation Of $E_c^{SC}$ Into GFK

Figure 4.6 represents a characteristic plot of both original and modified flotation rate constants vs. particle size. As seen, the famous elephant curve for the kinetic rate versus particle size is evidently seen with different variances. Moreover, intermediate particle size class for almost all configurations exhibits the maximum flotation rate constant. Dropping k for finer and coarser particles is applicable with the lower $E_c$ and $E_a/E_s$, respectively (Pyke et al., 2003).

Although the flotation rate constant for fine particle sizes becomes zero till 25µm for both mineral species using the modified model, it never reaches zero in the original model even for ultra-fine particles. This is the particle range that the modified model yields superior results by producing very low rate constant as reported in some studies (Traher and Warren 1976; Pease et al., 2005).

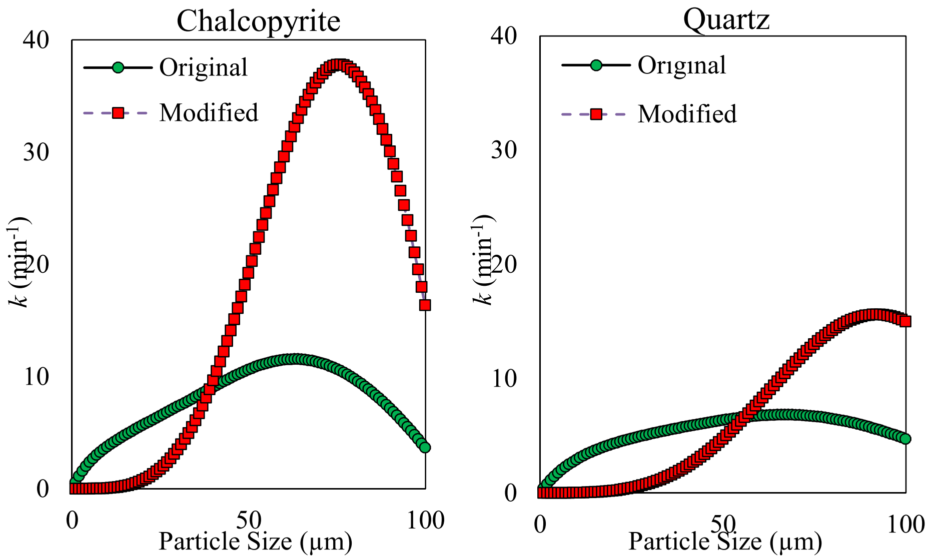


**Figure 4.6 :** Quartz and chalcopyrite's flotation rate constants as a function of particle diameters for original and modified models ($d_B = 1.4\times10^{-3}$ m, $v_B = 18$ cm/s, $\varepsilon = 38$ m$^2$/s$^3$, $\theta = 80°$, $G_{fr} = 3.5\times10^{-3}$ m$^3$/min).

Modified flotation rate constants calculated for quartz and chalcopyrite minerals reach maxima within the particle size of 90µm and 75µm, respectively. For the original model, however, the corresponding values are 68µm and 62µm, respectively. Thus, the comparison of the two models for both minerals reveals that the modified model overestimates the values for coarser particle sizes. Also, both models yield relatively greater values for chalcopyrite. The intersection of these models for chalcopyrite and quartz takes place at 40µm and 55µm, respectively; these points disclose two areas for each mineral where the two models display different outcomes. While below these critical points modified model underestimates the k values for the ultra-fine particles, above them it predicts k more than the expected value which is provided by original model. Interestingly the modified model estimates the rate constant close to zero for particles below 15µm and 20µm for chalcopyrite and quartz, respectively. It can be found that the effect of particle and water inertial forces in both models is relatively crucial and still not very clearly addressed in the literature as the flotation rate constant in each case drops significantly for different size classes. As a consequence, accurate prediction of the flotation rate constant by analytical methods can be obtained by incorporation of the all inertial aspects of particle and water in flotation system.

The role of particle density on k is shown in Figure 4.7 for quartz, chalcopyrite and galena (7.4g/cm$^3$). As the density of particles increases, which refers to an increase in inertial forces and St, the k value substantially rises especially for intermediate galena particles. The k value of modified flotation model apparently has two diverse functions on below and above 25µm. While, modified equation suppresses the k below 25µm, it leads to an overestimation of particles above this size.

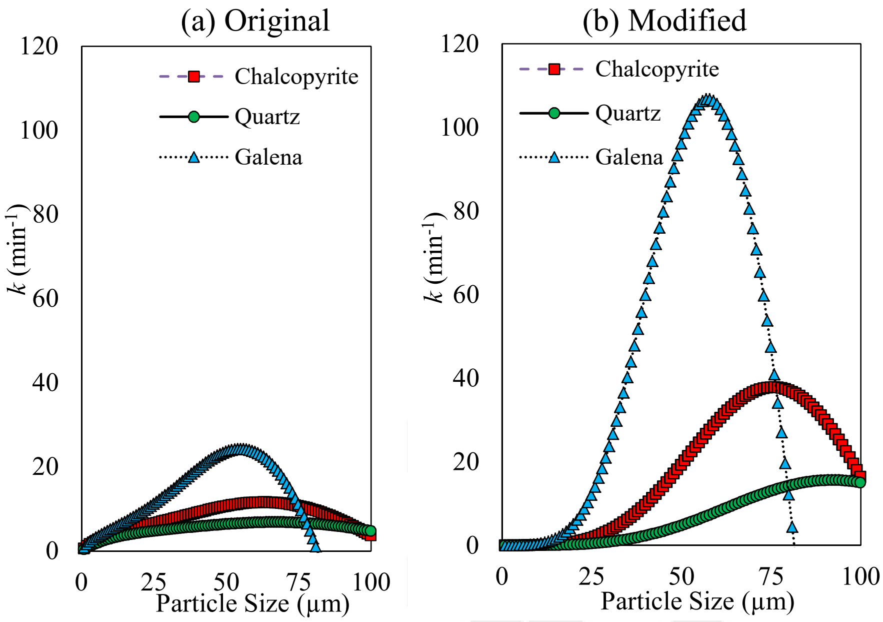


**Figure 4.7 :** Predicted flotation rate constants for quartz, chalcopyrite and galena under a certain condition as $d_B$=1.2×$10^{-3}$m, $v_B$=18cm/s, $\varepsilon$= 38$m^2/s^3$, $\theta$=80°, $G_{fr}$=3.5×$10^{-3}$ $m^3$/min.

Abandoning the negative inertial impact on Ec for coarser particles apparently creates a poor prediction of k in the modified equation. The $E_c^{GSE}$ properly includes both positive and negative inertial effects, which provides comparabily better k values. Evidently, by incorporation of inertial effect, k values for fine (<25µm) and intermediate/coarse (>25µm) respectively increase and decrease. Another key point is whether to consider of angle of tangency in this model. Furthermore, this model enables to tackle the issue of varying specific gravity of minerals during particle-bubble interactions. In other words, $E_c^{SC}$ provides a better response to the changes of the particle density compared to that with $E_c^{GSE}$.

Figure 4.8 shows the effect of bubble diameter on the k. It can be shown that increasing the bubble diameter results in an increase in the k-value of coarse particles. A plunge in k-value of fine particles is related to increasing bubble diameter leading to low Ec-value (Ahmed et al., 1985; Hassanzadeh et al., 2015). Contrarily, improving k-value of coarse particles with increasing the bubble diameter corresponds to the increasing Ea-value which is influenced by the increasing adhesion angle of coarse particles on bubble (Kouachi et al., 2010). A detailed study on evaluation of the k-value as a response of hydrodynamic parameters including dB is presented in chapter 6.

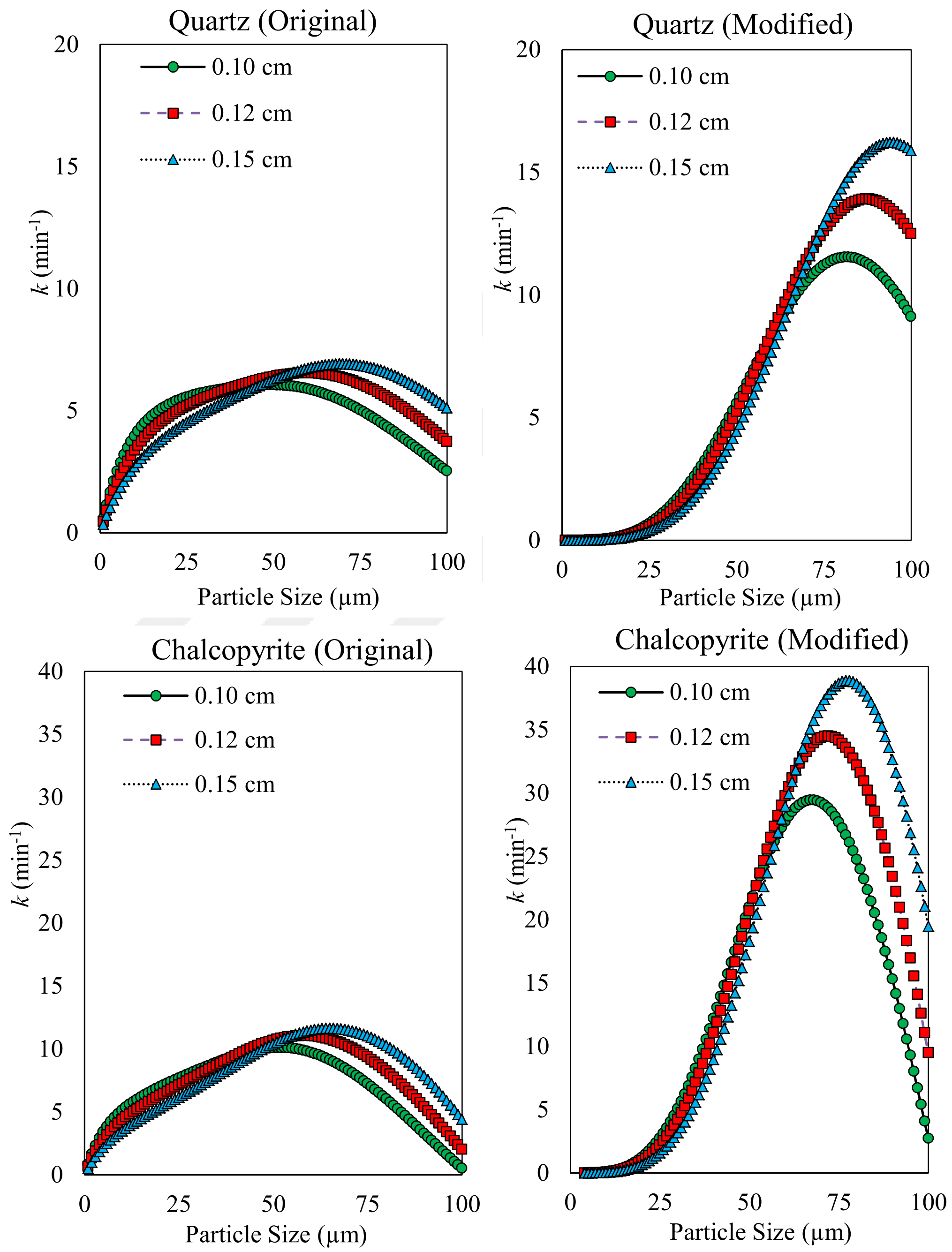


**Figure 4.8 :** Flotation kinetic rate obtained for quartz and chalcopyrite in the presence of bubble sizes of 0.10, 012 and 0.15cm ($v_B$=18cm/s, $\varepsilon$=38m$^2$/s$^3$, $\theta$=80°, $G_{fr}$=3.5×10$^{-3}$).

Figure 4.8 clearly displays the differences between the GFK model and its modified version. Apparently, the effect of $d_B$ becomes more significant for fine particle using GFK model compared to the modified one. The calculated k-value approaches zero below 25μm and 20μm for quartz and chalcopyrite, respectively. Indeed, these size classes are the intervals where inertial effects have greater impacts on flotation rate constants.

The maximum value obtained for k at intermediate particle size (50μm) for the GFK is in agreement with the experimental results reported by Pyke et al. (2003). Though, the obtained maximum k values using the modified model for coarse particles reveals some discrepancy with the results of Duan et al., (2003). The effect of increasing $d_B$ on the modified model discloses that there is a serious disagreement between the outcomes of theoretical and experimental data for larger bubble sizes. This might be ascribed to neglecting the particle and water inertial effects on k. This deviation which is found for the particle range studied (1-100μm), it can be used for quantitative incorporation of inertial force on the k.

Figure 4.9 shows the effect of $v_B$ on the k. As seen, an improvement on $d_B$ induces a considerable reduction in the k-value of coarse particles. Indeed, increasing $v_B$ only has a slight influence on $E_c$ but a substantial impact on $E_a$ and $Z_{pb}$, particularly for coarse particle sizes (Dai et al., 1998; Hassanzadeh et al., 2016).

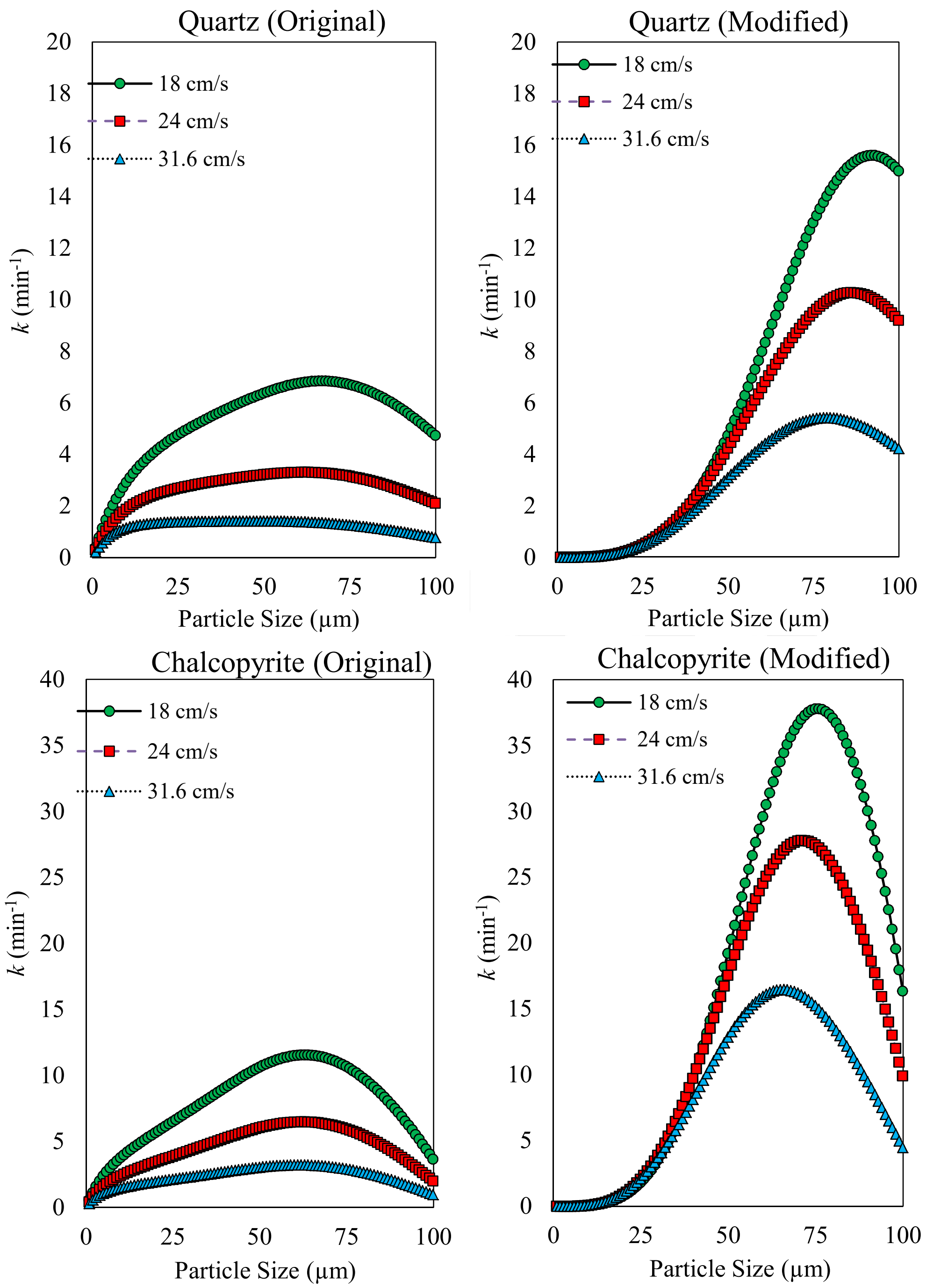


**Figure 4.9 :** Calculated $k$ values *vs.* quartz and chalcopyrite particle sizes for bubble velocities varying as 18, 24 and 31.6cm/s ($d_B$=1.2×10$^{-3}$m, $\varepsilon$=38m$^2$/s$^3$, $\theta$=80°, $G_{fr}$=3.5×10$^{-3}$ m$^3$/min).

Other than above, a profound comprehension of effective variables on flotation kinetic constant and its sub-processes in different scales may contribute to elaboration of a comprehensive flotation model. Evaluation of the results, suggest that the flotation kinetic model obtained from here requires re-consideration using up-scaling technique based on dimensional similitude and cell conditions applying different scales (from nano to industry) and taking advantage of computational fluid dynamic (CFD) method. This approach will allow researchers to create relatively similar conditions within the flotation cells on lab, pilot and industrial scales utilizing the dimensionless numbers such as Stokes (St), Reynolds (Re), Webber (We), Eotvos, Froude (Fr), Bond (Bo), Morton (Mo) and Tadaki (Ta) numbers as well as bubble surface area flux ($S_b$) and interfacial area of bubbles ($I_b$). For instance, the influence of particle density and bubble rising velocity can be simply discussed by two dimensionless numbers as Stokes ($K_{st} = \frac{\rho_p v_b d_p^2}{9\,\eta\,d_b}$) and bubble Reynolds ($Re_b = \frac{v_b \rho_f d_b}{\eta}$) numbers which is discussed in chapter 6. Also, more detail information concerning the dimensionless numbers can be found elsewhere (Truter, 2010)

## 4.4 Effect Of Particle Settling Velocity

Figure 4.10 demonstrates the effect of particle settling velocity as a function of particle size for both quartz and chalcopyrite. As mentioned previously, several models were applied to calculate the particle terminal velocity including Nguyen, Stokes, Oseen and Bruce models. Obviously, with increasing particle size, terminal particle settling velocity enhances which in turn leads to rising the collision probability. Also, it can be seen that the results obtained from different Equations in the particle range of 1-80µm for quartz are approximately same. However, above 80µm, a slight deviation can be observed among the models. The only exception is the values from Oseen and Bruce models which produced almost the same trends. Following this, the deviation between the settling velocities of the models starts from 60µm particle size rather than 80µm. Nevertheless, the particle settling velocity does not significantly change for particles finer than 20µm. In this range of particle size not only increasing particle size but also rising particle density from 2.6g/cm$^3$ to 4.1g/cm$^3$ demonstrate no difference on particle settling velocity.

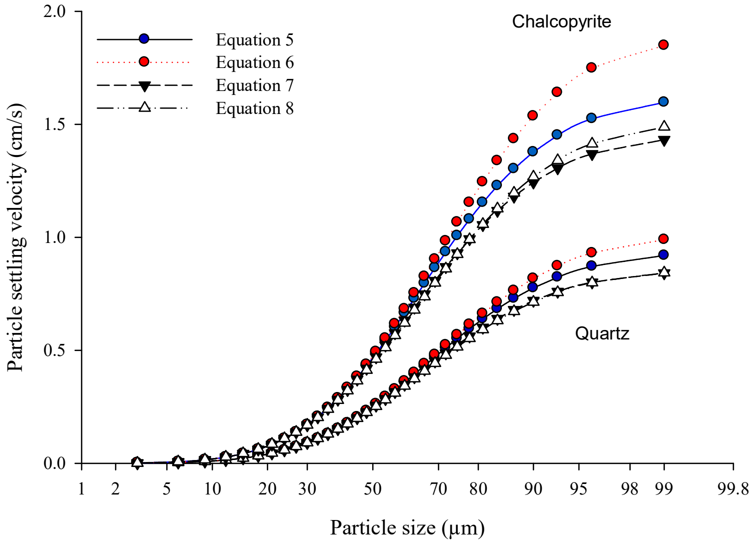


**Figure 4.10 :** Collision efficiency model as function of particle diameter: (a) Afruns-Kitchener model for chalcopyrite, (b) Afruns-Kitchener model for quartz, (c) Nguyen-Kmet model for chalcopyrite and (d) Nguyen-Kmet model for quartz ($d_B = 0.12$ cm, $v_B = 26 \mathrm{cm/s}$).

It can be claimed that, the particle settling velocity is profoundly effective at increasing particle diameters and particle densities. As seen, the results obtained using each model, the terminal settling velocity of chalcopyrite for a given particle size is greater than that for quartz. It clearly indicates the influence of specific gravity on particle settling velocity and collision efficacy. Furthermore, for both mineral types, the particle settling velocity results obtained from Stokes and Oseen models exhibit the maximum and minimum values, respectively. In addition, it is worth to note that equations 5 and 6 are more influenced at higher particle densities compared to the other parameters. As stated by Nguyen (1997) the prediction by the Oseen law is smaller than that by the Stokes law with a factor of $\frac{2}{1+\sqrt{1+Ar/24}}$.

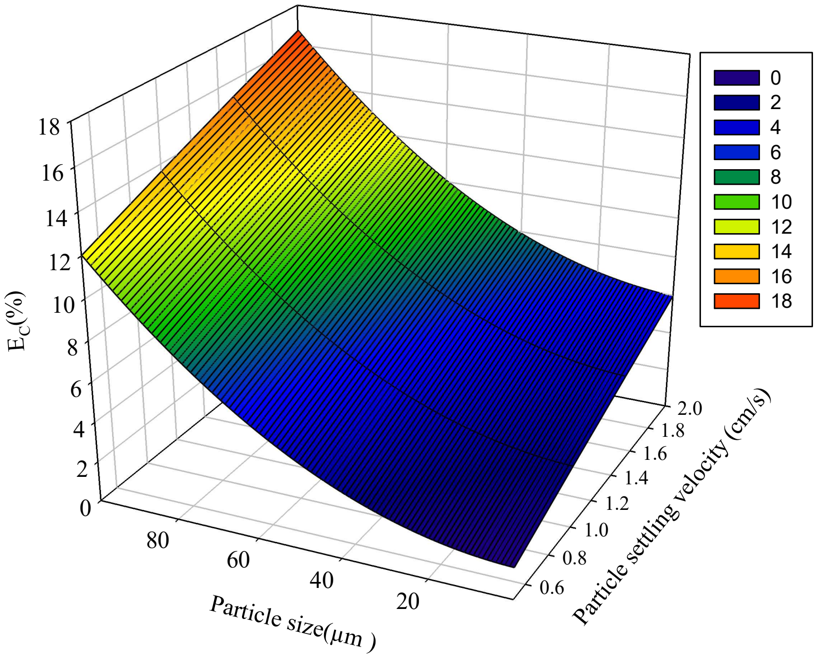


**Figure 4.11 :** Collision efficiency as a function of particle settling velocity and particle size using quartz particles and Afruns-Kitchener model ($d_B$ = 0.12cm, $v_B$ =31cm/s).

Figure 4.11 displays the collision efficiency as a function of particle settling velocity ($V_S$) and particle size ($d_P$) using quartz particles in the range of 1-100µm. The graph can be divided into three main sections including low $E_c$ zone (0-6%), intermediate zone (6-10%) and high zone (10-18%). The predominant section of the graph is apparently devoted to the $E_c$ values between 0-6% (low zone). For intermediate particle sizes with higher particle settling velocities, the $E_c$ rises up and reaches to the 6-10% (intermediate zone). Finally for coarse particles (>80µm) with the maximum particle terminal velocities (>1.5cm/s), the $E_c$s are in the highest domain and their values are in the range of 10-18% (high zone).

It can be claimed that for coarser particles, at constant the particle size is constant while the particle settling velocity enhances, wherease the $E_c$ increases sharply. For instance when the particle size is 60µm, when terminal particle settling velocity is 0.5cm/s, the $E_c$ equals to 1.46%. However, upon increasing the particle settling velocity from 0.5 cm/s to 1 cm/s, the $E_c$ significantly rises up from 1.46% to 7.17%. This considerable change cannot be observed for particles of settling velocities greater than 1cm/s. In this regard, Duineveld (1995) theoretically and experimentally showed that the hydrodynamic resistance increases with respect to the bubble surface deformation. Also, at rather high Reynolds numbers the terminal velocity decreases with increasing the bubble dimension. Naturally the bubble shape deformation arises earlier than the decrease in terminal velocity. In fact, it manifests itself in the retardation of the terminal velocity increase and its dependence on bubble dimension. In on other study by Chen and Stebe (1996), the theory of Marangoni retardation and bubble terminal velocity was improved by considering the physicochemistry of the surfactant in parallel with a more exact solution of the hydrodynamic problem. They found that, beyond the critical concentration, a bubble can reach to a constant terminal velocity independent of the surfactant concentration.

# 5. EFFECT OF BUBBLE PROPERTIES ON $E_c$

## 5.1 Evaluation Of Bubble Size Measurement Techniques

Bubble size can be measured using several approaches such as visualization technique (*i.e.*, photographic and image analysis) (Sam et al., 1996; Chen et al., 2001; Grau and Heiskanen, 2002; Soler et al., 2003; Gaillarda et al., 2015), conductivity probes (Yasumishi et al., 1986; Barigou and Greaves, 1992), interactive iterative approach (Yianatos et al., 1988; Xu and Finch 1990) drift flux analysis (Dobby et al., 1988; Banisi and Finch, 1994), capillary probes (Barigou and Greaves, 1992 a,b; Alves et al., 2002), liquid scattering (Vera et al., 2001), phase doppler anemometry (Schafer et al., 2000; Kulkarniet al., 2001), optical sensors (Randall, et al., 1989; Leifer et al., 2003), LTM-BSizer (Rodrigues and Rubio, 2003) and acoustic technique (Chu et al., 2016). These techniques are classified depending upon their operating principles. Each method has some drawbacks limiting its utility. Table 5.1 demonstrates different bubble measurement systems (BMSs) manifesting their difficulties. Other infrequently used methods are discussed elsewhere (Rodrigues and Rubio, 2003; Karimipour and Pugsley, 2011). Nevertheless, nowadays it is widely accepted that University of Cape Town (UCT), Helsinki University of Technology (HUT) and/or McGill bubble size analyzers (MBSA) are typically used to measure bubble diameter in both industrial and batch conditions with a reasonable accuracy. Hernandez-Aguilar et al., (2004) established a very useful outline in terms of comparison between UCT and MBSA outcomes. Miskovic (2011) also presented detailed explanations on methods of bubble size measurements.

**Table 5.1 :** A review of bubble size measurement approaches.

| Method | Drawback(s) |
|---|---|
| **Visualization technique** | Strong mismatching of the refractive indices between bubbles and water<br>Automatic sizing through image analysis routines have not been extensively implemented due to the common practical and fundamental problems associated with this method.<br>The impact of the inherently variant distance between the focus plane and the bubble. |
| **Optical probes** | Optical probes can be used only in transparent systems and at low gas holdup. Also, the use of optical probes in a three phase system is also considered problematic. |
| **Isokinetic collection probes** | Bubbles smaller than the capillary diameter cannot be transformed into slugs. Reducing the capillary size further may cause bubble breakup at the point of bubble entry and risk of the probe blockage increases as the capillary size decreases. |
| **Conductivity probes** | Bubbles that are rising in a direction not aligned with the two probes lead to major errors which seriously limits use of the probe in turbulent flow fields.<br>It's not applicable if the bubbles are not spherical and too small (<6 mm) |
| **LTM-BSizer** | This approach is applicable only when the liquid-phase is translucent.<br>liquid-gas mixture is withdrawn from the dispersion in some cases. |
| **Acoustic technique** | Complexity of the system while the number of bubbles increase. |
| **Phase doppler anemometry** | Edge and slit effects as well as unwanted scattering modes caused by the trajectory |
| **Capillary probes** | Bubbles smaller than the capillary diameter are not converted into slugs and cannot be identified reliably<br>Low liquid viscosity is also required. |

## 5.2 Role Of Bubble Size On Particle-Bubble Encounter

Comparison of all analytical encounter models and evaluation of the literature data with respect to predicting the Ec convinced us to use $E_c^{GSE}$ for evaluating the effect of $d_B$ on $E_c$. The quantitative data for further works was relied on the practical maximum velocity of bubbles with different diameters in tap water reported by Sam et al., (1996). Following this, $d_B$ was chosen as three levels including 0.08, 0.12 and 0.15cm.

Figure 5.1 displays the impact of $d_B$ on the $E_c$ using $E_c^{GSE}$. Generally speaking, coarse particles reach greater Ecs at all three bubble diameters. It should be noted that the constant particle density in this Figure enables us analyzing the bubble diameter effect. Also, it can be found that $E_c$ of chalcopyrite particles decreases for all sizes upon increasing $d_B$ from 0.08 to 0.15cm at all bubble velocities. The reason might be attributed to the mobile behavior of a single bubble as shown by (Sam et al., 1996). When $d_B$<0.12cm, bubbles follow almost in straight line in a flotation cell while for $d_B$>0.12cm, they start fluctuation and moving in a zigzag form along the cell. This indeed changes bubbles orientation, which directly influences the probability of particle-bubble encounter.

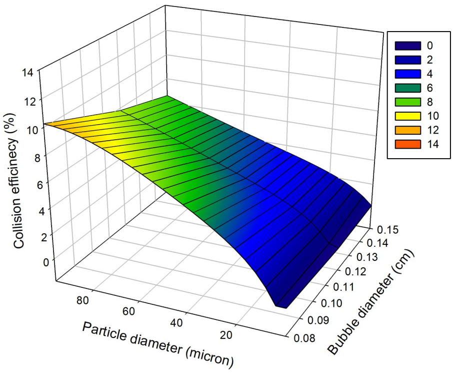


(a)

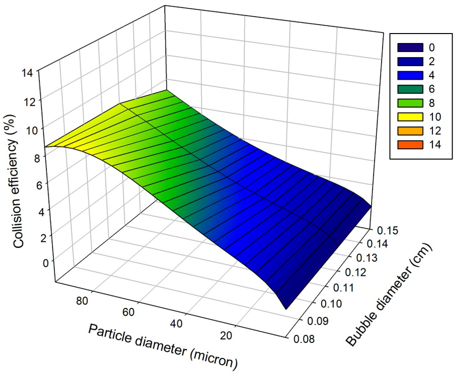


(b)

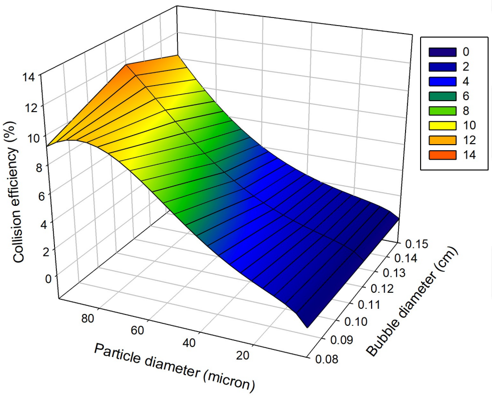


(c)

**Figure 5.1 :** Particle-bubble encounter efficiencies predicted by Dukhin's model demonstrating the role of bubble diameter at three levels.

Figure 5.1a illustrates the $E_c$-values as a function of $d_B$ with a stationary $v_B$=10cm/s for the particle sizes in the range of 1-100μm. According to the trend of data, Ec is categorized in three main zones *i.e.* low (0-4%), intermediate (4-8%) and high (8-14%) zones. This classification simplifies the evaluation and interpretation of the data versus $d_B$ and $v_B$. As seen, $E_c$ firstly rises with increasing particle size at a very high rate to certain extend and subsequently the rate keeps constant. The maximum $E_c$ (8%) obtained at $v_B$=10cm/s and $d_B$=0.08m for the particles finer than 60μm.

It is now well-known that fine particles can achieve greater $E_c$ in the presence of micro and nano-bubbles. This can be concluded in demonstrations shown in Figure 5.2. It exposes that the probability of encountering fine particle sizes with small bubbles is greater than that with large bubbles. This is in absolute agreement with the results of Tao (2004). However, it should be also noted that the bubble surface mobility and degree of contamination plays a very significant role on the phenomenon that is also a function of bubble size and consumed agent dosage. Bubble surface might be retarded either by chemical reagents in the medium *i.e.* collector, frother, dispersant, pH regulator and depressant or by adsorption of the impure ions existing in water composition.

In this regard, Shahbazi et al. (2010) experimentally measured $E_c$ for quartz particles with the sizes of 20, 30, 40, and 50µm in a Denver flotation cell. The calculated results under potential fluid regime of quartz yielded values in the range of 4.48−23.44%. However, according to impossibility of isolating the sub-processes from each other their outcomes do not identify each interaction separately for a given vB, dB and dp which is studied in detail in this section of the work.

Figure 5.1b displays the $E_c$ as a function of $d_B$ while $v_B$= 20cm/s. When $d_B$=0.08cm, the $E_c$ for fine particles (<20µm) and coarse particles (>70µm) respectively increases and decreases with a steeper slope change. However, for intermediate particle sizes (20µm <$d_p$<70µm) this parameter exhibits with a linear slope. The maximum $E_c$ for coarse particles is obtained in the hydrodynamic condition of $v_B$=20cm/s and $d_B$=0.12cm which is exactly related to bubble motion as a function of its size. Keeping this in mind, a schematic view in Figure 5.2 shows the effect of bubble diameter and its motion in a liquid phase demonstrating the role of bubble size and its velocity on the particle-bubble encounter interaction.

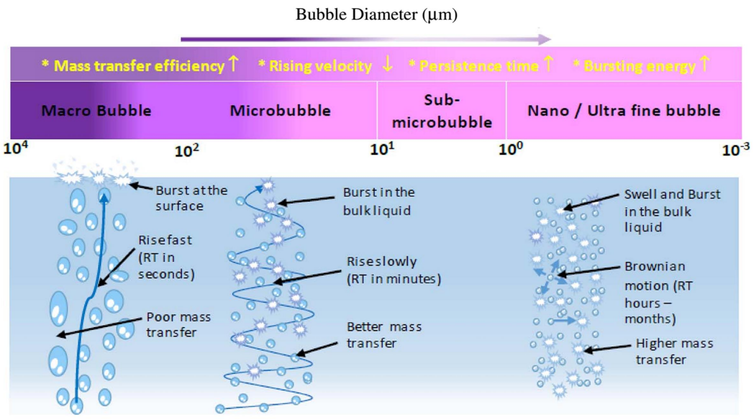


**Figure 5.2 :** Bubble movement based on its size and velocity.

Figure 5.1c exhibits the role of $d_B$ on $E_c$ for chalcopyrite particles at $v_B$=30cm/s. Evidently, the low zone of $E_c$ (0-4%) predominantly occupies the graph. Sparking of this zone, while $d_B$=0.12cm and 0.08 cm respectively, $d_p$<45µm and 40µm fall in this zone. It can be concluded that at $v_B$=30cm/s, the probability of particle ($d_p$=60µm) encountering with a bubble ($d_B$=0.15cm) is equivalent to a corresponding value of $E_c$ with $d_p$=45µm and for $d_B$=0.12cm and $d_p$=30µm and $d_B$=0.08cm. By comparing the Figure 5.1a, b and c, it can be asserted that when $v_B$= 30cm/s, the low zone is the most predominant part. Also, $E_c$ obtained for $v_B$=30cm/s compared with $v_B$=10 and 20cm/s is the minimum for the particle size range of 1-60µm.

### 5.3 A New Suggestive Criterion

After a careful evaluation of both $d_B$ and $v_B$ on $E_c$, a requirement for a novel ratio containing both terms was found essential. Thereby, a ratio is defined for obtaining $E_c$ by consideration of two bubble diameters, for example, 0.08 and 0.15cm. Figure 5.3 shows that for particles finer than 65µm, the index for bubble velocity of 30cm/s is the maximum. It declines substantially for particles coarser than 65µm. However, when the $v_B$ is the minimum (10cm/s), the suggestive index goes through a relatively broad maximum until $d_B$=65µm. It implies for intermediate class encountering with bubbles of 10cm/s velocity, the $E_c$ for the $d_B$=0.08cm is 1.9 times greater than the case of $d_B$=0.15cm. This rate is approximately 2 and 2.1 for the $v_B$=20 and 30cm/s, respectively. As seen in Figure 5.3, when $d_B$=0.08 and 0.15cm and bubble velocity is varying at lower levels, $E_c$ remains relatively constant for a wide range of particle size. When $v_B$ rises up to 20 and 30cm/s, for the particles of below 65µm, the smaller the bubble is the greater $E_c$. With respect to coarser particles (above 65µm) bubbles of 0.15cm show better performance in collision. One feasible cause for poor $E_c$ of ultrafine particles might be the low mass and required momentum for rupturing the bubble film.

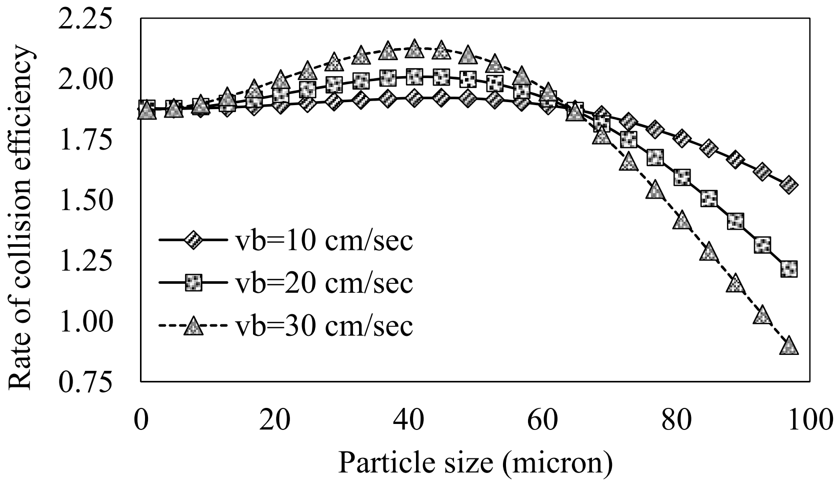


**Figure 5.3 :** An index for assessment of $E_c$ in the presence of various bubble velocities.

Table 5.2 presents the cumulative $E_c$ for ultra-fine particles with respect to selected $d_B$ and $v_B$ using $E_c^{GSE}$ and $E_c^{Sc}$. As seen the max. value (3.65%) can be obtained in the presence of $d_B$=0.08 and $v_B$=20cm/s. As a general trend, in the presence of a fixed $v_B$, by increasing the $d_B$ the $E_c$ rises up. A detailed explanation can be found elsewhere (Hassanzadeh et al., 2016).

**Table 5.2 :** Cumulative particle-bubble encounter probability for ultra-fine chalcopyrite particles as a function of bubble diameter and its velocity.

| Model name | GSE bubble velocity (cm/s) | | | Schulze bubble velocity (cm/s) | | |
|---|---|---|---|---|---|---|
| Bubble diameter (cm) | 10 | 20 | 30 | 10 | 20 | 30 |
| 0.08 | 2.20 | 3.65 | 3.10 | 0.15 | 0.1 | 0.13 |
| 0.12 | 1.25 | 2.42 | 2.06 | 0.17 | 0.07 | 0.08 |
| 0.15 | 2.32 | 1.94 | 1.64 | 0.05 | 0.04 | 0.03 |

### 5.4 Role Of Bubble Velocity On Particle-Bubble Encounter

To study the effect of $v_B$ on the $E_c$, the $v_B$ was chosen at three levels *i.e.* 10, 20 and 30cm/s due to the bubble terminal velocity in the presence of chemical reagents (Sam et al., 1996). An effective factor in this regard is $\theta_t$ changing versus $v_B$ (Figure 5.4). As seen a reduction in $\theta_t$ is obvious as a function of $v_B$ which is in connection with reducing the maximum possible collision angle. Consequently, reducing $\theta_t$ leads to a sudden reduction of possible free area for particles that in turn decreases the encounter probability with bubbles. In a very similar trend, Vaziri Hassas et al. (2016), experimentally found that the $\theta_t$ demonstrates a notable effect on $E_c$ and $E_a$.

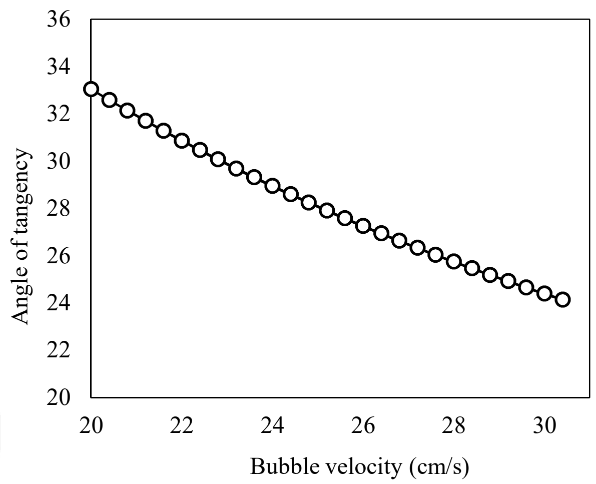


**Figure 5.4 :** Angle of tangency as a function of bubble velocity for 80µm chalcopyrite particle.

The effect of $v_B$ on $E_c$ *vs.* $d_p$ is shown in Figure 5.5a. As clearly can be observed for particles coarser than 80µm, minimum $E_c$ at $d_B$=0.08cm is obtained when $v_B$ is 20cm/s. However, $E_c$ faces a reduction of *ca.* 10% when $v_B$=10 or 20cm/s. It can be stated that the low zone is mainly covered by $d_p$<40µm but it falls into the range of $d_p$<25µm if $d_B$=0.08cm. This finding is in good agreement of theoretical and experimental reports of Yoon and Luttrell (1989) and Jameson (2010) in terms of the role of bubble size and its velocity in flotation cells. Generally speaking, fine particles follow the stream lines during their encounter with bubbles with respect to their low mass and momentum (mass and density). While, coarse particles have a good affinity to deviate from the streamlines for colliding with bubbles. However, in this sense, distinguishing the size and density effects is relatively hard which was argued in chapter three.

Interestingly, it can be seen in Figure 5.5b that for coarse particle sizes, the particle-bubble encounter probability can reach to values greater than 12% if $v_B$=30cm/s. the main reason can be contributed to the interceptional effect presented in chapter 1. In this context, Kouachi et al., (2015) reported that while dp>50µm, the interceptional component is the main mechanism of reaching maximum Ec.

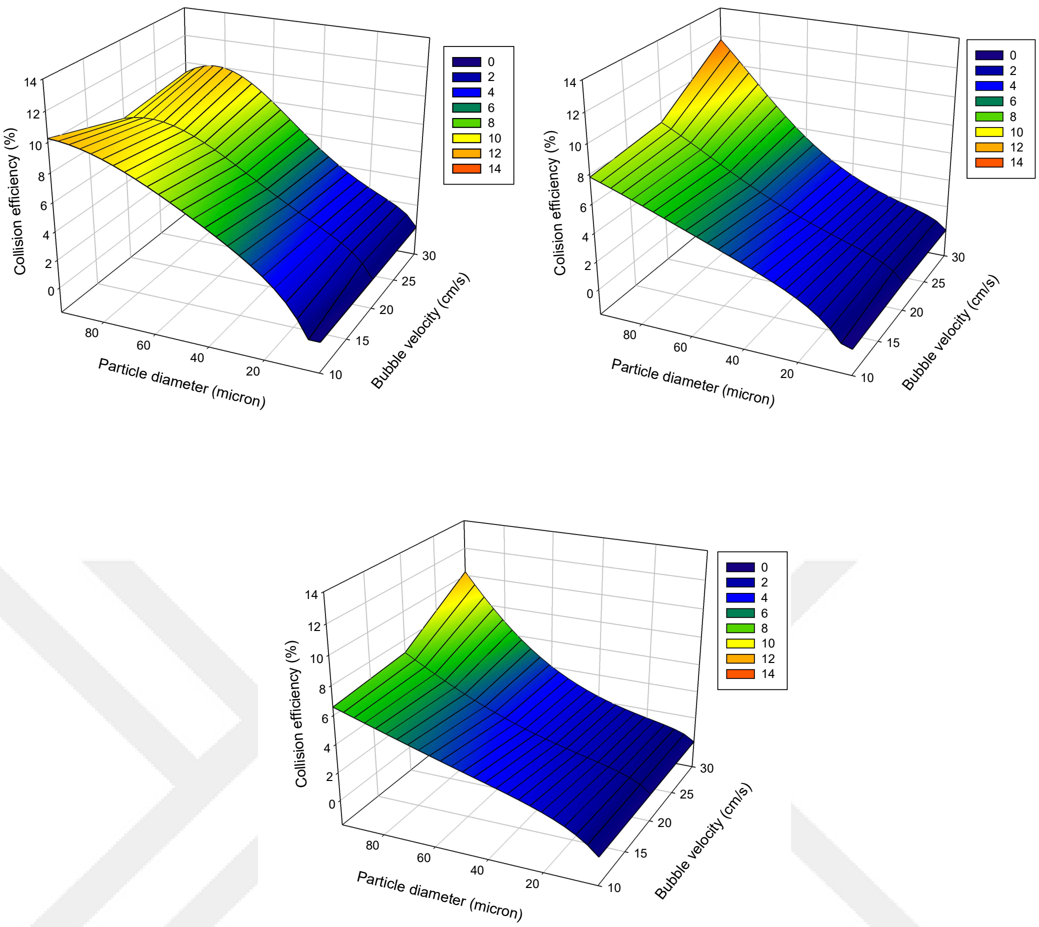


**Figure 5.5 :** Role of $v_B$ in particle-bubble encounter interaction at three levels of bubble diameters; (a) 0.08cm, (b) 0.12cm and (c) 0.15cm.

By taking both Figure 5.4 and Figure 5.5 into our account with respect to $\theta_t$, $d_B$ and $v_B$, $E_c$ is reduced upon rising the $v_B$ due to surface availability of bubbles. In this regards, Verrelli et al. (2014) pointed out that tind drops down from 200ms to 100ms owing to reduction of $\theta_t$ which considerably influnces $E_a$ and consequently $E_c$. An increase in $d_B$ causes reduction of $E_c$ at lower $v_B$ but the rate remains constant thereafter (Figure 5.5b and Figure 5.5c).

## 5.5 Stokes Critical Number's Impact On Particle-Bubble Encounter

Undoubtedly, the particle size is one of the most effective parameters on particle-bubble interactions, flotation rate constant and ultimate grade-recovery curve (Trahar, 1981; Xian-ping et al., 2011; Hassanzadeh et al., 2015; Azizi et al., 2015). St and G numbers can be very good indices for showing the effect of particle size

(Flint and Howarth, 1971) along with the role of viscous and inertial forces. These dimensionless numbers can be expressed as below:

$$St = \frac{\rho_p {d_p}^2 V_B}{9\mu d_B} \tag{5.1}$$

$$G = \frac{(\rho_p - \rho_f){d_p}^2 g}{18\mu V_B} \tag{5.2}$$

where all the terms were introduced in previous formulas.

By taking the selective ranges of $d_B$ and $v_B$ together with equation 5.1 and equation 5.2 into consideration, Table 5.3 was established for the purpose of showing the threshold with chalcopyrite particles where the inertial force sets off to be effective for a given $d_B$ and $v_B$. For this reason, the $St_{cr}$=0.1 is considered as the main criterion for this classification. According to the concept of these both formulas, the Table presented can be used for identification, effectiveness, and ineffectiveness of the particle inertial effect in the relevant range of bubble sizes and velocities. It can be also concluded that St is reduced upon increasing $d_B$ leads to increase in $E_c$ for fine particles if $d_B$ is low enough. Basically, for a constant $d_B$ (*e.g.* $d_B$=0.12cm), rising the $v_B$ from 10cm/s to 30cm/s induces the particle inertial effect for fine particle more significantly.

**Table 5.3 :** Obtained chalcopyrite particle diameters in the vicinity of critical Stokes number (*St*=0.1) and variation of bubble properties.

| | | $v_B$ (cm/s) | | |
|---|---|---|---|---|
| | | 10 | 20 | 30 |
| $d_B$ (cm) | 0.08 | 41μm | 29μm | 25μm |
| | 0.12 | 49μm | 37μm | 25μm |
| | 0.15 | 51μm | 43μm | 33μm |

### 5.6 Bubble Surface Property

In addition to $d_B$ and $v_B$, bubble surface contamination is another effective factor on particle-bubble encounter efficiency. Its impact is shown in Figure 5.6 by taking the advantage of $E_c^{GSE}$ and $E_c^{WP}$ for both mobile and immobile bubbles. As seen, in the entire particle size range, the corresponding $E_c$-value of $E_c^{WP}$ is greater than $E_c^{GSE}$ and $E_c^{WP-i}$ due to assuming a completely clean surface. In this sense, Schulze, 1993 reported that bubble surface immobilization reduces the $E_c$ by ca. 10-foldes. The discrepancies between $E_c^{GSE}$ and $E_c^{WP-mo}$ disclose the significant effect of retarded bubble on $E_c$. A relative difference between $E_c^{GSE}$ and $E_c^{WP-i}$ can be seen due to the inertial forces of coarse particles. As seen, the $E_c^{WP-}$ is very close to $E_c^{GSE}$ in comparison with the $E_c^{WP-m}$ clearly indicating the role of bubble contamination in particle-bubble encounter probability. A detailed argument concerning this subject is presented elsewhere (Hassanzadeh et al., 2017).

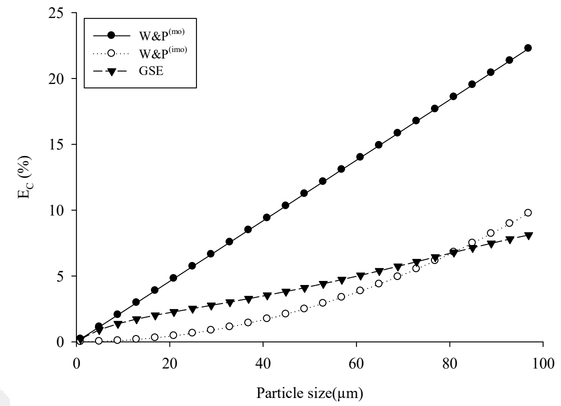


**Figure 5.6 :** $E_c$ versus degree of bubble surface mobility using $E_c^{SU}$, $E_c^{GSE}$ and $E_c^{WP}$.

## 5.7 Cross-Sectional Points And $St_{cr}$

Table 5.4 presents the estimated dps in connection with the Stcr and the points where both $E_c^{GSE}$ and $E_c^{CS}$ converge. As seen, there is a close agreement between the proposed cross-sectional point and the obtained particle sizes corresponding to the $St_{cr}$. The best fit is given for $d_B$=0.12cm and $v_B$=20cm/s. Furthermore, by increasing $v_B$ while the $d_B$ is kept constant, particle inertia impact is absolutely needed to be considered for even fine particles. With respect to St, Michael and Norey (1969) also counted 1/12 as $St_{cr}$ for a particle to reach the surface of a sphere or a bubble under the action of inertial forces. The $St_{cr}$ determines the deposition mechanism of particle on the surface of bubbles during encounter process. According to the theory of GSE, when St>>$St_{cr}$, inertial deposition of particles onto the bubble surfaces is the main collision mechanism. The particle inertial force has a positive effect on the $E_c$ and the $E_c$ depends on the magnitude of the St. This is in a very good agreement with the report of Ralston et al., (1999). They concluded that when the St is considerably large (St>>$St_{cr}$), inertial force is strong and becomes positive. In contrast, when St<<$St_{cr}$, particles move alongside the fluid streamlines and interception is the main collision mechanism. Below a $St_{cr}$, particle inertia has a strong negative effect (which is originated from the water inertial effect) on $E_c$. The proportion of this force becomes more effective as the St falls below $St_{cr}$.

**Table 5.4 :** A comparison of particle sizes obtained from both collision models and $St_{cr}$ *vs*. bubble size and its velocity.

| | $v_B$(cm/s), $d_B$=0.12cm | | | $d_B$(cm), $v_B$=20(cm/s) | | |
|---|---|---|---|---|---|---|
| | 10 | 20 | 30 | 0.08 | 0.12 | 0.15 |
| **Cross-sectional point** | 45µm | 37µm | 27µm | 32µm | 37µm | 37µm |
| **Particle size upon $St_{cr}$** | 49µm | 37µm | 25µm | 29µm | 37µm | 41µm |

# 6. ESTIMATION AND OPTIMIZATION OF $E_c$ AND $k$ USING RSM

## 6.1 Estimation Of $E_{coll}$

Figure 6.1 displays the particle–bubble interaction probabilities for 30 runs. Figure 6.1a shows the differences between the particle–bubble encounter efficiencies using generalized Sutherland equation ($E_c^{\mathrm{GSE}}$) and Yoon–Luttrell ($E_c^{YL}$) models. Figure 6.1b presents the values given by modified Dobby–Finch ($E_a^{DF}$) and Yoon–Luttrell (intermediate) ($E_a^{YL}$) attachment models. Also, Figure 6.1c indicates particle–bubble collection efficiencies using two types of model configurations (*i.e.* ($E_c^{\mathrm{GSE}}$, $E_a^{DF}$, $E_s^{SC}$) and ($E_c^{YL}$, $E_a^{YL}$, $E_s^{SC}$)). The first configuration of the models is typically used in numerical studies (Koh and Schwarz, 2003, 2006 and 2007; Govender et al., 2012) while the second one is used in analytical investigations (Pyke, 2003, Duan et al., 2003; Newell, 2006; Karimi et al., 2014 a,b).

It can be seen in Figure 6.1a that $E_c^{YL}$ and $E_c^{\mathrm{GSE}}$ have relatively similar trends. However, it can be found that $E_c^{YL}$ is much more dependent on particle diameter than $E_c^{\mathrm{GSE}}$. The minimum and maximum particle–bubble encounter efficiencies for $E_c^{YL}$ occur when the particle size is respectively coarser than 78µm (runs 13, 21, and 25) and finer than 33µm (runs 8, 12, 14, 20, and 23) regardless of the values of other factors. However, it appears that the $E_c^{\mathrm{GSE}}$ takes the combination of the factors into account. In this regard, Schulze (1989) and Dai et al., (1998) noted that the assumptions involved in predicting $E_c^{YL}$ are unrealistic. Following this, Dai et al., (2000) compared experimental and predicted encounter efficiencies for several models in a specific flotation condition ($d_p$<70µm, $d_B$=0.08 and 0.15cm, $v_B$=31.60 and 19.60cm/s and $\rho_p$=2.65g/cm$^3$) assuming that the particle–bubble stability is equal to unity. It was pointed out that $E_c^{YL}$ underestimates Ec in comparison with $E_c^{\mathrm{GSE}}$ due to ignoring the particle inertial forces and assuming a uniform distribution of collision over the entire upper half surface of the bubble; this is in a relatively good agreement with our findings. Also, King (2001) indicated the dependence of theoretical and experimental collision efficiencies on different bubble (0–1.2mm) and particle (12, 18, 27, 31 and 41µm) sizes. For theoretical estimations, $E_c^{YL}$ and Afruns–Kitchener ($E_c^{AK}$) collision model were used for coal and quartz, respectively. It was concluded that theoretical predications overestimate Ec by a factor of about two for bubbles approaching 1mm in diameter.

As shown by Figure 6.1b, except for a few runs (3, 6, 13, 18, 21 and 25) $E_a^{YL}$ varies very slightly in the vicinity of one. In other words, the estimated value of the particle–bubble attachment efficiency using Yoon–Luttrell model does not change upon varying the effective factors. However, $E_a^{DF}$ shows different values as a function of 30 runs. In this regard, Shahbazi et al., (2009) used $E_a^{YL}$ for predicting particle–bubble attachment probability of quartz in a mechanical flotation cell and reported that the results were approximately zero for all experiments. Kouachi et al., (2010) analyzed the $E_c^{YL}$ and $E_a^{YL}$ under various flotation conditions for quartz and galena minerals. It was reported that a large maximum collision angle (90°) used in the Yoon–Luttrell model resulted in small attachment efficiencies. Newell (2007) proposed a new attachment model (1/W attachment model) based on the ratio between the rate of interaction force controlled interparticle collision with and without electrostatic double layer repulsion. Experimental attachment efficiencies compared with corresponding values of 1/W attachment model, $E_a^{YL}$ and $E_a^{DF}$. It was disclosed that $E_a^{DF}$ and 1/W attachment model agreed with experimental findings contrary to $E_a^{YL}$ which showed entirely opposite behavior.

Finally, it is found in Figure 6.1c that the collection efficiencies estimated by applying the configuration I (*i.e.* $E_c^{YL}$, $E_a^{YL}$, $E_s^{SC}$ as collision, attachment and stability models) gives greater values than using the configuration II (*i.e.* $E_c^{\mathrm{GSE}}$, $E_a^{DF}$ and $E_s^{SC}$).

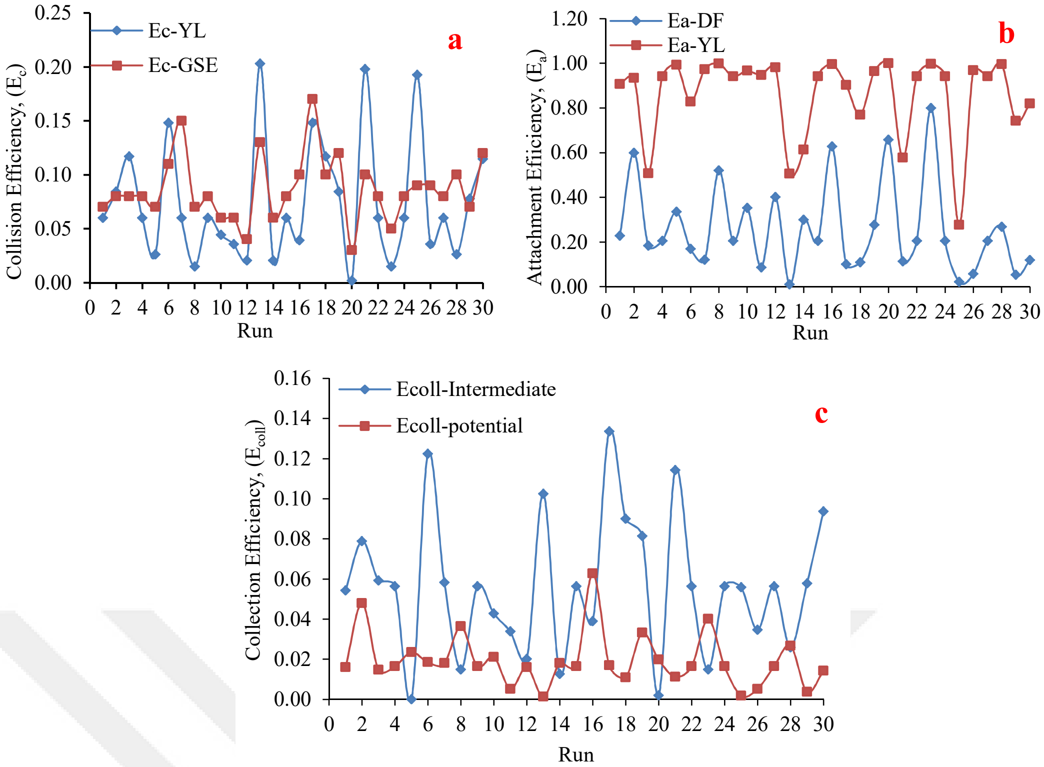


**Figure 6.1 :** A comparison between the particle-bubble interactions using two model configurations: (a) encounter (Dukhin (GSE) *vs.* Yoon-Luttrell (YL)), (b) attachment (Dobby-Finch (DF) *vs.* Yoon-Luttrell (YL)) and (c) configuration I vs. configuration II.

### 6.2 Estimation And Optimization Of $E_c$

A series of 30 tests with appropriate combinations of particle size (A), particle density (B), bubble size (C) and bubble velocity (D) were conducted using the central composite design method. The design matrix of these variables in coded units is given in Table 6.1 along with the predicted values of the response ($E_c$ as the particle–bubble encounter efficiency). The factors were studied with their codified values to simplify the calculations and for uniform comparison. The factors are coded according to the following equation:

$$x_i = \frac{X_i - X_0}{\Delta X} \tag{6.1}$$

where $x_i$ is the dimensionless coded value of the ith factor, $X_i$ is the actual value of the factor, $X_0$ is the value of $X_i$ at the center point and $\Delta X$ is the step change value.

**Table 6.1 :** Central composite design with actual/coded values for the parameters and results of the particle-bubble encounter efficiency.

| Run | Particle size ($d_p$)($\mu m$) ($A$) | Particle density ($\rho_p$)($g/cm^3$) ($B$) | Bubble size ($d_B$)($cm$) ($C$) | Bubble velocity ($v_B$)($cm/s$) ($D$) | Collision efficiency ($E_c$) |
|---|---|---|---|---|---|
| **1** | 55 (0) | 4.10 (2) | 0.08 (0) | 20 (0) | 0.07 |
| **2** | 78 (1) | 3.40 (1) | 0.09 (1) | 15 (-1) | 0.08 |
| **3** | 78 (1) | 3.40 (1) | 0.09 (1) | 25 (1) | 0.08 |
| **4** | 55 (0) | 2.70 (0) | 0.08 (0) | 20 (0) | 0.08 |
| **5** | 33 (-1) | 3.40 (1) | 0.06 (-1) | 15 (-1) | 0.07 |
| **6** | 78 (1) | 3.40 (1) | 0.06 (-1) | 15 (-1) | 0.11 |
| **7** | 55 (0) | 1.30 (-2) | 0.08 (0) | 20 (0) | 0.15 |
| **8** | 33 (-1) | 2.00 (-1) | 0.09 (1) | 15 (-1) | 0.07 |
| **9** | 55 (0) | 2.70 (0) | 0.08 (0) | 20 (0) | 0.08 |
| **10** | 55 (0) | 2.70 (0) | 0.10 (2) | 20 (0) | 0.06 |
| **11** | 33 (-1) | 3.40 (1) | 0.06 (-1) | 25 (1) | 0.06 |
| **12** | 33 (-1) | 3.40 (1) | 0.09 (1) | 25 (1) | 0.04 |
| **13** | 78 (1) | 2.00 (-1) | 0.06 (-1) | 25 (1) | 0.13 |
| **14** | 33 (-1) | 2.00 (-1) | 0.09 (1) | 25 (1) | 0.06 |
| **15** | 55 (0) | 2.70 (0) | 0.08 (0) | 20 (0) | 0.08 |
| **16** | 55 (0) | 2.70 (0) | 0.08 (0) | 10 (-2) | 0.10 |
| **17** | 78 (1) | 2.00 (-1) | 0.06 (-1) | 15 (-1) | 0.17 |
| **18** | 78 (1) | 2.00 (-1) | 0.09 (1) | 25 (1) | 0.10 |
| **19** | 78 (1) | 2.00 (-1) | 0.09 (1) | 15 (-1) | 0.12 |
| **20** | 10 (-2) | 2.70 (0) | 0.08 (0) | 20 (0) | 0.03 |
| **21** | 100 (2) | 2.70 (0) | 0.08 (0) | 20 (0) | 0.10 |
| **22** | 55 (0) | 2.70 (0) | 0.08 (0) | 20 (0) | 0.08 |
| **23** | 33 (-1) | 3.40 (1) | 0.09 (1) | 15 (-1) | 0.05 |
| **24** | 55 (0) | 2.70 (0) | 0.08 (0) | 20 (0) | 0.08 |
| **25** | 78 (1) | 3.40 (1) | 0.06 (-1) | 25 (1) | 0.09 |
| **26** | 33 (-1) | 2.00 (-1) | 0.06 (-1) | 25 (1) | 0.09 |
| **27** | 55 (0) | 2.70 (0) | 0.08 (0) | 20 (0) | 0.08 |
| **28** | 33 (-1) | 2.00 (-1) | 0.06 (-1) | 15 (-1) | 0.10 |
| **29** | 55 (0) | 2.70 (0) | 0.08 (0) | 30 (2) | 0.07 |
| **30** | 55 (0) | 2.70 (0) | 0.05 (-2) | 20 (0) | 0.12 |

In order to describe the effect of factors on particle–bubble encounter efficiency, it is first necessary to choose a suitable empirical model. Therefore, experimental data ($E_c$) in Table 6.1 were fitted to a full quadratic second order model equation by applying multiple regression analysis for Ec using Design Expert software (Demo v. 7.0.0, Stat–Ease, Inc.). Consequently, the final equation (equation A.1) representing the particle–bubble encounter efficiency ($E_c$) in terms of coded factors after removing insignificant terms was obtained as shown in Appendix A.

Evidently, the regression coefficients of all four factors together with interactions of the AB (particle size and particle density) and BC (particle density and bubble size) terms were found to be significant. The analysis of variance (ANOVA) was also applied to estimate the adequacy of the model and its significance at the 95% confidence level. The coefficient of determination, $R^2$ was found to be 0.97, which means that the model could explain 97% of the total variations in the system. The p–value was found <0.0001 indicating the significance of the model due to being smaller than 0.05.

Figure 6.2 shows the perturbation plot of the effects of the main factors on the particle–bubble collision efficiency ($E_c$), which is simulated from model fitting (equation A.1, Appendix A). This plot helps compare the effect of all the factors at a particular point in the design space. A steep slope or curvature in a factor displays whether the efficiency is sensitive to that particular factor. In addition, 3D response surface plots were applied to gain a better understanding of the influence of factors and their interactive effects. Figure 6.3 displays the response surface plots of the effect of four factors on the particle–bubble collision efficiency.

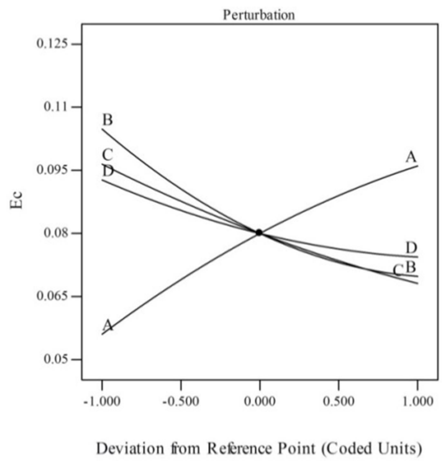


**Figure 6.2 :** Perturbation plot showing the relative significance of factors on the $E_c$.

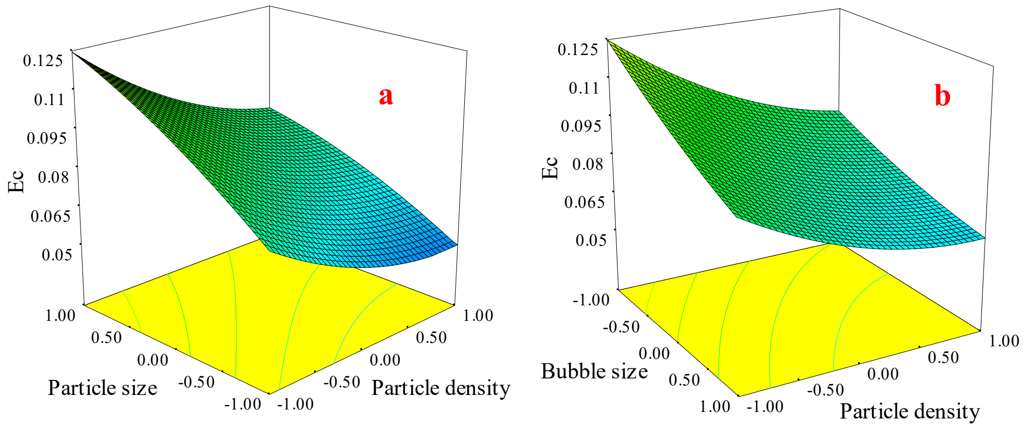


**Figure 6.3 :** 3D response surface plots showing the effect of two factors on the $E_c$: (a) particle size and particle density; (b) bubble size and particle density.

Figures 6.2 and 6.3 reveal that the order of significance of the studied factors is as particle size, particle density, bubble diameter, and bubble velocity ($d_p > \rho_p > d_B > v_B$). In other words, particle size positively affects the $E_c$ most whereas particle density, bubble size and velocity influence negatively under the studied flotation conditions. The effect of particle size has been extensively illustrated in the literature; the Ec increases with increasing the particle size particularly in quiescent conditions due to interceptional, gravitational and inertial forces (Schulze, 1989; Dai et al., 2000; Ralston et al., 2002; Hassanzadeh et al., 2018). As reported in several studies (Reay and Ratcliff, 1973; Ahmed and Jameson, 1985; Dobby and Finch, 1987; Tao, 2004), small bubbles enhance the probability of particle–bubble encounter specifically in the case of fine particles. A detailed study on the effect of bubble size and velocity is given elsewhere (Hassanzadeh et al., 2016).

In this regard, Eskanlou et al., (2017) conducted experimental tests and estimated the particle–bubble encounter efficiencies for pyrite and chalcopyrite using multiple linear regression (MLR) and artificial neural network (ANN) techniques. The best fitted equation was identified as equation 6.2 ($R^2$=0.60) using the MLR method. However, the coefficient of the respective testing sets achieved was 0.99 using a feed–forward ANN approach with 6–15–15–2 arrangement showing its substantial privilege to the MLR technique.

$$E_c = 72.92 + 0.01S_B - 0.25\lambda - 42.17C_p + 0.02\,\mathrm{Re}_B + 0.13d_p - 5.71\rho_p \qquad (6.2)$$

where $E_c$ is the particle–bubble encounter efficiency. $S_B$, λ, $C_P$, $Re_B$, $d_p$ and $\rho_p$ are respectively bubble surface area flux, micro–turbulence, particle circularity, bubble Reynolds number, particle size and particle density.

The most influential factors on $E_c$ were introduced as $S_B$, $Re_B$ and $d_p$. However, it can be found from equation 6.2 that $C_P$ had stronger impact on $E_c$ than λ, $d_p$ and $\rho_p$. Also, micro–turbulence negatively influenced $E_c$ which is a complete disagreement with fundamental concepts of the particle–bubble interaction (Duan et al., 2003; Pyke et al., 2003; Govender et al., 2013; Cheng et al., 2017).

The influence of particle density and bubble rising velocity can be discussed by two dimensionless numbers as Stokes ($St = \frac{\rho_p v_B d_p^2}{9\,\eta\, d_B}$) and bubble Reynolds ($Re_b = \frac{v_B \rho_f d_B}{\eta}$) numbers. The St is used to characterize the behavior of particles suspended in a fluid flow. It is defined as the ratio of the characteristic time of a particle to a characteristic time of the flow. A particle with a low Stokes number ($St<<1$) follows fluid streamlines and inertial forces have practically no effect on the motion of the particle. However, a particle with a large Stokes number ($St>>1$) is dominated by its inertia and continues along its initial trajectory. The $Re_B$ is generally used to assess the flow conditions of fluid in proximity to particles and described as the inertial forces to the viscous forces of the fluid. Stokes flow (so–called creeping flow) conditions apply when the $Re_B$ is very much less than unity ($Re_B<<1$) and potential flow conditions apply at $80<Re_B<500$. An increase in $\rho_p$ and $v_B$ increases the St. Thus, the particle–bubble encounter interaction will change from interception to inertial. This facilitates collisions between particles and bubbles. An increase in $v_B$ also affects the fluid flow conditions around the bubble surface. At a greater $v_B$ potential flow conditions apply, which are more advantageous for particle–bubble encounter than Stokes flow conditions (King, 2001).

Furthermore, it can be observed that the role of particle density on $E_c$ is greater than bubble size and velocity. It is worth noting that unlike other features of the particle, the role of particle density on the particle–bubble encounter has not been practically investigated due to some difficulties involved in the process. It is recently shown by analytical and numerical methods that there are two distinct zones where particle densities play completely different roles. In the first zone, increasing the particle density leads to reducing the $E_c$ due to the negative effect of inertia of water flow.

However, in the second zone, increasing the particle density follows by an increase in the $E_c$ as it overcomes the negative effect of water flow inertia by the particle inertia (Nguyen et al., 2006; Liu and Schwarz, 2009; Firouzi et al., 2011; Hassanzadeh et al., 2017; Kouachi et al., 2017).

Figure 6.4 shows the significant interaction effects of AB and BC on the $E_c$. As can be seen, at high and low levels of particle density, increasing the particle size and reducing the bubble size results in an increase in the particle–bubble encounter efficiency. Also, it is observed from Figure 6.4 that at high and low levels of particle size and bubble size, encounter efficiency is reduced with increasing the particle density.

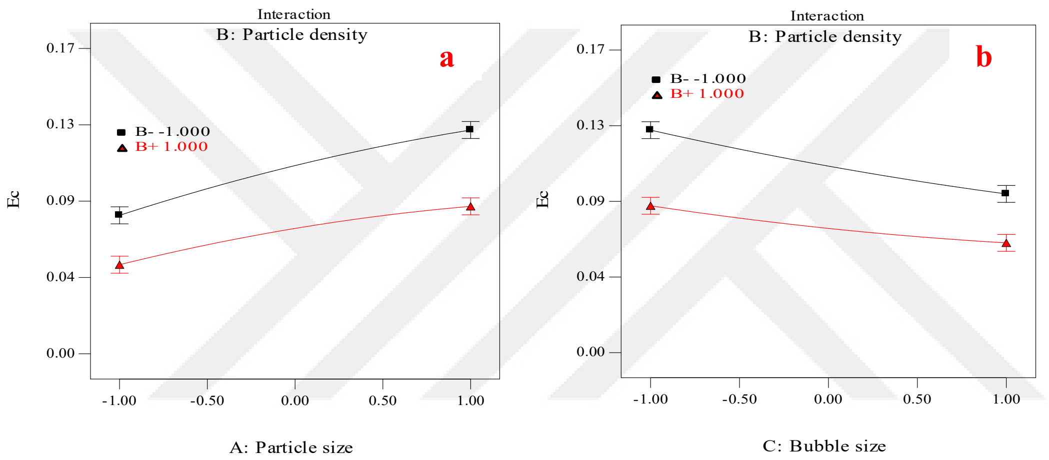


**Figure 6.4 :** Interaction effect plot between a) particle size and particle density; and b) particle density and bubble size on the particle-bubble encounter efficiency ($E_c$).

The particle–bubble encounter efficiency was optimized to obtain the maximum efficiency using Design Expert software. Figure 6.5 demonstrates the trend of factors for movement towards the optimal point. Evidently, changing the parameters toward the optimal point decreases the particle–bubble encounter efficiency. The optimum particle size, particle density, bubble size and bubble velocity were found to be 78µm, 2g/cm$^3$, 0.06cm and 15cm/s, respectively. Under these conditions, the maximum particle–bubble encounter efficiency was determined about 0.1575.

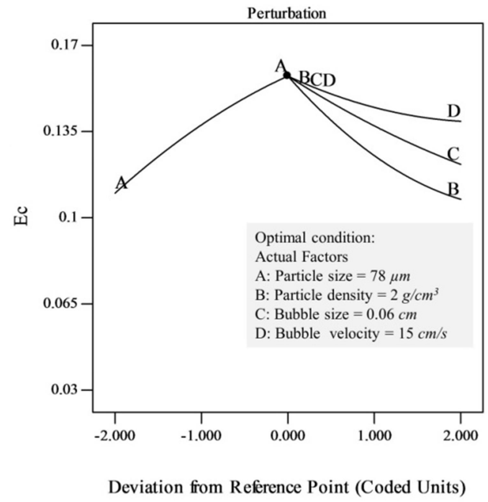


**Figure 6.5 :** Perturbation plot showing the optimal conditions of factors to obtain the maximum particle-bubble encounter efficiency.

### 6.3 Estimation And Optimization Of K

Table 6.2 represents the coded and values of five factors and the response (i.e. the flotation rate constant) for 50 runs using CCD method. Appropriate combinations of five factors as particle size (A), particle density (B), bubble size (C) bubble velocity (D) and turbulence dissipation rate (E) were used in this study. The obtained results from ANOVA analysis showed that $R^2$ and $R^2_{adj.}$ were 0.95 and 0.93 together with the p–value of < 0.0001 showing the significance of the model. As can be seen in Table 6.2, the minimum and maximum flotation rate constants are 0.13 (Run 10) and 10.24 (Run 39), respectively. In this regard, Safari and Deglon (2018) used a large pile of data to derive empirical correlations for describing the relationship between the attachment/detachment rate constants and the particle size, particle density, bubble size, collector dosage and energy input. The obtained kinetic rates were in the range of 0.1–10 which is in good agreement with the presented results. Shi and Fornasiero (2009) studied the effects of particle size, density and cell turbulence on flotation rate and recovery of pure quartz, chalcopyrite and galena. The rate of flotation increased with increasing particle size up to a maximum value before decreasing for coarser particles. The particle size for maximum flotation rate was found to decrease with increasing mineral density. The flotation rate also increased with agitation rate up to a maximum value before decreasing at high agitation rates.

**Table 6.2 :** Central composite design with actual/coded values for the parameters and results of the flotation kinetics rates.

| Run | ($d_p$)($\mu m$) ($A$) | ($\rho_p$)($g/cm^3$) ($B$) | ($d_B$)($cm$) ($C$) | ($v_B$)($cm/s$) ($D$) | ($\varepsilon$) ($m^2/s^3$) ($E$) | ($k$) ($1/min$) |
|---|---|---|---|---|---|---|
| **1** | 33 (-1) | 2.00 (-1) | 0.07 (-1) | 15 (-1) | 21 (-1) | 4.50 |
| **2** | 78 (1) | 2.00 (-1) | 0.07 (-1) | 15 (-1) | 21 (-1) | 2.61 |
| **3** | 33 (-1) | 3.40 (1) | 0.07 (-1) | 15 (-1) | 21 (-1) | 7.33 |
| **4** | 78 (1) | 3.40 (1) | 0.07 (-1) | 15 (-1) | 21 (-1) | 4.50 |
| **5** | 33 (-1) | 2.00 (-1) | 0.09 (1) | 15 (-1) | 21 (-1) | 5.27 |
| **6** | 78 (1) | 2.00 (-1) | 0.09 (1) | 15 (-1) | 21 (-1) | 4.73 |
| **7** | 33 (-1) | 3.40 (1) | 0.09 (1) | 15 (-1) | 21 (-1) | 5.29 |
| **8** | 78 (1) | 3.40 (1) | 0.09 (1) | 15 (-1) | 21 (-1) | 4.65 |
| **9** | 33 (-1) | 2.00 (-1) | 0.07 (-1) | 25 (1) | 21 (-1) | 0.48 |
| **10** | 78 (1) | 2.00 (-1) | 0.07 (-1) | 25 (1) | 21 (-1) | 0.13 |
| **11** | 33 (-1) | 3.40 (1) | 0.07 (-1) | 25 (1) | 21 (-1) | 0.93 |
| **12** | 78 (1) | 3.40 (1) | 0.07 (-1) | 25 (1) | 21 (-1) | 0.27 |
| **13** | 33 (-1) | 2.00 (-1) | 0.09 (1) | 25 (1) | 21 (-1) | 1.01 |
| **14** | 78 (1) | 2.00 (-1) | 0.09 (1) | 25 (1) | 21 (-1) | 0.47 |
| **15** | 33 (-1) | 3.40 (1) | 0.09 (1) | 25 (1) | 21 (-1) | 1.87 |
| **16** | 78 (1) | 3.40 (1) | 0.09 (1) | 25 (1) | 21 (-1) | 1.33 |
| **17** | 33 (-1) | 2.00 (-1) | 0.07 (-1) | 15 (-1) | 27 (1) | 5.61 |
| **18** | 78 (1) | 2.00 (-1) | 0.07 (-1) | 15 (-1) | 27 (1) | 3.76 |
| **19** | 33 (-1) | 3.40 (1) | 0.07 (-1) | 15 (-1) | 27 (1) | 8.93 |
| **20** | 78 (1) | 3.40 (1) | 0.07 (-1) | 15 (-1) | 27 (1) | 6.65 |
| **21** | 33 (-1) | 2.00 (-1) | 0.09 (1) | 15 (-1) | 27 (1) | 5.91 |
| **22** | 78 (1) | 2.00 (-1) | 0.09 (1) | 15 (-1) | 27 (1) | 5.23 |
| **23** | 33 (-1) | 3.40 (1) | 0.09 (1) | 15 (-1) | 27 (1) | 9.23 |
| **24** | 78 (1) | 3.40 (1) | 0.09 (1) | 15 (-1) | 27 (1) | 10.01 |
| **25** | 33 (-1) | 2.00 (-1) | 0.07 (-1) | 25 (1) | 27 (1) | 0.77 |
| **26** | 78 (1) | 2.00 (-1) | 0.07 (-1) | 25 (1) | 27 (1) | 0.24 |
| **27** | 33 (-1) | 3.40 (1) | 0.07 (-1) | 25 (1) | 27 (1) | 1.47 |
| **28** | 78 (1) | 3.40 (1) | 0.07 (-1) | 25 (1) | 27 (1) | 0.59 |
| **29** | 33 (-1) | 2.00 (-1) | 0.09 (1) | 25 (1) | 27 (1) | 1.17 |
| **30** | 78 (1) | 2.00 (-1) | 0.09 (1) | 25 (1) | 27 (1) | 0.56 |
| **31** | 33 (-1) | 3.40 (1) | 0.09 (1) | 25 (1) | 27 (1) | 2.17 |
| **32** | 78 (1) | 3.40 (1) | 0.09 (1) | 25 (1) | 27 (1) | 1.53 |
| **33** | 10 (-2) | 2.70 (0) | 0.08 (0) | 20 (0) | 24 (0) | 3.13 |
| **34** | 100 (2) | 2.70 (0) | 0.08 (0) | 20 (0) | 24 (0) | 1.33 |
| **35** | 55 (0) | 1.30 (-2) | 0.08 (0) | 20 (0) | 24 (0) | 0.97 |
| **36** | 55 (0) | 4.10 (2) | 0.08 (0) | 20 (0) | 24 (0) | 3.19 |
| **37** | 55 (0) | 2.70 (0) | 0.05 (-2) | 20 (0) | 24 (0) | 0.95 |
| **38** | 55 (0) | 2.70 (0) | 0.10 (2) | 20 (0) | 24 (0) | 3.66 |
| **39** | 55 (0) | 2.70 (0) | 0.08 (0) | 10 (-2) | 24 (0) | 10.24 |
| **40** | 55 (0) | 2.70 (0) | 0.08 (0) | 30 (2) | 24 (0) | 0.43 |
| **41** | 55 (0) | 2.70 (0) | 0.08 (0) | 20 (0) | 18 (-2) | 2.47 |
| **42** | 55 (0) | 2.70 (0) | 0.08 (0) | 20 (0) | 30 (2) | 3.07 |
| **43*** | 55 (0) | 2.70 (0) | 0.08 (0) | 20 (0) | 24 (0) | 2.79 |

*Run 43 is the average for 8 central tests.

It can be found by ANOVA (Table A.2, Appendix A) that the degree of influence of the important factors on k is bubble velocity, particle density, turbulence, particle size, and bubble diameter (*i.e.* $v_B > \rho_p > \varepsilon > d_p > d_B$). Regarding these results, Safari and Deglon (2018) presented the order of $\rho_p > \varepsilon > d_B > d_p$ upon developing an attachment–detachment kinetic model. The literature data for a turbulence system is almost unclear. Vazirizadeh et al. (2015) also studied the relative effect of gas hold–up ($\varepsilon_g$), interfacial area of bubbles ($I_B$) and bubble surface area flux ($S_b$). It was reported that for fine (53–75µm) and intermediate particles (75–106µm), $S_B$ has the strongest effect than $\varepsilon_g$ and $I_B$ on flotation kinetic constant (i.e. $S_B > \varepsilon_g > I_B$) which is in good agreement with other studies (Gorian et al., 1997; Massinaei et al., 2009). As the particle size increased (106–150µm), the contribution of the $S_b$ decreased and importance of $\varepsilon_g$ and $I_b$ increased ($I_b > \varepsilon_g > S_b$) which is in agreement with the results given by Kracht et al., (2005). Following this, Eskanlou et al., (2017) studied the effect of bubble surface area flux ($S_B$), micro–turbulence (λ), article circularity ($C_p$), bubble Reynolds number ($Re_B$), particle size ($d_p$) and particle density ($\rho_p$) on flotation rate constants of chalcopyrite and pyrite in a laboratory Denver mechanical flotation cell using MLR and ANN approaches. SB and λ were identified as the most effective factors on k. According to the obtained results and outcomes presented in the literature, it can be concluded that the relative influence of flotation variables on flotation kinetics rates in both batch and industrial cells is unclear and requires further studies.

Figure 6.6 displays response surface plots focusing on the interactive effects and respective flotation rate constants. The shapes of the contour and response surface plots show the nature and extent of the interactions of the different components. It is obvious from the results presented in Figure 6.7 that the flotation rate constant depends strongly on the interaction among factors. It can be found that the ranking of the significant interaction on the flotation kinetics is as follows: interactive effects of bubble velocity and turbulence>particle density and bubble velocity>particle density and turbulence>particle size and bubble size.

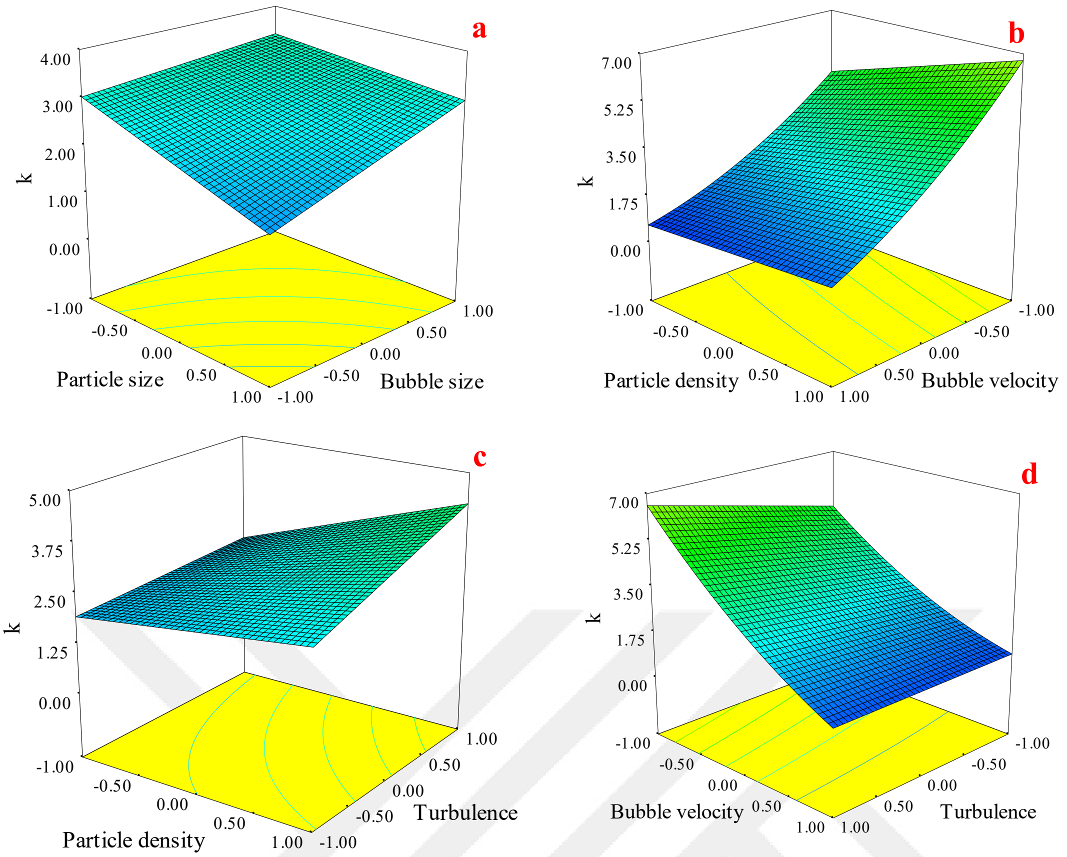


**Figure 6.6 :** 3D response surface plots showing the effect of two factors on the flotation kinetics rates (*k*, *min*$^{-1}$): (a) particle size and bubble size; (b) particle density and bubble velocity; (c) particle density and turbulence; (d) bubble velocity and turbulence.

It can be pointed out that interaction of $\varepsilon.v_B$ negatively impacts on k. Regarding the $\varepsilon.v_B$ effect, Amini et al. (2013) examined the influence of turbulence kinetic energy (TKE) on bubble size in two mechanical flotation cells with the same geometry but different sizes as laboratory (5L) and full–scale (60L) cells. It was reported that increasing TKE reduced bubble Sauter mean diameter ($d_{32}$) in the 5L cell until a critical value ($0.18 m^2/s^2$) after which there was no significant further influence. The TKE had no effect on the $d_{32}$ in the 60L cell. The literature data indicated inconsistent results, some demonstrating a reduction in the d32 at increasing impeller speed (Grau et al., 2005; Shahbazi et al., 2009), others showing little to no effect (Finch et al., 2008). Nevertheless, none of these studies examined the interaction effect of $\varepsilon.v_B$ on k.

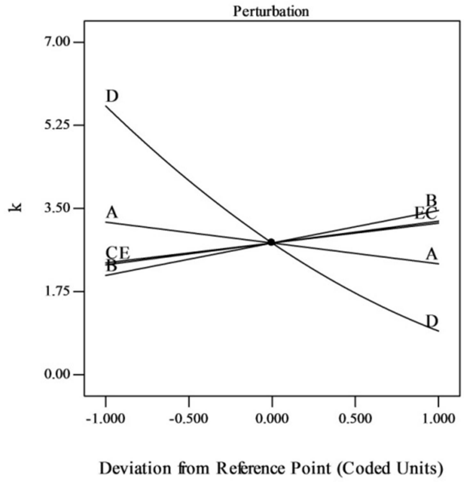


**Figure 6.7 :** Perturbation plot showing the relative significance of factors on the flotation kinetics rate ($k$, $min^{-1}$).

Interaction graphs were constructed to provide better understanding and insight of interactive effects among factors on flotation kinetics, which are displayed in Figure 6.8. As can be seen, at high level of particle sizes (78µm), increasing the bubble size resulted in an increase at the flotation rate constant (Figure 6.8a). The increment in the bubble size leads to a slight increase of flotation kinetics at low level of particle sizes (33µm) (Figure 6.8a). It is also obvious from the results that the bubble size has less significant on the kinetic rate, which is probably attributed to the fact that, the range chosen for this parameter (33–78µm) is too small to have any confidence in the outcome of the tests. Meanwhile, it is observed that at high and low levels of particle density and turbulence, kinetic rate strongly decreases with increased bubble velocity. It can be also seen that the bubble velocity has maximum influence on the flotation kinetic (Figure 6.8b and 6.8d). In addition, it is found from Figure 6.8c that the turbulence has a positive effect on the flotation kinetics of high density particles in the range studied; turbulence has a negligible effect on the kinetics at low particle densities.

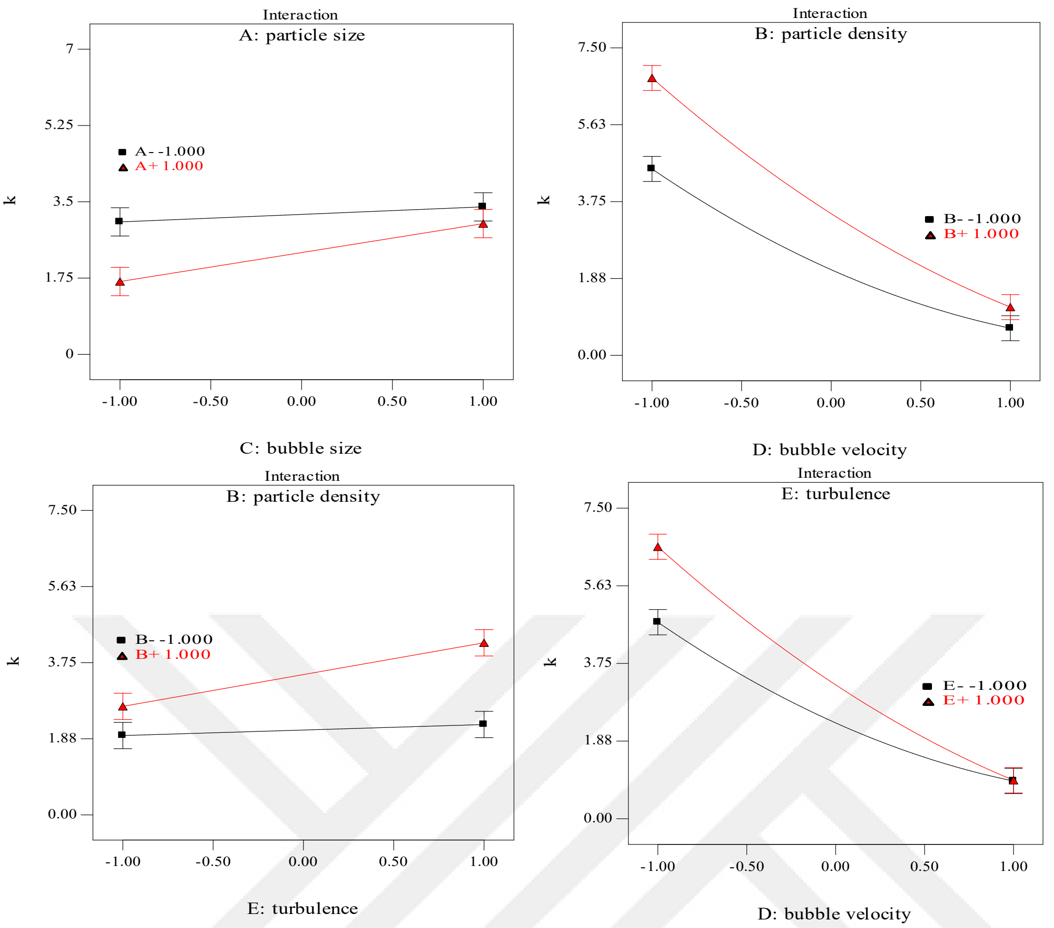


**Figure 6.8 :** Interaction effect plot between a) particle size and bubble size; b) particle density and bubble velocity; c) particle density and turbulence; and d) bubble velocity and turbulence on the flotation kinetic rates.

The impact of turbulence dissipation rate (varies at 18, 21, 24, 27 and 30$m^2/s^3$) in a constant gas flow rate (3500$cm^3$/min) is shown in Figure 6.9. The following states in Figure 6.9 (a–e) take place with the flotation cell while the $\varepsilon$ factor slowly increases. In the first graph (Figure 6.9A), dispersion of particles and bubbles is very poor and they only disperse in the center of the vessel. By increasing the $\varepsilon$ up to 24$m^2/s^3$ (Figure 6.9b and 6.9c), particles and bubbles distribute over the entire cross–section of the cell above the agitator. Under these conditions, only small mass transfer intensities are feasible at low kinetic rates. However, once the turbulence dissipation rate rises to 30 $m^2/s^3$ (Figure 6.9d and 6.9e), particles and bubbles distribute in the lower part of the cell leading to improved particle–bubble interactions and greater mass transfer rates.

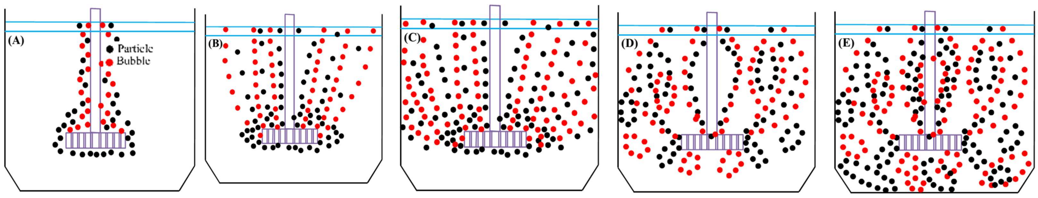


**Figure 6.9 :** A schematic view of increasing turbulence dissipation rate from 18 to $30m^2/s^3$, (a) $18m^2/s^3$, (b) $21m^2/s^3$, (c) $24m^2/s^3$, (d) $27m^2/s^3$, (e) $30m^2/s^3$ on dispersion of particles and bubbles inside the flotation cell.

In order to find an optimum condition with the highest flotation rate constant, equation (B1) in Appendix B was optimized using quadratic programming of the mathematical software package (Design Expert) within the experimental range studied (Figure 6.10). The optimal conditions suggested by Design Expert software are: particle size of 33µm, particle density of 3.4g/cm$^3$, bubble size of 0.09cm, bubble velocity of 15cm/s and turbulence dissipation rate of 27m$^2$/s$^3$. Under these optimal conditions, the maximum flotation kinetic rate of 8.61min-1 was approximately obtained.

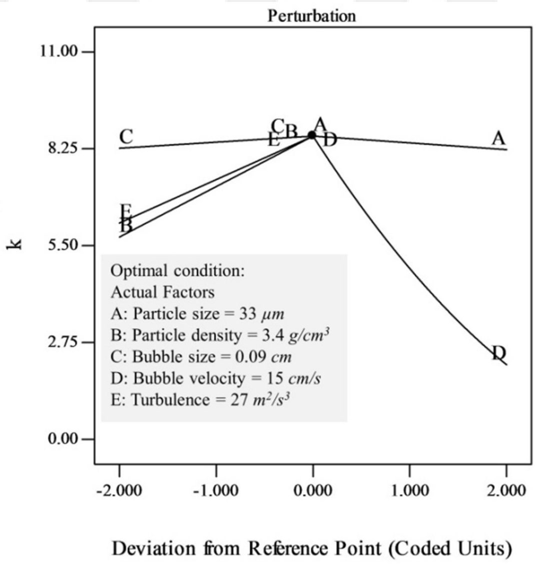


**Figure 6.10 :** Perturbation plot showing the optimal conditions of factors to obtain the maximum flotation kinetics rate ($k$, $min^{-1}$).

# 7. CONCLUSIONS

Particle–bubble encounter probability ($E_c$) is identified as the most initiative and crucial aspect between the three main sub-processes in particle-bubble interaction. It is undoubtedly the most effective phenomenon influencing the flotation rate constant in flotation processes. It is mainly controlled by hydrodynamic characteristic of the cell such as pulp density, impeller speed (power consumption), energy dissipation rate (cell turbulence), air flow rate, particle and bubble surface contamination, their sizes and velocities and particle density. Both the theoretical and physical concepts concerning its determination in static and dynamic systems together with the effect of flotation factors on it are very limited. Its theoretical and numerical modeling whether in quiescent (laminar) and turbulent conditions is also suffered from many irrational simplifications by applying a great number of assumptions.

Therefore, selection of the best methodology for its determination requires initially understanding the available works and presented studies in this regards. Therefore, the presented thesis aimed to firstly compile all of investigations focused on its estimation in the format of a comprehensive review study. For this, the studies categorized in three groups based on the type of methodology as theoretical and analytical approaches, numerical including DEM and CFD techniques and experimental (direct and indirect) methods. Thereafter, the thesis identify the role of some key hydrodynamic parameters such as energy dissipation rate, bubble size, its velocity and bubble surface mobility, particle size and its density together with their internal interactions. The modeling of particle-bubble encounter interaction is exclusively studied analytically and numerically. The key privileges and constrains of them pointed in the present work. In the end, the relation between particle-bubble collision efficiency and flotation rate constant are optimized and assessed using a response surface technique (*i.e.* central composite design).

The obtained results of each chapter are stated separately as following:

## 7.1 Outcomes Obtained From A Comprehensive Review Study

The comprehensive reviewing available data disclosed that the models used analytical solving of Naiver-Stokes equation for streamlines is only limited to a specific hydrodynamic conditions. The interceptional models used for analyzing the $E_c$ consider several simplifications such as sphericity of both particles and bubbles, isotropic and homogeneous distribution of energy dissipation rate and consideration of low bubble Reynolds number and assuming the stabilized streamlines for fluid by time and space.

The comparison between three common methods for estimation of $E_c$ revealed that the main concerns of analytical modeling were disregarding the microhydrodynamic resistance forces and particle trajectory together with its angle of tangency in greater Stokes values. However, the best correlation among numerical and analytical modeling was obtained for fine and ultra-fine particles due to low impact of inertial forces in this particle range. Despite the limitation of numerical methods in some cases, they were identified as the powerful techniques for evaluation of particle-bubble interactions in very intensive turbulent conditions. In addition to that, a great lack of observation and measurement methods was reported in detail, which requires further studies. Among the studied hydrodynamic characteristics, particle density and energy dissipation rate were introduced as the main causes of discrepancies between these three methods. It was also reported that water inertial forces and their roles on particle-bubble encounter probability by varying hydrodynamic conditions was not adequately addressed in flotation systems. It was also found that the impact of micro and nano-bubble for improving the collision efficiencies specifically for fine particles require more scientific investigations.

## 7.2 Impact Of Particle Characteristics On $E_c$ And $K$

In this section, the role of particle size and its density on $E_c$ and $k$ was analyzed in detail by taking advantage of differences between two models ($E_c^{GSE}$ and $E_c^{Sc}$) focusing on water inertial force, $\beta$ and $\theta_t$ terms. The aim was to find the particle size range where the particle and water inertial forces are significantly influenced on $E_c$ and $k$ under different hydrodynamic conditions. For calculation of flotation rate constant the following parameters were kept stationary; $\varepsilon$=38 $m^2/s^3$, $G_{fr}$=3.5×10-3 $m^3$/min while the $v_B$ varied from 18 to 31.6 cm/s, and $d_B$ from 0.12 to 0.15cm.

It was found that $E_c^{GSE}$ and $E_c^{Sc}$ only support each other for fine particle sizes while the difference is clearly observed for coarser and denser particles. Additionally, the results revealed the imperative impact of water inertial and microhydrodynamic forces by variation of particle size and density. By substituting the $E_c^{GSE}$ with $E_c^{Sc}$ in GFK model, a substantial discrepancy was detected over a wide range of particle size. This exceeded variation was argued in conjunction with the inertial forces of both particles and bubbles for quartz, chalcopyrite and galena minerals. Applying the $E_c^{SC}$ to the GFK showed a sever error for estimation of flotation rate constant by discounting the inertial forces. Finally, it was concluded that elimination of inertial effects in theoretical modeling might lead to two to four-fold greater prediction of the flotation rate constant.

### 7.3 Effect Of Bubble Properties On $E_c$

This section highlights the effect of $d_B$, $v_B$ and mobility degree of bubbles on the $E_c$. The particle-bubble encounter probabilities were calculated using $E_c^{GSE}$ and $E_c^{Sc}$ while the $d_B$ and $v_B$ changed in three levels *i.e.* 0.08, 0.12 and 0.15cm and 10, 20 and 30cm/s, respectively. Chalcopyrite mineral was selected for this study while its size varied in the range of 1-100µm. Additionally, bubble surface contamination was analyzed by means of $E_c^{WP}$.

It was found that for particle finer than 32µm when $d_B$ and $v_B$ were 0.08cm and 20cm/s, respectively the particle inertial impact on the $E_c$ is insignificant. However, its impact becomes more substantial for coarse particle sizes and requires taken into account for obtaining accurate analyses. In addition to that, when the $d_B$ was fixed (0.l2cm), diminishing $v_B$ from 30 to 20cm/s, the particle inertial force can be discounted for a wider particle range.

For the first time in the literature, $E_c$ was categorized into three zones as follows:

- low zone (0-4%); corresponded values of $E_c$ for particle range of 1-10µm (ultra-fine) and 10-20µm (fine)
- intermediate zone (4-8%); corresponded values of $E_c$ in particle range of 20-70µm

➢ high zone (8-14%); coarse particles over 70µm

The low zone was introduced where the $E_c$ is in its lowest values where the collision frequency can be considerably improved by a correct combination of nano, micro and macro-bubbles. The intermediate one was relatively depending on bubble properties. However, the high zone includes the $E_c$ from 8-14% where the coarser particles lead to greater values for $E_c$.

Finally, it was pointed out that $E_c^{GSE}$ of chalcopyrite particles increased by increasing $d_p$ and decreases by increasing the $d_B$. The principle reason of poor encounter probability for UF particles was related to their low momentums.

### 7.4 Estimation And Optimization Of $E_c$ And $k$

This work deals with the estimation and optimization of particle–bubble encounter interaction ($E_c$) and flotation rate constant (k) using central composite design methodology (CCD). The effect of four and five factors was studied on the $E_c$ and k, respectively. The parameters were considered as particle size (10, 33, 55, 78 and 100µm), particle density (1.3, 1.0, 2.7, 3.4 and 4.1g/cm$^3$), bubble size (0.05, 0.06, 0.08, 0.09 and 0.1cm), bubble velocity (10, 15, 20, 25 and 30cm/s) and turbulence dissipation rate (18, 21, 24, 27, 30m$^2$/s$^3$). Two model configurations were used to estimate the particle–bubble sub–processes (collision, attachment and stability) as (I) generalized Sutherland equation ($E_c^{\mathrm{GSE}}$), modified Dobby–Finch ($E_a^{DF}$) and modified Schulze stability models ($E_s^{SC}$) and (II) Yoon–Luttrell ($E_c^{YL}$), Yoon–Luttrell (intermediate) ($E_a^{YL}$) and modified Schulze stability models ($E_s^{SC}$) (*i.e.* ($E_c^{\mathrm{GSE}}$, $E_a^{DF}$, $E_s^{SC}$) and ($E_c^{YL}$, $E_a^{YL}$, $E_s^{SC}$)).

It was revealed that the second configuration provided greater values than the first one. The results further showed that the order of effective factors on the particle–bubble encounter efficiency was as particle size, particle density, bubble diameter, and bubble velocity in a quiescent condition. The maximum Ec was obtained at $d_p$=78µm, $\rho_p$=2g/cm$^3$, $d_B$=0.08cm and $v_B$=15cm/s. The interrelated influence of particle size and particle density as well as particle density and bubble size on Ec was identified significant. The maximum flotation kinetic rate of 8.61min-1was achieved at $d_p$=33µm, $\rho_p$=3.4g/cm$^3$, $d_B$=0.09cm, $v_B$=15cm/s and $\varepsilon$ =27m$^2$/s$^3$. The influential degree of the important factors on k was found as bubble velocity, particle density, turbulence, particle size, and bubble diameter. It was revealed that there is not a clear statement in the literature and good agreement with studies concerning the relative importance of effective parameters on flotation kinetic constant. Further specific studies are required to address this issue from practical and modeling points of view.

To summarize the key findings, the following bull points can be stated:

- The present study is the first work in the literature highlighting applications, constrains and privileges of the most common three methods: experimental (direct and indirect), analytical and numerical (CFD) simultaneously for estimation of particle-bubble interactions in flotation cells. The obtained results from this thesis evidently show that despite the analytical approaches are commonly used in many research studies; they are restricted owing to poor estimation of collision angle, Stokes number, particle density and microhydrodynamic forces.
- Initially, it is found in this work that the omitting negative inertial forces would result in 2-4 folds higher estimation of flotation kinetics depending upon variation in numerical densities and particle sizes.
- Optimization of the particle-bubble encounter efficiency (Ec) and flotation kinetic rate (k) in the absence and presence of turbulence dissipation rate are reported for the first time in the field of mineral processing using a central composite design (CCD) by DX7 software.
- The relative significance of factors (particle size, bubble diameter, bubble velocity, particle density and turbulence) on $E_c$ and k is shown for the first time to be incoherent in the literature. According to the obtained results under the conditions studied, particle size and bubble velocity are the most effective factors on the particle-bubble encounter and flotation rate constant, respectively.
- For first-time the intersection of three collision models (*i.e.* Sutherhland, Schulze and Dukhin) is suggested as an alternative method for estimating the critical Stokes number ($St_{cr\text{-}st}$) as a function of bubble surface properties (bubble size, its diameter and mobility). The results of the presented approach highly correlate the obtained data given by Stokes.

- For the first time the exact thresholds for identifying the positive and negative effects of particle inertia are reported.
- With respect to flotation modeling from microscopic aspect, researchers have utilized two common configurations for determination of the particle-bubble collection efficiency (capture efficiency) as (I) generalized Sutherland equation ($E_c^{\mathrm{GSE}}$), modified Dobby–Finch ($E_a^{DF}$) and modified Schulze stability ($E_s^{SC}$) models and (II) Yoon–Luttrell ($E_c^{YL}$), Yoon–Luttrell (intermediate) ($E_a^{YL}$) and modified Schulze stability ($E_s^{SC}$) models (*i.e.* ($E_c^{\mathrm{GSE}}$, $E_a^{DF}$, $E_s^{SC}$) and ($E_c^{YL}$, $E_a^{YL}$, $E_s^{SC}$)), respectively. The results indicate that the collection efficiency (Ecoll) calculated by configuration (I) is greater than that calculated by configuration (II). Initiatory, it is found that interceptional models applied to analytical aproaches (configuration I) overestimate the $E_{coll}$ compared to that using computational fluid dynamic technique (configuration II).

### 7.5 Future Work

The efficient design and optimization of flotation processes requires robust computational tools able to capture the physics of the process but at the same time versatile enough to allow extensive parametric studies. The first principles based modelling of the flotation process is not a viable task since it includes several size scales starting from those of the flotation device and ending to the scale of the thin film separating particle and bubble. At the heart of the modelling of flotation, process is the bubble-particle collision function. The vast majority of the relevant literature work refers to non-turbulent flows but a few recent approaches have been also suggested for the derivation of this function for turbulent flows. Therefore, after a complete evaluation of the presented techniques, the list of further required fundamental investigations suggested on the basis of the identified knowledge gap in the literature.

- distinguishing particle and water inertial impacts under intensively turbulent conditions for particle with wide domain of sizes and densities.

- more to the point and fundamental works in terms of interactions among hydrodynamic properties using directionless numbers on particle–bubble encounter probabilities.
- optimizing the hydrodynamic factors by maximizing particle-bubble encounter efficiency and flotation rate constant.
- establishment a reliable set-up for direct measurement of static and dynamic particle-bubble interactions in a batch flotation cell.

numerical modeling of the processes by applying both computational fluid dynamic and discrete element methods.

- observation and tracking trajectory of particles with different densities in a various size fraction sizes encountering with mobile and immobile bubbles in both collection and froth zone.

## REFERENCES


**Abrahamson, A.** (1975). Collision rates of small particles in a vigorously turbulent fluid, *Chemical Engineering Science*, *30*, 1371–1379.

**Agar, G.E., Chia, J., Requis, L.** (1989). Flotation rate measurements to optimize an operating circuit, *Minerals Engineering*, *4*, 47–60.

**Ahmed, N., and Jameson, G.J.** (1985). The effect of bubble size on the rate of flotation of fine particles, *International Journal of Mineral Processing, 14*, 195–215.

**Ahmed, N., Jameson, G.J. (**1989). Flotation kinetic, *Mineral Processing and Extractive Metallurgy Review*, *5*, 77–99.

**Albijanic, B., Subasinghe, G.K.N., Park, C.H.** (2015). Flotation kinetic models for fixed and variable pulp chemical conditions, *Minerals Engineering, 78*, 66-68.

**Amini, E., Bradshaw, D.J., Finch, J.A., Brennan, M.** (2013). Influence of turbulence kinetic energy on bubble size in different scale flotation cells, *Minerals Engineering*, *45*, 146–150.

**Anfruns, J.F., Kitchener, J.A.** (1977). Rate of capture of small particles in flotation. *Transactions of the Institution of Mining and Metallurgy* (Sect. C), *86*, 9–15.

**Arbiter, N. and Harris C. C.** (1962). *Flotation kinetic in froth flotation*, 50th Anniversary Volume (ed. D. W. Fuerstenau), 215-246, (Rocky Mountain Fund Series).

**Assemi, S., Nguyen, A., Miller, J.D.** (2008). Direct measurement of particle–bubble interaction forces using atomic force microscopy, *International Journal of Mineral Processing*, *89* (1-4), 65–70.

**Azizi, A., Hassanzadeh, A., Fadaei, B.** (2015). Investigating of the first-order flotation kinetic models for Sarcheshmeh copper sulphide ore, *International Journal of Mining Science and Technology*, *25*, 849-854.

**Banisi, S., and Finch, J. A.** (1994). Technical note reconciliation of bubble size estimation methods using drift flux analysis. *Minerals Engineering*, *7***(12)**, 1555-1559.

**Basarova, P., Machon, V., Hubicka, M., Horn, D.** (2010). Collision processes involving a single rising bubble and a larger stationary spherical particle, *International Journal of Mineral Processing, 94*(1–2), 58–66.

**Batchelor, G.K.** (1976). in W.T. Koiter (Ed.), *Theoreticai and Applied Mechanics*, North Holland, p. 33.

**Bloom, F., Heindel, T.J.** (2002). On the structure of collision and detachment frequencies in flotation models, *Chemical Engineering Science*, *57*, 2467–2473.

**Bloom, F., Heindel, T.J.** (1997). Mathematical modelling of the flotation deinking process, *Mathematical Computation Modelling*, *25*(5), 13-58.

**Bournival, G., Ata, S., Wanless, E.G.** (2016). Behviour of bubble interfaces stabilized by particles of different densities, *Langmuir, 32*, 6226-6238.

**Brabcova, Z., Karapantsios, K., Kostoglou, M., Basarova, P., Matis, K.** (2015). Bubble–particle collision interaction in flotation systems, *Colloids and Surfaces A: Physicochemical and Engineering Aspects, 473*(20), 95–103.

**Brenner, H.** (1961). The slow motion of a sphere through a viscous fluid towards a plane surface, *Chemical Engineering Science,* ***16***, 242-251.

**Bruce, H.K. (**2003). *Modeling of hindered-settling column separations,* Ph.D thesis in mineral processing. Pennsylvania State University, 11–13.

**Bu, X., Xie, G., Peng, Y., Ge, L., Ni, C.** (2017). Kinetic of flotation. Order of process, rate constant distribution and ultimate recovery, *Physicochemical Problems of Mineral Processing*, *53*(1), 342-365.

**Camp, T.R. and Stein, P.C.** (1943). Velocity gradients and integral work in fluid motion, *Journal of Boston Society and Civil Engineering*, *30(4)*, 219.

**Chen, F., Gomez, C.O., Finch, J.A.** (2001). Bubble size measurement in flotation machines, *Minerals Engineering, 14*(4), 427–432.

**Chen, J., Stebe, K.J.** (1996). Marangoni retardation of the terminal velocity of a settling droplet: the role of surfactant physico-chemistry, *Journal of Colloid and Intereface Science, 178*, 144–155.

**Cheng, G., Shi, C., Yan, X., Zhang, Z., Xu, H., Lu, Y.** (2017). A study of bubble-particle interactions in a column flotation process, *Physicochemical Problems of Mineral Processing*, *53*(1), 17-33.

**Cho, Y.S., Laskowski, J.S.** (2002). Effect of flotation frothers on bubble size and foam stability, *International Journal of Mineral Processing, 64*, 69–80.

**Cilek, E.C.** (2004). Estimation of flotation kinetic parameters by considering interactions of the operating variables, *Minerals Engineering*, *17*, 81–85.

**Clift, R., Grace, J.R., Weber, M.E.** (1978). *Bubbles, Drops, and Particles*. Academic Press, New York.

**Crawford, R., Ralston, J. (**1988). The influence of particle size and contact angle in mineral flotation, *International Journal of Mineral Processing*, *23*, 1–24.

**Cuong, M., Nguyen, A.V. Nguyen, Miller, J.D.** (2006). Computational validation of the Generalized Sutherland Equation for bubble–particle encounter efficiency in flotation, *International Journal of Mineral Processing*, ***81***, 141–148.

**Dai, Z.** (1998). *Particle–bubble heterocoagulation*, PhD Thesis, University of South Australia, Australia.

**Dai, Z., Dukhin, S., Fornasiero, D., Ralston, J.** (1998). The inertial hydrodynamic interaction of particles and rising bubbles with mobile surfaces, *Journal of colloid and interface science*, *197*, 275–292.

**Dai, Z., Fornasiero, D. and Ralston, J.** (1999). Particle–bubble attachment in mineral flotation, *Journal of Colloid and Interface Science*, *217*(1), 70-76.

**Dai, Z., Fornasiero, D., Ralston, J.** (2000). Particle–bubble collision models-A review, *Advances in Colloid and Interface Science, 85*, 231–256.

**Dashti, A., Eskandari Nasab, M.** (2013). Optimization of the performance of the hydrodynamic parameters on the flotation performance of coarse coal particles using design expert (DX8) software, *Fuel*, *107*, 593–600.

**Davis, R.H.** (1993). Microhydrodynamics of particulate suspensions, *Advance in Colloid and Interface Science*, ***43***, 17-50.

**Deglon, D.A., Egya-Mensah, D., Franzidis, J. P.** (2000). Review of hydrodynamics and gas dispersion in flotation cells on South African platinum concentrators, *Minerals Engineering*, *13*, 235–244.

**Derjaguin, B., Dukhin, S.** (1993). Theory of flotation of small and medium-size particles, *Progress in Surface Science*, *43*(1), 241–266.

**Derjaguin, B.V. and Dukhin, S.S.** (1960). Theory of flotation of small and medium-size particles, *Transactions of the Institute of Mining and Metallurgy, 70*, 221-246.

**Derjaguin, B.V., Dukhin, S.S.** (1993). Theory of Flotation of small and medium sized particles, *Progress in Surface Science*, *43*(1-4), 241–246.

**Derjaguin, B.V., Dukhin, S.S., Rulyov, N.N.** (1986). Microflotation, Khimija, Moscova,.

**Do, H.** (2010). *Development of a turbulent flotation model from first principles*. (Ph.D. Thesis). Virginia Polytechnic Institute and State University, USA.

**Dobby, G.S., Finch, J.A.** (1987). Particle size dependence in flotation derived from a fundamental model of the capture process. *International Journal of Mineral Processing, 2*(3–4), 241–260.

**Dowling, E.C., Klimpel, R.R., Aplan, F.F.** (1985). Model discrimination in the flotation of a porphyry copper ore, *Minerals and Metallurgical Processing*, *2*(2), 87-101.

**Duan, J., Fornasiero, D., Ralston, J.** (2003). Calculation of the flotation rate constant of chalcopyrite particles in an ore, *International Journal of Mineral Processing, 72*, 227–237.

**Duineveld, P.C.** (1995). The rise velocity and shape of bubbles in pure water at high Reynolds number*, Journal of Fluid Mechanics, 292*, 325-3

**Dukhin S.S., Miller, R., Loglio, G.** (1998). Physico-chemical hydrodynamic of rising bubble, *Drops and Bubbles in Interfacial Research*, 367–432.

**Dukhin, S. S., and Rulyov, N. N.** (1977). *Kolloidn Zh.*, *39*, p. 270.

**Dukhin, S.S.** (1983). Critical value of the Stokes number and the Sutherland formula. *Kolloidnyi Zhurnal (in Russian), 45*(2), 207–218.

**Dukhin, S.S.** (1982). Role of inertial forces in flotation of small particles, *Kolloidnyi Zhurnal (in Russian)*, *44*(3), 431-441.

**Dukhin, S.S., Kretzschmar, G., Miller, R.** (1995). *Dynamics of Adsorption at Liquid Interfaces*, 1st Edition, ISBN: 9780444881175, Elsevier Science

**Dukhin, S.S., Rulev, N.N.** (1977). Hydrodynamic interaction between a solid spherical particle and a bubble in the elementary act of flotation, *Kolloid. Zh.*, *39*(2), 270–275.

**Dukhin, S.S., Schulze, H.J.** 1987, Inertial-hydrodynamic interaction of particle with bubble in elementary act of flotation at supercritical Stokes numbers, *Kolloidn. Zh.*, *49*(4), 644–654.

**Ek, C.** (1992). *Flotation kinetic. In Innovations in Flotation Technology*, (Mavros, P. and Matis, K. A., Eds.), Nato ASISeries, Dordrecht, The Netherlands: Kluwer Academic Publishers, *208*, 183–209.

**Eskanlou, A., Shahbazi, B., Vaziri Hassas, B.** (2018). Estimation of flotation rate constant and collision efficiency using regression and artificial neural networks, *Separation Science and Techn*ology, *53*, 374-388.

**Evans, G.M., Doroodchi, E., Lane, G.L., Koh, P.T.L., Schwarz, M.P.** (2008). Mixing and gas dispersion in mineral flotation cells, *Chemical Engineering Research and Design*, *86*, 1350–1362.

**Fallenius, K.** (1987). Turbulence in flotation cells, *International Journal of Mineral Processing*, *21*(1–2), 1-23.

**Fan, M., Tao, D., Honaker, R., Luo, Z.** (2010). Nanobubble generation and its applications in froth flotation (part II): fundamental study and theoretical analysis, *Mining Science and Technology*, *20*, 159–177.

**Finch, J.A., Nesset, J.E., Acuna, C.** (2008). Role of frother on bubble production and behaviour in flotation, *Minerals Engineering*, *21*, 949–957.

**Firouzi, M. and Nguyen, A.V.** (2014a). Effects of monovalent anions and cations on drainage and lifetime of foam films at different interface approach speeds, *Advanced Powder Technology*, *25*, 1212-1219.

**Firouzi, M. and Nguyen, AV.** (2014b). Novel methodology for predicting the critical salt concentration of bubble coalescence inhibition, *Journal of Physical Chemistry C*, *118*, 1021-1026.

**Firouzi, M. and Nguyen, AV.** (2014c). On the effect of van der Waals attractions on the critical salt concentration for inhibiting bubble coalescence, *Minerals Engineering*, *58*, 108-112.

**Firouzi, M. and Nguyen, A.V.** (2017). The Gibbs-Marangoni stress and nonDLVO forces are equally important for modeling bubble coalescence in salt solutions, *Colloids and Surfaces A: Physicochemical and Engineering Aspects*, *515*, 62-68.

**Firouzi, M., Howes, T. and Nguyen, A.V.** (2015). A quantitative review of the transition salt concentration for inhibiting bubble coalescence , *Advances in Colloid and Interface Science*, *222*, 305-318.

**Firouzi, M., Nguyen, A.V., Hashemabadi, H.** (2011). The effect of microhydrodynamics on bubble–particle collision interaction, *Minerals Engineering, **24***, 973–986.

**Flint, L.R., Howarth, W.J.** (1971). The collision efficiency of small particles with spherical air bubbles. *Chemical Engineering Science, 26*(8), 1155–1168.

**Fornasiero, D., Filippov, L.O.** (2017). Innovations in the flotation of fine and coarse particles, *Journal of Physics: Conference Series, 879*, 012002, pp. 1-6.

**Gammelsater, R., Bech, K., Johansen, S.T.** (1997). *Enhanced flotation of inclusions to bubbles due to turbulence*. In: Huglen, R. (Ed.), Light Metals. TMS, 1007–1011.

**Gaudin, A.M.** (1957). *Flotation*. McGraw-Hill, New York.

**Gharai M., and Venugopal, R.** (2016). Modeling of flotation process-An overview of different approaches, *Mineral Processing and Extractive Metallurgy Review*, *37*(2), 120-133.

**Gorain, B., Franzidis, J., Manlapig, E.** (1996). Studies on impeller type, impeller speed and air flow rate in an industrial scale flotation cell, Part 3: effect on superficial gas velocity. *Minerals Engineering*, *9*, 639–654.

**Gorain, B.K., Franzidis, J.P., Manlapig, E.V.** (1997). Studies on impeller type, impeller speed and air flow rate in an industrial scale flotation cell. 4. Effect of bubble surface area flux on flotation performance, *Minerals Engineering, 10*(4), 367–379.

**Govender, D., Lelinski, D., Traczyk, F.** (2012). Hybrid energy flotation™- on the optimization of fine and coarse particle kinetic in a single row, *The Journal of The Southern African Institute of Mining and Metallurgy*, *113*, 285-296.

**Grammatika, M., Zimmerman, W.B.** (2001). Microhydrodynamics of flotation processes in the sea surface layer, *Dynamics of Atmospheres and Oceans*, *34*, 327–348.

**Grau, R.A., Laskowski, J.S., Heiskanen, K.** (2005). Effect of frothers on bubble size, *International Journal of Mineral Processing*, *76*, 225–233.

**Guven, O., Celik, M.S.** (2016). Interplay of particle shape and surface roughness to reach maximum flotation efficiencies depending on collector concentration, *Mineral Processing and Extractive Metallurgy Review*, *37*(6), 412-417.

**Guven, O., Celik, M.S., Drelich, J.W.** (2015). Flotation of methylated roughened glass particles and analysis of particle–bubble energy barrier, *Minerals Engineering*, *79*, 125-132.

**Hamielec, A.E., Storey, S.H., Whitehead, J.M.** (1963). Viscous flow around fluid spheres at intermediate Reynolds numbers (II), *Canadian Journal of Chemical Eng*ineering, *41*, 246-251.

**Han, M., Kim, W., Dockko, S.** (2001). Collision efficiency factor of bubble and particle ($\alpha_{bp}$) in DAF: theory and experimental verification, *Water Science and Technology*, *43*(8), 139–144.

**Happel, J., Brenner, H.** (1963). *Low Reynolds number hydrodynamics*. Martinus Nijhoff Publishers, Hague, Netherlands.

**Harris, C. C.** (1978). Multiphase model of flotation machine behavior, *International Journal of Mineral Processing*, *5*, 107–129

**Hassanzadeh A., Kouachi, S., Hasanzadeh, M., Celik, M.S**. (2017). A new insight to the role of bubble properties on inertial effect in particle–bubble interaction, *Journal of Dispersion Science and Technology*, *38*(7), 953-960.

**Hassanzadeh, A.** (2017). Measurement and modeling of residence time distribution of overflow ball mill in continuous closed circuit, *Geosystem Engineering*, *20*(5), 251-260.

**Hassanzadeh, A., Farhadi, E., Azizi, A.** (2015). Modeling and analysis of residence time distribution in industrial mechanical flotation cells, *Proceedings of the 24th International Mining Congress and Exhibition of Turkey*, Antalya, Turkey,14-17 April, 757-763.

**Hassanzadeh, A., Firouzi, M., Albijanic, B., Celik, M.S.** 2018, A review on determination of particle-bubble encounter using analytical, experimental and numerical methods, *Minerals Engineering*, *122*, 296-311.

**Hassanzadeh, A., Hasanzadeh, M.** (2016). A study on selective flotation in low and high pyretic copper sulfide ores, *Separation Science and Technology*, *51*, 2214–2224.

**Hassanzadeh, A., Karakaş, F.** (2017a). The kinetic modeling of chalcopyrite and pyrite, and the contribution of particle size and sodium metabilsulfite to the flotation of copper complex ores, *Particular Science and Technology*, *35*(4), 455-461.

**Hassanzadeh, A., Karakaş, F.** (2017b). Recovery improvement of coarse particles by stage addition of reagents in industrial copper flotation circuit, *Journal of Dispersion Science and Technology*, *38*(2), 309–316.

**Hassanzadeh, A., Vaziri Hassas, B., Kouachi, S., Brabcova, Z., Çelik, M.S.** (2016). Effect of bubble size and velocity on collision efficiency in chalcopyrite flotation, *Colloids and Surfaces A: Physicochemical and Engineering Aspects*, *498*(5), 258-267.

**Hassnzadeh, A., Azizi, A.** (2015). Flotation circuit efficiency enhancement regarding increase of rougher cells throughput, *Proceedings of the 24th International Mining Congress and Exhibition of Turkey*, Antalya, Turkey, 14-17 April, 1175–1179.

**Heindel, T., Bloom, F.** (1999). Exact and approximate expression for bubble-particle collision, *Journal of Colloid and Interface Science*, *213*, 101–111.

**Hewitt, D., Fornasiero, D. and Ralston, J.** (1995). Bubble-particle attachment, *Journal of the Chemical Society*, *Faraday Transactions*, *91*(13), 1997-2001.

**Hobbs, A.**, (2009). Simulation of an aggregate dryer using coupled CFD and DEM methods, *International Journal of Computational Fluid Dynamic*, *23*(2), 199–207.

**Huang Z., Legendre D., Guiraud, P.** (2011). A new experimental method for determining particle capture efficiency in flotation, *Chemical Engineering Science, 66*, 982–997.

**Imaizumi T., Inoue, T.**, (1963). Kinetic considerations of froth flotation, *Proceedings of the 6th International Mineral Processing Congress*, Cannes, France, 581-593

**Ireland, P.M., Jameson, G. J.** (2014). Collision of a rising bubble–particle aggregate with a gas–liquid interface, *International Journal of Mineral Processing*, *130*, 1–7.

**Jameson, G.J.** (2010). New directions in flotation machine design. *Minerals Engineering, 23*, 835–841.

**Jameson, G.J., Nam, S., Young, M.M. (**1977). Physical factors affecting recovery rates in flotation, *Mining Science of Engineering*, *9*(3), 103–108.

**Jenson, V.G.** (1959). Viscous flow round a sphere at low Reynolds numbers (<40), *Proceedings of the Royal Society, A249*, 346-366.

**Jiang, L., Krasowska, M., Fornasiero, D., Koh, P., Ralston, J.** (2010). Electrostatic attraction between a hydrophilic solid and a bubble, *Physical Chemistry Chemical Physics*, *12*, 14527–14533.

**Jiang, Z.W. and Holtham, P.N.** (1986). Theoretical model of collision between particles and bubbles in flotation. *Transactions of the Institution of Mining and Metallurgy*, *95*, C187-C193.

**Johansen, S.T., Fredriksen, A., Rasch, B.** (1995). Particle flotation to bubbles in rotor-stirred reactors for melt treatment. Light Metals, *The Minerals, Metals and Materials Society*, 1203–1206.

**Jordan, C.E., Spears, D.R.** (1990). Evaluation of a turbulent flow model for fine-bubble and fine-particle flotation, *Minerals and Metallurgical Processing*, *7*(2), 65–73.

**Jowett, A. and Safvi, S. M.** (1960) Refinements in methods of determining flotation rates, *Transactions of the AIME*, *217*, 351–357.

**Kalyani, V.K., Pallavika, Gouri Charan T, Sanjay C.** (2005) Optimization of a laboratory scale froth flotation process using response surface methodology. *International Journal of Coal Preparation and Utilization*, *25*, 141–53.

**Karakas, F., Vaziri Hassas, B.** (2016). Effect of surface roughness on interaction of particles in flotation, *Physicochemal Problems in Mineral Processing*, *52*(1), 18–34.

**Karimi, M., Akdogan, G., Bradshaw, S.M.** (2014a). A computational fluid dynamics model for the flotation rate constant, Part I: Model development, *Minerals Engineering*, *69*, 214–222.

**Karimi, M., Akdogan, G., Bradshaw, S.M.** (2014b). A CFD-kinetic model for the flotation rate constant, Part II: Model validation, *Minerals Engineering*, *69*, 205–213.

**Kelly, E.G., Carlson, C.E.** (1991). Two flotation models: resolution of a conflict. *Minerals Engineering, 4*(12), 1333-1338.

**Kelsall, D. F.** (1961). Application of probability in the assessment of flotation systems, *Bull. Institution of Mining and Metallurgy*, *70*(4), 650, 191–204.

**King, R.P.** (2001). *Modeling and Simulation of Mineral Processing Systems*, Department of Metallurgical Engineering, University of Utah, USA, 293–320.

**Klimpel, R.R.** (1980). *Selection of chemical reagents for flotation. Mineral Processing Plant Design*, 2nd ed (Mullar, A. L. and Bhappu, R. B., Eds.), New York: AIME, pp. 907–934.

**Koh, P.T.L., Manickam, M., Schwarz, M.P.** (2000). CFD simulation of particle–bubble collisions in mineral flotation cells, *Minerals Engineering, 13*(14-15), 1455-1463.

**Koh, P.T.L., Schwarz M.P.** (2007). CFD model of a self-aerating flotation cell, *International Journal of Mineral Processing, 85*, 16–24.

**Koh, P.T.L., Schwarz M.P.** (2003). CFD modelling of bubble–particle collision rates and efficiencies in a flotation cell, *Minerals Engineering, 16*, 1055–1059.

**Koh, P.T.L., Schwarz, M.P.** (2006). CFD modelling of bubble–particle attachments in flotation cells, *Minerals Engineering, 19*, 619-626.

**Koh, P.T.L., Schwarz, M.P.** (2007). CFD model of a self-aerating flotation cell, *International Journal of Mineral Processing*, *85*, 16–24.

**Kouachi, S., Bouhenguel, M., Amirech, A., Bouchemm, A.** (2010). Yoon–Luttrell collision and attachment models analysis in flotation and their application on general flotation kinetic model, *Desalination*, *264(3*), 228-235.

**Kouachi, S., Hassanzadeh, A., Bouhenguel, M., Vaziri Hassas, B., Çelik, M.S.** (2015). Contribution of interceptional effect to collision efficiency of particle bubble encounter in flotation, *Proceedings of the XVI Balkan Mineral Processing Congress*, Belgrade, Serbia, 339–345.

**Kouachi, S., Vaziri Hassas, B., Hassanzadeh, A., Celik M.S., Bouhenguel, M.** (2017). Effect of negative inertial forces on particle–bubble collision via implementation of Schulze collision efficiency in general flotation rate constant equation, *Colloids and Surfaces A: Physicochemical Engineering Aspects, 517*, 72–83.

**Kracht, W., Vallebuona, G., Casali, A.** (2005). Rate constant modelling for batch flotation, as a function of gas dispersion properties. *Minerals Engineering*, *18*(11), 1067–1076.

**Kulkarani, A.A., Joshi, J.B.** (2005). Bubble formation and bubble rise velocity in gas-liquid systems: a review. *Industrial and Engineering Chemistry Research*, *44*, 5873-5931.

**Lane, G.L.** (2005). *Numerical modelling of gas–liquid flow in stirred tanks*. (Ph.D. Thesis). University of Newcastle, Australia.

**Langmuir, I., Blodgett, K.** (1945). Mathematical investigating of water droplet trajectories, *Journal of Meteorology*, *5*, 175.

**Laskowski, J.S., Cho, Y.S., Ding, K.J.** (2003). Effect of frothers on bubble size and foam stability in potash ore flotation systems. *Canadian Journal of Chemical Engineering*, *81*, 63–69.

**Legendre, D., Sarrot, V., Guiraud, P.** (2009). On the particle inertia-free collision with a partially contaminated spherical bubble, *International Journal of Multiphase Flow*, *35*, 163–170.

**Lehr, F., Millies, M., Mewes, D.** (2002). bubble-size distributions and flow fields in bubble columns, *Fluid Mechanics and Transport Phenomena*, *48*, 2426-2243.

**Leistner, T., Peuker, U.A., Rudolph, M.** (2017). How gangue particle size can affect the recovery of ultrafine and fine particles during froth flotation, *Minerals Engineering*, *109*, 1–9.

**Leppinen, D.M.** (1999). Trajectory analysis and collision efficiency during microbubble flotation, *Journal of Colloid and Interface Science, 212*, 431-442.

**Levich, V. G.** (1962). *Physiochemical Hydrodynamics*, New Jersey, Prentice Hall.

**Levin, L.I.** *Research into the physics of coarsely disperse aerosols*, Isd. Akad. Nauk SSSR,

**Li, H., Afacan, A., Liu, Q., Xu, Z.** (2015). Study interactions between fine particles and micron size bubbles generated by hydrodynamic cavitation, *Minerals Engineering, 84*, 106–115.

**Liu, T.Y., Schwarz, M.P.** (2009a). CFD-based modelling of particle–bubble collision efficiency with mobile bubble surface in a turbulent environment, *International Journal of Mineral Processing*, *90*, 45–55.

**Liu, T.Y., Schwarz, M.P.** (2009b). CFD-based multiscale modelling of bubble–particle collision efficiency in a turbulent flotation cell. *Chemical Engineering Science, 64*, 5287-5301.

**Lyman, G.J.** (1983). *Enhancement of coarse particle recovery in froth flotation of coal* J.K.M.R.C. Report, in Nicholson, op cit.

**Malysa, K., Krasowska, M., Krzan, M.** (2005). Influence of surface active substances on bubble motion and collision with various interfaces, *Advances in Colloid and Interface Science*, *114–115*, 205-225.

**Mao, L. and Yoon, R.H.** (1997). Predicting flotation rates using a rate equation derived from first principles. *International Journal of Mineral Processing, 51*(1-4), 171-181.

**Martinez-L, A., Uribe, A.S., Carrillo, F.R.P., Coreno, J.A., Ortiz, J.C.** (2003). Study of celestite flotation efficiency using sodium dodecyl sulfonate collector: factorial experiment and statistical analysis of data. *International Journal of Mineral Processing*, *70*, 83–97.

**Massinaei, M., Kolahdoozan, M., Noaparast, M., Oliazadeh, M., Yianatos, J., Shamsadini, R., Yarahmadi, M.** (2009). Hydrodynamic and kinetic characterization of industrial columns in rougher circuit, *Minerals Engineering*, *22*(4), 357–365.

**Maxwell, R., Ata, S., Wanless, E.J., Moreno-Atanasio, R.** (2012). Computer simulations of particle–bubble interactions and particle sliding using discrete element method. *Journal of Colloid and Interface Science, 381*, 1-10.

**Mehrotra, S. P. and Padmanabhan, N. P. H.** (1990). Flotation kinetic—a review, *Transactions of The Indian Institute of Metals*, *43*, 9–21.

**Meyer, C.J., Deglon, D.A.** (2011). Particle collision modeling-A review, *Minerals Engineering*, *24*, 719–730.

**Miettinen, T.** (2007). *Fine particle flotation*, PhD Thesis, University of South Australia, Australia.

**Miettinen, T., Ralston, J., Fornasiero, D.** (2010). The limits of fine particle flotation, *Minerals Engineering, 23*, 420–437.

**Mika, T. S. and Feurstenau, D. W.** (1968). A microscopic model of the flotation process, *Proceeding of the VIII International Mineral Processing Congress,* Leningrad, Russia, 246-269.

**Motarjemi, M., and Jameson, G.J.** (1978). Mass transfer from very small bubbles-the optimum bubble size for aeration, *Chemical Engineering Science*, *33*, 1415–1423.

**Mukherjee, M.,** (2004). *Bubble solid interaction*. (MSc. Thesis). Center for Advanced Study, Department of Metallurgy, Faculty of Engineering, Indian Institute of Science, India.

**Natanson, G.L.** (1957). Diffusional precipitation of aerosols on a streamlined cylinder with a small capture coefficient, *Proceedings of the Academy of Sciences of the USSR Physical Chemistry Section*, *112*, 21-25.

**Nesset, J.E., Hernandez-Aguilar, J.R., Acuna, C., Gomez, C.O., Finch, J.A.** (2006). Some gas dispersion characteristics of mechanical flotation machines, *Minerals Engineering*, *19*, 807–815.

**Newell, R., Grano, S.** (2006). Hydrodynamics and scale up in Rushton turbine flotation cells: Part 2. Flotation scale-up for laboratory and pilot cells, *International Journal of Mineral Processing*, *81*, 65–78.

**Newell, R.** (2006). *Hydrodynamics and scale-up in Rushton turbine flotation cells*. (Ph.D. Thesis). University of South Australia, Australia.

**Nguyen, A.V.** (1994). The collision between fine particles and single air bubbles in flotation. *Journal of Colloid and Interface Science, 162*, 123-128.

**Nguyen, A.N., Evans G.M.** (2004). Movement of fine particles on an air bubble surface studied using high-speed video microscopy, *Journal of Colloid and Interface Science, 273*(1), 271–277.

**Nguyen, A.V., Kmet, S.** (1992). Collision efficiency for fine mineral particles with single bubble in a countercurrent flow regime, *International Journal of Mineral Processing, 35*, 205-223.

**Nguyen, A.V.** (1998). Particle–bubble encounter probability with mobile bubble surfaces, *International Journal of Minereral Processing,* ***55***, 73–86.

**Nguyen, A.V., An-Vo, D.A., Tran-Cong, T., Evans, G.M.** (2016). A review of stochastic description of the turbulence effect on bubble-particle interactions in flotation, *International Journal of Mineral Processing, 156*(10), 75-86.

**Nguyen, A.V., Evans, G.M.** (2002). Axisymmetric approach of a solid sphere toward a non-deformable planar slip interface in the normal stagnation flow—development of global rational approximations for resistance coefficients. *International Journal of Multiphase Flow, 28*, 1369-1380.

**Nguyen, A.V., Ralston, J., Schulze, H.J.** (1998). On modeling of bubble-particle attachment probability in flotation, *International Journal of Mineral Processing*, *53*, 225–249,

**Nguyen, A.V., Schulze, H.J.** (2004). *Colloidal Science of Flotation*. Marcel Dekker, New York. p. 840.

**Nguyen, A.V., Schulze, H.J., and Ralston, J.** (1997). Elementary steps in particle-bubble attachment, *International Journal of Mineral Processing*, *51*, 183–195.

**Nguyen, C., Nguyen, A.N., Miller, J.D.** (2006). Computational validation of the Generalized Sutherland Equation for bubble–particle encounter efficiency in flotation, *International Journal of Mineral Processing*, *81*, 141–148.

**Nguyen, P.T., Nguyen, A.V.** (2009). Validation of the generalized Sutherland equation for bubble–particle encounter efficiency in flotation: Effect of particle density, *Minerals Engineering, 22*, 176-181.

**Ni, C., Xie, G., Jin, M., P, Y., Xia, W.** (2016). The difference in flotation kinetic of various size fractions of bituminous coal between rougher and cleaner flotation processes, *Powder Technology*, *292*, 210–216.

**Nonaka, M., Inoue, T., Imaizumi, T.** (1982). A microhydrodynamic flotation model and its application to the flotation process. *XIV International Mineral Processing Congress*, Toronto. II-9.1-III-9.18.

**Pease, J.D., Curry, D.C. and Young M.F.** (2005). Designing flotation circuits for high fines recovery, *Proceeding of the Centenary of Flotation Symposium*, Brisbane, Australia, 905–912.

**Phan, C.M., Nguyen, A.V., Miller, J.D., Evans, G.M., Jameson G.J.** (2003). Investigations of bubble–particle interactions, *International Journal of Mineral Processing*, *72*, 239–254.

**Popli, K.** (2017). *Real-time process monitoring for froth flotation processes using image processing and dynamic fundamental models*. (Ph.D. Thesis). University of Alberta, Canada.

**Popli, K., Sekhavat, M., Afacan, A., Dubljevic, S., Liu, Q., Prasad, V.** (2015). Dynamic modeling and real-time monitoring of froth flotation, *Minerals*, *5*, 570-591.

**Pyke, B.** (2003). *Particle–bubble capture in turbulent flotation systems*. (Ph.D. Thesis). University of South Australia, Australia.

**Pyke, B., Fornasiero, D., Ralston, J.** (2003). Particle–bubble heterocoagulation under turbulent conditions, *Journal of Colloid Interface Science, 265*, 141–151.

**Quinn, J. J., Kracht, W., Gomez, C., Gagnon, C., & Finch, J.** (2007). Comparing the effect of salts and frother (MIBC) on gas dispersion and froth properties. *Minerals Engineering*, *20*(14), 1296-1302.

**Radoev, B.P. Alexandrova, L.B., Tchaljovska, S.D.** (1990). On the kinetics of froth flotation, *International Journal of Mineral Processing*, *28*(1-2), pp. 127-38.

**Rafiei Mehrabadi, A.A.** (2009). Effects of frother type on single bubble rise velocity. (Ph.D. Thesis). McGill University, Montreal, Canada.

**Ralston, J., Dukhin, S.S.** (1999). The interaction between particles and bubbles, *Colloids and Surfaces A: Physicochemical and Engineering Aspects*, *151*, 3–14.

**Ralston, J., Dukhin, S.S., Mishchuk, N.A.** (2002). Wetting film stability and flotation kinetics, *Advances in Colloid and Interface Science, 95*, 145-236.

**Ralston, J., Dukhin, S.S., Mishchuk, N.A.** (1999). Inertial hydrodynamic particle-bubble interaction in flotation, *International Journal of Mineral Processing*, *56*, 207–256.

**Ralston, J., Fornasiero, D., Hayes, R.** (1999). Bubble–particle attachment and detachment in flotation, *International Journal of Mineral Processing*, *56*, 133–164.

**Reay, D., and Ratcliff, G.A.** (1975). Experimental testing of the hydrodynamic collision model of fine particle flotation, *The Canadian Journal of Chemical Engineering*, *53*, 481.

**Reay, D., Ratcliff, G.A.** (1973). Removal of fine particles from water by dispersed air flotation. Effects of bubble size and particle size on collection efficiency. *The Canadian Journal of Chemical Engineering, 51*(2), 178–185.

**Rooki, R. Doulati Ardejani, F., Moradzadeh, A., Kelessidis, V.C., Nourozi, M.** (2012). Prediction of terminal velocity of solid spheres falling through Newtonian and non-Newtonian pseudoplastic power law fluid using artificial neural network, *International Journal of Mineral Processing, 110–111*, 53–61.

**Rubioa, J., Souza, M.L., Smith, R.W.** (2002). Overview of flotation as a wastewater treatment technique, *Minerals Engineering*, *15*(3), 139-155.

**Safari, M., Deglon, D.** (2018). An attachment-detachment kinetic model for the effect of energy input on flotation, *Minerals Engineering*, *117*, 8–13.

**Saffman, P.G. and Turner, J.S.** (1956). On the collision of drops in turbulent clouds, *Journal of Fluid Mechanics, 1*, 16-30.

**Sahoo, S.K., Suresh, N., Varma, A.K.** (2016). Performance evaluation of basic flotation kinetic models using advanced statistical techniques, *International Journal of Coal Preparation and Utilization*, 1-23.

**Sam, A., Gomez, C.O., Finch, J.A.** (1996). Axial velocity profiles of single bubbles in water/frother solutions, *International Journal of Mineral Processing*, *47*, 177–196.

**Sarrot, V., Huang, Z., Legendre, D., Guiraud, P.** (2007). Experimental determination of particles capture efficiency in flotation, *Chemical Engineering Science, 62*, 7359-7369.

**Schimmoller, B.K., Luttrell, G.H. Yoon, R.H.** (1993) A combined hydrodynamic-surface force model for bubble-particle collection. *XVIII International Mineral Processing Congress,* Sydney, 751-756.

**Schubert, H. and Bischofberger, C.** (1978). On the hydrodynamics of flotation machines, *International Journal of Mineral Processing*, *5*, 131-142.

**Schubert, H.** (2005). Nanobubbles, hydrophobic effect, heterocoagulation and hydrodynamics in flotation, *International Journal of Mineral Processing*, *78*, 11-21.

**Schubert, H.** (1999). On the turbulence-controlled microprocesses in flotation machines, *International Journal of Mineral Processing*, *56*, 257-276.

**Schubert, H.J.** (2008). On the optimization of hydrodynamics in fine particle flotation, *Minerals Engineering*, *21*(12–14), 930-936.

**Schuhmann R.** (1942). Flotation kinetics I. Methods for steady-state study of flotation *problems, J. Phys. Chem*., *46*, 891–902.

**Schulze, H.J.** (1977). New theoretical and experimental investigations on stability of bubble particle aggregates in flotation: A theory on the upper particle size of floatability, *International Journal of Mineral Processing*, *4*, 241–259.

**Schulze, H.J.** (1989). Hydrodynamics of bubble-mineral particle collisions, *Mineral Processing and Extractive Metallurgy Review*, *5*, 43–76.

**Schulze, H.J.** (1992). Probability of particle attachment on gas bubbles by sliding, *Advances in Colloid and Interface Science*, *40*(30), 283-305.

**Schulze, H.J.,** (1993). Flotation as a heterocoagulation process: possibilities of calculating the probability of flotation, *Surfactant Science Series* (Coagulation and Flocculation), *47*, 321–354.

**Schulze, H.J., Gottschalk G.** (1981). Preliminary experimental investigations of hydrodynamic interaction between particles and a gas bubble, *Aufbereitungstechnik (in German)*, *22*, 254-263.

**Shahbazi, B., Rezai, B., Koleini, S.M.J.** (2010). Bubble–particle collision and attachment probability on fine particles flotation, *Chemical Engineering and Processing, 49*, 622–627.

**Shahbazi, B., Rezai, B., Koleini, S.M.J.** (2009). The effect of hydrodynamic parameters on probability of bubble–particle collision and attachment, *Minerals Engineering*, *22*, 57–63.

**Shen LH, Johnsson F, Leckner B.** (2004). Digital image analysis of hydrodynamics two dimensional bubbling fluidized beds, *Chemical Engineering Science*, *59*, 2607–2617.

**Sherrell, I.M.** (2004). *Development of a flotation rate equation from first principles under turbulent flow conditions*, Ph.D. Thesis, Mining and Minerals Engineering, Virginia Polytechnic Institute and State University, Blacksburg, Virginia, U.S.A.

**Shi, Y., Fornasiero, D.** (2009). Effects of particle size and density, and turbulence on flotation recovery, Engineering our Future: Are we up to the Challenge?, *Engineers*, Australia, 528-236.

**Shrimali, K., Jin, J., Vaziri Hassas, B., Wang, X., Miller, J.D.** (2016). The surface state of hematite and its wetting characteristics, *Journal of Colloid and Interface Science*, *477*, 16–24,

**Smoluchowski, M.** (1917). Versuch einer mathematischen theorie der koagulations-kinetik kollöider losungen. *Zeitschrift für Physikalische Chemie (in German)*, *92*, 129.

**Sobhy, A., Tao, D.** (2013). Nanobubble column flotation of fine coal particles and associated fundamentals, *International Journal of Mineral Processing, 124*, 109–116.

**Sundaram, S. and Collins, L.R.** (1997). Collision statistics in an isotropic particle-laden turbulent suspension. Part 1. Direct numerical simulations, *Journal of Fluid Mechanics*, *335*, 75-109.

**Sutherland, K.** (1948). The physical chemistry of flotation XI. Kinetics of the flotation process. *The Journal of Physical and Colloid Chemistry, 52*(2), 394–425.

**Tao, D.** (2004). Role of bubble size in flotation of coarse and fine particles-A review, *Separation Science and Technology*, *39*, 741–760.

**Temesgen, T., Bui, T.T., Han, M., Kim, T.I., Park, H.** (2017). Micro and nanobubble technologies as a new horizon for water-treatment techniques: A review, *Advances in Colloid and Interface Science*, *246*, 40-51.

**Trahar, W.J.** (1981). A rational interpretation of the role of particle size in flotation, *International Journal of Mineral Processing*, *8*(4), 289-327.

**Trahar, W.J., and Warren, L.J.** (1976). The floatability of very fine particles-A review. *International Journal of Mineral Processing*, *3*, 103-131.

**Tsai, J.C., Kumar, M., Chen, S.Y., Lin, J.G.** (2007). Nano-bubble flotation technology with coagulation process for the cost-effective treatment of chemical mechanical polishing wastewater, *Separation and Purification Technology, 58*, 61–67.

**Vanthuyne, M., Maes, A., Cauwenberg, P.** (2003). The use of flotation techniques in the remediation of heavy metal contaminated sediments and soils: an overview of controlling factors, *Minerals Engineering*, *16*(11), 1131-1141.

**Vaziri Hassas, B., Caliskan, H., Guven, O., Karakaş, F., Cinar, M., Celik, M.S.** (2016). Effect of roughness and shape factor on flotation characteristics of glass beads, *Colloids and Surfaces A: Physicochemical and Engineering Aspects*, *492*, 88-99.

**Vazirizadeh, A. (**2015). *The relationship between hydrodynamic variables and particle size distribution in flotation*, (Ph.D. Thesis). Laval University, Canada.

**Vazirizadeh, A., Bouchard, J., Villar, R.D., Barvarz, M.G., Duchesne, C.** (2015). On the relationship between hydrodynamic characteristics and the kinetic of flotation. Part II: Model validation, *Minerals Engineering*, *74*, 198–206.

**Venditti, R.A.** (2004). A simple flotation de-inking experiment for the recycling of paper, *Journal of Chemical Education*, *81*(5), 693.

**Verrelli, D.I., Albijanic, B.** (2015). A comparison of methods for measuring the induction time for bubble-particle attachment, *Minerals Engineering*, *80*, 8-13.

**Verrelli, D.I., Bruckard, W.J., Koh, P.T.L., Schwarz, M.P., Follink, B.** (2014). Particle shape effect in flotation. Part 1: Microscale experimental observations, *Minerals Engineering*, *58*, 80–89.

**Verrelli, D.I., Koh, P.T.L., Bruckard, W.J., Schwarz, M.P.** (2012). Variations in the induction period for particle–bubble attachment, *Minerals Engineering*, *36–38*, 219-230.

**Verrelli, D.I., Koh, P.T.L., Nguyen, A.V.** (2011). Particle–bubble interaction and attachment in flotation, *Chemical Engineering Science*, *66*, 5910–5921.

**Wang, C.Q., Wang, H., Fu, J.G., Liunt, Y.N.** (2015). Flotation separation of waste plastics for recycling—A review, *Waste Management*, *41*, 28-38.

**Wang, G., Ge, L., Mitra, S., Evans, G.M., Joshi, J.B., Chen, S.** (2018). A review of CFD modeliing studies on the flotation process, *Minerals Engineering*, *127*, 153-177.

**Wang, L., Lee, H.G., Hayes, P.** (1996). Prediction of the optimum bubble size for inclusion removal from molten steel by flotation, *ISIJ International*, *36*(1), 7-16.

**Wang, W., Zhou, Z., Nandakumar, K., Xu, Z., Masliyah, J.H.** (2003). Effect of surface mobility on the particle sliding along a bubble or a solid sphere, *Journal of Colloid and Interface Science*, *259*, 81-88.

**Weber, M.E.** (1981). Collision efficiency for small particles with a spherical collector at intermediate Reynolds numbers. *Journal of Separation Process Technology, 2*, 29-33.

**Weber, M.E., Paddock, D.** (1983). Interceptional and gravitational collision efficiencies for single collectors at intermediate Reynolds numbers. *Journal of Colloid and Interface Science, 94*(2), 328–335.

**Wierink, G., Tiitinen, J., Heiskanen, K.** (2009). Mapping of collision regimes in flotation modelling, *Proceeding of the Seventh International Conference on CFD in the Minerals and Process Industries*, CSIRO, Melbourne, Australia. P. 1-9.

**Wills, B.A.** (2006). *Mineral Processing Technology*, Butterworth Heinemann, UK

**Woodburn, E. T.** (1970). Mathematical modeling of flotation process, *Minerals Science and Engineering*, *2*(2), 3–17

**Woodburn, E.T., King, R.P., Colborn, R.P.** (1971). The effect of particle size distribution on the performance of a phosphate flotation process. *Metallurgical and Materials Transactions B, 2*, 3163-3174.

**Xian-ping, L., Xue-kun, T., Li-ping, H., Li-ying, L.** (2011). Effects of size distribution on flotation kinetics of Chalcopyrite, *International Conference on Environment Science and Engineering, IPCBEE*, *8*, IACSIT Press, Singapore, 81-85.

**Yoon, R.H.** (1991). Hydrodynamic and surface force in bubble-particle interactions, *Proceeding 17th 1MPG, Dresden*. p. 474.

**Yoon, R.H. and Mao, L.** (1996). Application of extended DLVO theory, IV. Derivation of flotation rate equation from first principles, *Journal of Colloid and Interface Science*, *181*(2), 613-626.

**Yoon, R.H., and Luttrell, G.H.** (1986). The effect of bubble size on fine coal flotation, *Coal Preparation*, *2*(3), 179–192.

**Yoon, R.H., Luttrell, G.H.** (1989). The effect of bubble size on fine particle flotation. *Mineral processing and Extractive Metallurgy Review, 5*, 101–122.

**Yoon, R.H., Soni, G., Huang, K., Park, S., Pan, L.** (2016). Development of a turbulent flotation model from first principles and its validation, *International Journal of Mineral Processing*, *156*(10), 43-51.

**Yoon, R.H., Yordan, J.L.** (1986). Zeta-potential measurements on microbubbles generated using various surfactants, *Journal of Colloid Interface Science, 113*, 430–438.

**Yuan, X.M., Palsson, B.I., Forssberg, K.S.E.** (1996). Statistical interpretation of flotation kinetic for a complex sulphide ore. *Minerals Engineering, 9*(4), 429-442.

**Zhang, Y., Finch, J.A.** (2001). A note on single bubble motion in surfactant solutions. *Journal of Fluid Mechanics, 429*, 63–66.

**Zheng, Y.Y. and Zhao, C.C.** (1993). A study of the kinetics on induced-air flotation for oil-water separation. *Seperation Science and Technology*, *28*, 1233-1240.

**Zuniga, H.G.** (1935). The efficiency obtained by flotation is an exponential function of time, *Bol. minero Soc. nacl. mineria (chile)*. *47*, 83-86.

## APPENDICES

**APPENDIX A:** ANOVA tables

The equation represents the particle–bubble encounter probabilities in terms of coded factors after removing insignificant terms given by Design Expert software.

$$E_c = +0.08 + 0.02\times A - 0.017\times B - 0.014\times C - 0.009167\times D - 0.00375\times A\times B$$
$$+0.00375\times B\times C - 0.003958\times A^2 + 0.007292\times B^2 + 0.002292\times C^2 + 0.003542 \quad \text{(A.1)}$$

**Table A.1:** ANOVA results of quadratic model to predict the $E_c$.

| Source | Sum of Squares | DF | Mean Square | F Value | p-value Prob > F | |
|---|---|---|---|---|---|---|
| **Model** | 0.027 | 10 | 2.67E-03 | 59.76 | < 0.0001 | significant |
| **A-particle size** | 9.60E-03 | 1 | 9.60E-03 | 214.59 | < 0.0001 | |
| **B-particle density** | 7.35E-03 | 1 | 7.35E-03 | 164.29 | < 0.0001 | |
| **C-bubble size** | 4.82E-03 | 1 | 4.82E-03 | 107.67 | < 0.0001 | |
| **D-velocity** | 2.02E-03 | 1 | 2.02E-03 | 45.08 | < 0.0001 | |
| **AB** | 2.25E-04 | 1 | 2.25E-04 | 5.03 | 0.037 | |
| **BC** | 2.25E-04 | 1 | 2.25E-04 | 5.03 | 0.037 | |
| **$A^2$** | 4.30E-04 | 1 | 4.30E-04 | 9.61 | 0.0059 | |
| **$B^2$** | 1.46E-03 | 1 | 1.46E-03 | 32.6 | < 0.0001 | |
| **$C^2$** | 1.44E-04 | 1 | 1.44E-04 | 3.22 | 0.0887 | |
| **$D^2$** | 3.44E-04 | 1 | 3.44E-04 | 7.69 | 0.0121 | |
| **Residual** | 8.50E-04 | 19 | 4.47E-05 | | | |
| **Pure Error** | 0 | 5 | 0 | | | |
| **Cor Total** | 0.028 | 29 | | | | |
| **Std. Dev.** | 6.69E-03 | | | | | |
| **$R^2$** | 0.9692 | | | | | |
| **Adj $R^2$** | 0.953 | | | | | |
| **Adeq Precision** | 32.921 | | | | | |

Final equation given by the software in terms of coded factors for calculation of the flotation rate constants.

$$k = +2.77 - 0.44 \times A + 0.68 \times B + 0.42 \times C - 2.37 \times D + 0.46 \times E + 0.25 \times A \times C$$
$$- 0.43 \times B \times D + 0.32 \times B \times E - 0.45 \times D \times E + 0.51 \times D^2 \quad \text{(A.2)}$$

**Table A.2:** ANOVA results of quadratic model to predict the flotation rate constants.

| Source | Sum of Squares | DF | Mean Square | F Value | p-value Prob > F | |
|---|---|---|---|---|---|---|
| **Model** | 321.28 | 10 | 32.13 | 69 | < 0.0001 | significant |
| **A-particle size** | 8.31 | 1 | 8.31 | 17.85 | 0.0001 | |
| **B-particle density** | 20.22 | 1 | 20.22 | 43.43 | < 0.0001 | |
| **C-bubble size** | 7.57 | 1 | 7.57 | 16.27 | 0.0002 | |
| **D-bubble velocity** | 242.93 | 1 | 242.93 | 521.73 | < 0.0001 | |
| **E-turbulence** | 9.15 | 1 | 9.15 | 19.65 | < 0.0001 | |
| **AC** | 1.94 | 1 | 1.94 | 4.16 | 0.0483 | |
| **BD** | 5.81 | 1 | 5.81 | 12.47 | 0.0011 | |
| **BE** | 3.35 | 1 | 3.35 | 7.2 | 0.0107 | |
| **DE** | 6.5 | 1 | 6.5 | 13.97 | 0.0006 | |
| **$D^2$** | 15.5 | 1 | 15.5 | 33.28 | < 0.0001 | |
| **Residual** | 18.16 | 39 | 0.47 | | | |
| **Pure Error** | 0 | 7 | 0 | | | |
| **Cor Total** | 339.44 | 49 | | | | |
| **Std. Dev.** | 0.68 | | | | | |
| **$R^2$** | 0.9465 | | | | | |
| **Adj $R^2$** | 0.9328 | | | | | |
| **Adeq Precision** | 37.719 | | | | | |

**CURRICULUM VITAE**

**Name Surname** : Ahmad HASSANZADEH

**Place and Date of Birth** : Khoy, 12.10.1986

**E-Mail** : hassanzadeh@itu.edu.tr

**EDUCATION** :

- **B.Sc.** : 2010, Sahand University of Technology, Mining Engineering
- **M.Sc.** : 2012, Bahonar University of Kerman, Mining Engineering Faculty, Mineral Processing Engineering Division,

**PROFESSIONAL EXPERIENCE AND REWARDS:**

- 2010 Mining Engineer, Azerabadegan Cement Plant
- 2010-2013 Process and Plant Engineer- NICICO.

**PUBLICATIONS, PRESENTATIONS AND PATENTS ON THE THESIS:**

- **Hassanzadeh, A**., Firouzi, M., Albijanic, B., Çelik M.S. 2018. A Review On Determination Of Particle-Bubble Encounter Using Analytical, Experimental And Numerical Methods, *Minerals Engineering*, 122, 296-311.
- **Hassanzadeh, A**., Kouachi, S., Hasanzadeh, M., Çelik M.S. 2017. A New Insight To The Role Of Bubble Properties On Inertial Effect In Particle-Bubble Interaction, *Journal of Dispersion Science and Technology*, 38(07), 953-960.
- **Hassanzadeh, A**., Vaziri Hassas, B., Kouachi, S., Brabcova, Z., Çelik M.S., 2016. Effect Of Bubble Size And Velocity In Chalcopyrite Flotation, *Colloids and Surfaces A. Physicochemical and Engineering Aspects*, 498, 258-267.
- Kouachi, S., Vaziri Hassas, B., **Hassanzadeh, A**., Çelik M.S., Bouhenguel, M., 2017. Effect Of Negative Inertial Forces On Bubble-Particle Collision Via Implementation Of Schulze Collision Efficiency In General Flotation Rate Constant Equation, *Colloids and Surfaces A. Physicochemical and Engineering Aspects*, 517(20), 72-83.
  - Bouhenguel, M., Kouachi, S., **Hassanzadeh, A**., Vaziri Hassas, B., Çelik M.S., 2016. Investigation Of The Effect Of The Maximum Collision Angle

On The Yoon-Luttrell Attachment Model, 15th International Mineral Processing Symposium, Istanbul, Turkey, October 19-21, 1040-1050.

- Kouachi, S., **Hassanzadeh, A**., Bouhenguel, M., Vaziri Hassas, B., Çelik M.S., 2015. Contribution Of Interceptional Effect To Collision Efficiency Of Particle Bubble Encounter In Flotation, XVI Balkan Mineral Processing Congress, Belgrade, Serbia, 17-19th June, 339-345.

**OTHER PUBLICATIONS, PRESENTATIONS AND PATENTS:**

- Hoang, D.H., Heitkam, S., Kupka, N., **Hassanzadeh, A**., Peuker, U.A., Rudolph, M., 2019. Froth Properties And Entrainment In Lab-Scale Flotation: A Case Of Carbonaceous Sedimentary Phosphate Ore, *Chemical Engineering Research and Design,* 142, 100–110.
- Vaziri Hassas, B., Guven, O., **Hassanzadeh, A**., 2018. An Investigation Of The Recovery And Kinetics During The Flotation Of Residual Petroleum Coke In Lime Calcination Exhaust Tailings, *International Journal of Coal Preparation and Utilization*, 1-11,
- **Hassanzadeh, A**., 2018. A Survey On Troubleshooting Of Closed-Circuit Grinding System, *Canadian Metallurgical Quarterly*, 57(03), 328-340.
- Agheli, S., **Hassanzadeh, A**., Vaziri Hassas, B., Azizi, A., Hasanzadeh, M., 2018. An Investigation On Effect Of Pyrite Content Of Feed And Configuration Of Locked Particles On Rougher Flotation Of Copper In Low And High Pyritic Ore Types, *International Journal of Mining Science and Technology*. 28(02), 167-176.
- **Hassanzadeh, A**. 2017. Measurement And Modeling Of Residence Time Distribution Of Overflow Ball Mill İn Continuous Closed Circuit, *Geosystem Engineering,* 20(05), 251–260.
- **Hassanzadeh, A**., 2018. A New Statistical View To Modeling Of Particle Residence Time Distribution In Full-Scale Overflow Ball Mill Operating İn Closed-Circuit, *Geosystem Engineering,* 21(04), 199-209.
- **Hassanzadeh, A**., Karakas, F., 2017, Recovery Improvement Of Coarse Particles By Stage Addition Of Reagents In Industrial Copper Flotation Circuit, *Journal of Dispersion Science and Technology,* 38(02), 309-316.
- **Hassanzadeh, A**., Hasanzadeh, M., 2016. A Study On Selective Flotation İn Low And High Pyretic Copper Sulfide Ores, *Separation Science and Technology,* 5(13), 2214-2224.
- **Hassanzadeh, A**., Hasanzadeh, M., 2016. Chalcopyrite And Pyrite Floatabilities In The Presence Of Sodium Sulphide And Sodium Metabisulfite In A High Pyritic Copper Complex Ore, *Journal of Dispersion Science and Technology,* 38(06), 782-788.